Molecular links between retinal determination factors and the oscillator mechanism

A thesis submitted to the University of Manchester for the degree of Ph.D
in the Faculty of Life Sciences

2010

Indrayani Ghangrekar

Table of contents

Word count: 36281

List of figures

Chapter 1

Chapter 2

Chapter 3

Chapter 4

Chapter 5

Chapter 6

List of tables

Chapter 1

Chapter 2

Chapter 4

Abstract

The past two decades have highlighted the utility in using the fruit fly *Drosophila* as a model organism for unravelling the molecular and functional complexities of two important fields of research: the systems that guide retinal determination (RD) and circadian rhythms (the daily body clock or oscillator). RD and clock factors are of great interest as they are: (1) highly conserved in vertebrates; (2) also essential for other physiological systems; (3) implicated in several congenital disorders and other diseases.

The RD factors operate within a network in which several of their interactions have been described. Two such factors, *eyes absent (eya)* and *sine oculis (so),* are known to function as a unit to direct transcriptional regulation during photoreceptor (PR) differentiation. The regulation of *eya* and *so* by a transcriptional repressor at the heart of the clock mechanism, *vrille (vri),* is here investigated. Two distinct observations advocated exploration of a link between *vri* and *eya*/ *so* is of interest. (1) *vri* is a core component of the clock and interacts with RD but the RD function is unknown. (2) Recent evidence suggests that an RD factor directly upstream of *eya* and *so*, *twin-of-eyeless (toy)*, interacts with the oscillator mechanism through direct and indirect pathways. It is possible that the indirect influences of *toy* on the oscillator are mediated via *eya* and/ or *so*. Interactions between *eya, so* and *vri* during RD and within oscillator cells are investigated here.

Eye development function was studied using immunohistochemistry and transgenic manipulation. VRI is not expressed within the developed PRs; rather, expression of VRI is down-regulated prior to differentiation. In addition, conversely to the hypothesised role, VRI is co-expressed with EYA in some regions. Together with data from transgenic manipulation of VRI regional expression, I propose that VRI is predominantly part of a developmental pathway but can attenuate *eya* and *so* expression.

The VRI binding site has been described previously and several sites were identified within *eya*/ *so* loci, some of which were tested in an *in vitro* binding assay. Two such sites were located adjacent to a known enhancer of *so*. I generated two transgenic fly lines containing: 1) an extension of the original enhancer to contain the VRI sites; and 2) a similar construct with the VRI sites ablated. Comparison of the original enhancer to those from the current study confirmed that the VRI sites attenuate expression and that intervening regions must contain binding sites for other transcription factors.

In adult brains over a circadian light-dark cycle, EYA protein was expressed in three of the central brain clock neurones. Furthermore, expression of *eya* and *so* transcripts in adult heads, PRs and the brain, changed over the light/ dark cycle independently of the clock – indicating that their expression is modulated over the light-dark cycle but not by the oscillator mechanism.

These data suggest interactions between eye development factors *eya*/ *so* and oscillator components, or, the light/ dark cycle exist. These interactions may be important for tissue-specific circadian physiology as well as the overall oscillator mechanism and offer an intriguing route for future investigation.

Declaration

I, Indrayani Ghangrekar, declare that no portion of the work referred to in this thesis has been submitted in support of an application for another degree or qualification of this or any other university or other institute of learning.

All of the work described here was carried out by me apart from:

- Figure 1.4 is from Glossop, unpublished result.
- Figure 1.5 is from Helfrich-Förster *et al.*, 2007.
- Figure 4.11 is from Helfrich-Förster, 2003.

Copyright statement

Dedication

I would like to dedicate this work to three people who, in their own unique ways, inspire and motivate me. Thank you for your love, support and encouragement, my life is so much richer for having you in it. I love you.

Mum, you are my role model for hard work and taught me to always be passionate about whatever I do. Without your efforts, love, patience and encouragement, I would not be the person I am today.

Mithu, you are so much more than a sister to me, I feel so lucky that we are the best of friends and have the connection that we do. Thank you for all the food, teas, coffees, playtimes and for helping me to 'eat an elephant'.

Dylan, my love, my best friend, thank you so much for your continued patience and support through the stress and tears and still having a smile and a hug for me at the end. Your encouragement, silliness, jokes and jibes really helped me to persevere when I felt like I could do no more and kept me cheerful, smiling and grounded.

Acknowledgements

I feel most privileged to have been given the opportunity to study for a PhD. I would like to thank my supervisor Dr. Nicholas Glossop for the opportunity and his continued encouragement and support throughout my studies. He has always been very generous with his time and advice and his enthusiasm and excitement about the project is infectious, for which I am very grateful. I also thank him for always being supportive of my desire to undertake public engagement projects, I have greatly benefitted from the experience and am proud of my achievements. Thanks also to my advisor Prof. Robert Lucas and my co-supervisor for their support and words of advice throughout my PhD. I am deeply indebted to my good friend and brother-in-law, Johan Oldekop, for keeping me motivated during thesis writing, offering numerous helpful suggestions and, together with my sister, ensuring I ate well and healthily.

I have been lucky in being surrounded by excellent colleagues, I am especially thankful for Annette Allen, Helena Bailes, Richard Baines, Heather Brooke, Graham Coutts, Thifeen Deen, Wei-Hsiang Lin, Nara Muraro and Verena Wolfram for friendship, advice and companionship during lunch and coffee breaks.

My loved ones, friends and family, have been supportive throughout and I am very fortunate to have them in my life.

This work would not have been possible without funding from the BBSRC and the kind donations of reagents or animals from other research groups. The Bioimaging Facility microscopes used in this study were purchased with grants from BBSRC, Wellcome and the University of Manchester Strategic Fund. Special thanks goes to Peter March, Jane Kott and Robert Fernandez for their help with the microscopy. Part of this work was carried out in the Faculty's Fly Facility, established through funds from University and the Wellcome Trust (087742/Z/08/Z).

About the author

I obtained a 2:1 classification for my undergraduate degree in Neuroscience with a Modern Language (Japanese) in 2006. In the summer after the first year of my undergraduate studies, I assisted Prof. Hugh Piggins' technician with immunostaining of hamster brains for six weeks. Following my second year, I continued my Japanese studies and undertook a research project at the University of Tsukuba, Japan. Prof. Katsuo Furukubo-Tokunaga was my advisor for the research project in which I carried out *in situ* hybridisation on *Drosophila* larval brains to investigate developmentally relevant genes expressed in the mushroom bodies out of a short-list identified from studies of the adult. My final year undergraduate project, supervised by Dr. Owen Jones, involved cloning of cyan fluorescent protein downstream of a *Chlamydomonas reinhardtii* photosensitive cation channel for further functional testing. I commenced my PhD studies in January 2007 under the guidance of Dr. Nicholas Glossop.

List of abbreviations

Abbreviation	*Term*
APS	ammonium persulphate
BO	Bolwig's organ
bp	base pairs
CLK-GP50	Guinea Pig 50 anti-CLK
Clk/CLK	Clock *gene*/PROTEIN
CNS	central nervous system
cyc/CYC	cycle *gene*/PROTEIN
DABCO	diazabicyclo [2.2.2] octane
DIG	digoxigenin
DN1s	dorsal neurones group 1
DN2s	dorsal neurones group 2
DN3s	dorsal neurones group 3
DNs	dorsal neurones
dpp/DPP	decapentaplegic *gene*/PROTEIN
DR	developmental regulatory
ECL	enzymatic chemiluminescence
EGF	epidermal growth factor
EGFR	epidermal growth factor receptor
EMSA	electrophoretic mobility shift assay
ey/EY	eyeless *gene*/PROTEIN
eya/EYA	eyes absent *gene*/PROTEIN
GFP	green fluorescent protein
GP-a-VRI	guinea pig anti-VRI antibody
H-B eyelet	Hofbauer-Buchner eyelet
H-B tract	Hofbauer-Buchner tract
hh/HH	hedgehog *gene*/PROTEIN
IHC	immunohistochemistry
IR	immunoreactivity
kb	kilo base pairs
L1-3	larval stage 1-3

lLNvs	large ventral lateral neurones
LNds	dorsal lateral neurones
LNs	lateral neurones
LNvs	ventral lateral neurones
MF	morphogenetic furrow
ºC	degrees centigrade
OL	optic lobe
PBS	phosphate buffered saline
PBX	phosphate buffered saline with 0.3% Triton X-100
PDF	pigment dispersing factor
PDFR	pigment dispersing factor receptor
pdp1/PDP1(ε)	PAR domain protein 1(ε isoform) *gene*/PROTEIN
PFA	paraformaldehyde
pGEM-TE	pGEM-T Easy plasmid
PR	photoreceptor
PXDN	PBS with 0.3% sodium deoxycholate and 5% donkey normal serum
RDGN	retinal determination gene network
rh1/ninaE/RH1	rhodopsin 1 *gene*/PROTEIN
Rh6	rhodopsin 6
R*x*	photoreceptor number ***x***
SDS	sodium dodecyl sulphate
sLNvs	small ventral lateral neurones
so/SO	sine oculis *gene*/PROTEIN
SSC	saline-sodium citrate buffer
TBST	Tris-sodium chloride-Tween20-Blocking buffer
TEMED	tetramethylethylenediamine
TF	transcription factor
TGFß	transforming growth factor beta
toy/TOY	twin of eyeless *gene*/PROTEIN
TST	Tris-sodium chloride-Tween20 buffer
V/P box	VRI/ PDP1ε box
VNC	ventral nerve cord

vri/VRI	vrille *gene*/PROTEIN
wg/WG	wingless *gene*/PROTEIN

Chapter 1 General introduction

Two areas that have been extensively researched in the fruit fly *Drosophila melanogaster* are development and the maintenance of circadian rhythms: both of which show striking parallels in mice and humans. The study of development is of interest because of the many areas in biology that are involved in this process, for example, apoptotic mechanisms; cell-cell interactions; signal transduction; transcriptional regulation; congenital disorders; stem cell biology; and evolution. Many upstream components that regulate development are highly conserved across phyla and help us to understand the evolution of inter- and intra-cellular interactions. Moreover, some factors that are involved in the development of an organism can also be employed in later, non-developmental stages, so, understanding the role they play during development can inform about mechanisms in the mature system.

Chronobiology – the study of behavioural, molecular and physiological cycles – is attractive as it shows a high level of functional conservation. The ability to anticipate, co-ordinate and adapt behavioural, metabolic and physiological functions to environmental changes imparts a significant survival advantage. Biorhythms may be linked to a variety of environmental changes, however, the influence of the daily light-dark cycle is most extensively researched. Indeed, evidence for the importance of daily biorhythms lies in several established links between disruption of daily rhythms and pathophysiology ranging from cell proliferation (Reddy *et al.,* 2005); cardiac function (Durgan and Young, 2010); neurodegeneration (Bao *et al.,* 2008); to pharmacokinetics (Lévi *et al.,* 2008), to name a few.

Daily oscillations may be studied on a whole animal behavioural level, optimal function of an organ or, at the molecular level. The molecular oscillator mechanism comprises a set of factors that show rhythmic changes in gene transcription and protein turnover and form a feedback regulatory network. Moreover, the molecular oscillator has been observed in several different cell

types – neurones within the central nervous system (CNS) that influence behaviour and in cells comprising organs that show daily changes in function. Currently, there is a lack of data about the molecular oscillator and how it interacts with tissue-specific factors within cells of a given organ to mediate physiological changes that are linked to the light-dark cycle. The compound eyes of the fruit fly are formed of approximately eight hundred individual photoreceptive units, or ommatidia (Voas *et al.*, 2004). All eight photoreceptors (PRs, R1-R8) within each ommatidium and the PRs of the ocelli, simple eyes located medially on dorsal head, contain cell-autonomous oscillators (Cheng and Hardin, 1998). The PRs thus comprise the largest tissue-specific oscillators of the adult fly head and were used here to begin exploring links between retinal determination factors and the oscillator mechanism. I will set the scene for these studies by outlining the relevant aspects of eye development and circadian rhythms of *Drosophila melanogaster*.

1.1 Eye development

Development of the adult visual systems, the compound eye and the ocelli, of *Drosophila* is initiated during embryonic development, remains dormant during early larval stages and resumes from late larval stages until emergence of the adult (Cohen, 1993; Poulson, 1994). Many of the key factors involved in eye development have been identified and found to interact within a feedback network rather than a binary cascade (reviewed in Kumar, 2009b). The factors that form this network may be split into two categories: (1) the retinal determination gene network (RDGN) factors; so described because of eye-specific mutant phenotypes and the ability to trans-determine tissue of other imaginal discs towards an eye fate when ectopically expressed. (2) developmental regulatory (DR) factors of signalling cascades that have pleiotropic roles throughout development in a multitude of tissues. Co-ordination between the RDGN and the DR factors is required for generation of the reiteratively patterned retina. Here, I am going to focus on the activation of two of the RDGN factors, *eyes absent* (*eya*) and *sine oculis* (*so*). During eye

development, *eya* and *so* expression is completely overlapping. In addition, the proteins dimerise to form a transactivation complex (Pignoni *et al.*, 1997). As a result of this close relationship, *eya* and *so* are frequently studied in conjunction and here also, referred to with reference to one another.

A cluster of fourteen cells at the posterior ventral part of this optic placode form the precursors of the larval visual system called Bolwig's organ (BO, Suzuki and Saigo, 2000). The cells first adopt a neural fate and then begin to develop a PR identity. The BO innervates the region containing a subset of the larval central brain circadian neurones to entrain those neurones to the light-dark cycle throughout larval development (Malpel *et al.*, 2002). During pupal development, the B-O PRs and projections are retained in this functional capacity but are now known as part of an extra-retinal structure called the Hofbauer-Buchner (H-B) eyelet (Helfrich-Förster *et al.*, 2002). The current study focuses on the development of the compound eye PRs as they also have intrinsic oscillator function whereas the H-B eyelet PRs do not. However, the PRs of the eyelet, together with the compound eye and ocellar PRs and a non-opsin, blue light molecular photoreceptor all contribute to the entrainment of the central brain circadian neurones in the adult fly (Helfrich-Förster *et al.*, 2001; Helfrich-Förster *et al.*, 2002).

1.1.1 Specification and early development

The adult visual system primordia arise as two bilaterally symmetrical groups of epithelial cells that meet at the dorsal midline to form a V-shape in the procephalic region (Cohen, 1993). Following patterning and organisation of the germ layers, regions of the epithelium dedicated to make any of the adult organs begin to invaginate to form flattened sacs of tissue known as imaginal discs (imaginal = of the imago, imago = adult; Campos-Ortega and Hartenstein, 1985). The eye imaginal disc is fused to the antennal imaginal disc and indeed they have a common origin, being specified by the same factors, and are indistinguishable at the molecular level until later stages (Kumar and Moses, 2001a). Following invagination, the discs do not develop

further until larval stages. The two *Pax-6* genes, *twin of eyeless* (*toy*) and *eyeless* (*ey*), are expressed from the embryonic origin of the eye disc and persist through to adult stages; both are RDGN components (Quiring *et al.*, 1994; Czerny *et al.*, 1999; Halder *et al.*, 1995; Pappu and Mardon, 2002).

The larva goes through three distinct developmental stages known as instars (Bodenstein, 1994), where progression from one larval instar to the next involves shedding of the cuticle. Successive larval stages are larger and have more developed and readily identifiable mouthparts; hereafter referred to as L1, L2 and L3. Throughout L1, L2 and early L3 larval development, larvae are devoted to feeding. This behaviour changes near the end of L3 – where larvae emerge from the food and begin 'wandering', or crawling to find a place to settle for puapariation. This behaviour coincides with developmental changes occurring within the eye disc.

During L1 to mid-L2 stages, discs grow by cell proliferation but development of eye identity remains dormant (Czerny *et al.*, 1999; Kammermeier *et al.*, 2001). Eye or antennal identity is acquired later, during the mid- to late-L2 stage, by the antagonistic action of two DR factors (see Table 1.1; Kumar and Moses, 2001a).

1.1.2 Determination and differentiation of photoreceptors

The major regulatory interactions that initiate eye precursor cell differentiation with reference to *eya* and *so* are summarised in Figure 1.1, an extended overview of interactions is listed in Table 1.1. The development of the disc into an eye begins during mid- to late-L3 and appears as a wave of differentiation, termed the morphogenetic furrow (MF), on the apical surface of the disc that moves as a DV-oriented line across the disc from posterior to anterior (Wolff and Donald, 1993). As the MF passes across the disc, hexagonal arrays of cells develop posterior to it and reflect the shape of the adult ommatidia. These cell arrays comprise the eight post-mitotic PR neurones that have terminally differentiated.

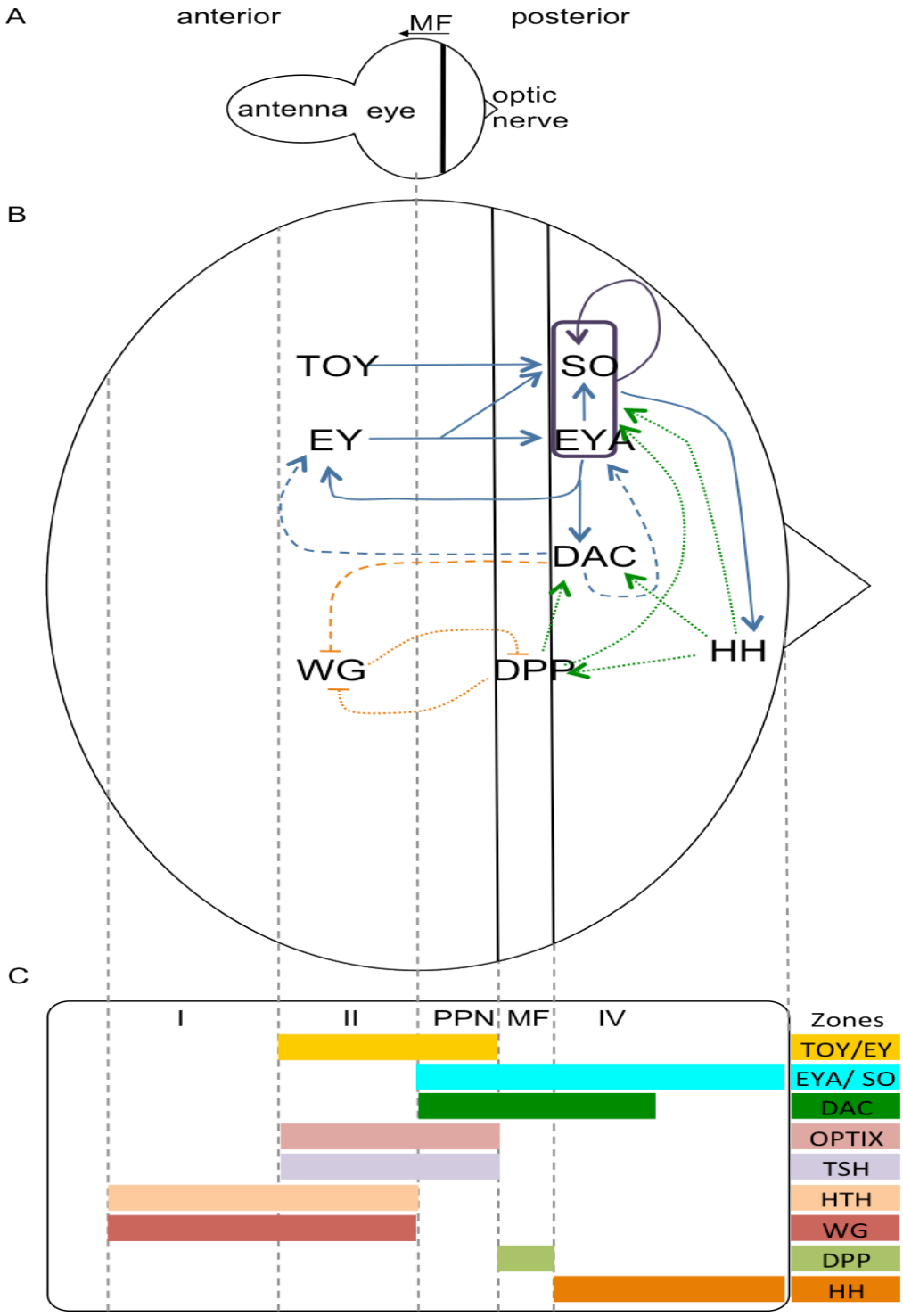

Figure 1.1 A schematic of the L3 eye disc. (A) The layout of the eye antennal disc during late L3. (B) Enlarged eye disc from (A); some retinal determination genes and MF-associated factors are shown together with their interactions. Solid blue arrows indicate direct, known transcriptional activation between retinal determination genes; purple box indicates EYA-SO complex; dashed blue arrows show predicted activation by DAC; dashed orange line with bar shows predicted inhibition by DAC; dotted lines show regulation by morphogens where the exact pathway has not been characterised: dotted green arrows show positive regulation, dotted orange lines with bars show negative regulation. (C) Adapted and expanded from Bessa *et al.* (2002), dotted lines outline zones of the eye disc. Shaded areas show the expression domains of the molecules indicated on the right. MF, morphogenetic furrow; PPN, pre-proneural zone; refer to text for further gene information (Czerny *et al.*, 1999; Halder *et al.*, 1995; Pappu and Mardon, 2002; Chen *et al.*, 1997; Halder *et al.*, 1998; Baonza and Freeman, 2002; Chen *et al.*, 1999; Pignoni *et al.*, 1997; Bonini *et al.*, 1993; Bonini *et al.*, 1997; Punzo *et al.*, 2002; Chanut and Heberlein, 1997; Bessa *et al.*, 2002).

Table 1.1 Summary of the roles of core eye determination factors and developmental regulators closely linked to eye determination. See Figure 1.1 for information about expression zones of the L3 eye disc; TF – transcription factor. (Bessa *et al.*, 2002; Kumar and Moses, 2001a-c; Pignoni *et al.*, 1997; Halder *et al.*, 1998; Chen *et al.*, 1999; Curtiss and Mlodzik, 2000; Pappu *et al.*, 2003; Baonza and Freeman, 2002; Czerny *et al.*, 1999; Punzo *et al.*, 2001; Pauli *et al.*, 2005; Pappu *et al.*, 2005; Chanut and Heberlein, 1997; Chen *et al.*, 1997; Kenyon *et al.*, 2005; Seimiya and Gehring, 2000; Ostrin *et al.*, 2006; Mardon *et al.*, 1994; Salzer *et al.*, 2009)

Gene	Category, *protein type*	Role during eye development
twin of eyeless (toy)	RDGN, *Pax6*	Expressed from eye primordium stage and in anterior eye disc zones II and PPN, down-regulated as MF advances. Activates *ey* initially; subsequently *eya* (inferred by homology with *ey*) and *so*.
eyeless (ey)	RDGN, *Pax6*	Expressed from eye primordium stage and in anterior eye disc zones II and PPN, down-regulated as MF advances. Activates *toy, eya*, *so* and *optix*; is activated by EYA-SO
eyes absent (eya)	RDGN, *Eya*	Expressed in eye disc zones PPN, MF and IV. Complexes with SO and/ or DAC to activate gene expression of *so, ey, dac* (anterior of zone IV only), *hh, string, lozenge* and *atonal*.
sine oculis (so)	RDGN, *Six*	Expressed in eye disc zones PPN, MF and IV. Complexes with EYA and/ or DAC to activate gene expression of *so, ey, dac* (anterior of zone IV only), *hh, string, lozenge* and *atonal*. Can dimerise with GROUCHO to repress *dac* in posterior of zone IV.
dachshund (dac)	RDGN, *Ski/Sno*	Expressed in eye disc zones PPN, MF and

		anterior of IV. Complex and unresolved role, may form dimers with EYA or SO, and/ or form a trimeric DAC-SO-EYA complex.
optix	RDGN, *Six*	Expressed in anterior eye disc zones II and PPN. Closely related to SO, partners with a transcriptional co-repressor, GROUCHO.
teashirt (tsh)	RDGN, zinc finger TF	Expressed in anterior eye disc zones II and PPN. Context-dependent role – together with HTH, EY and WG, repression of *eya* and *dac* in anterior eye disc distal to MF; together with EY, promotion of *eya* and *dac* proximal to MF.
homothorax (hth)	RDGN, homeobox	Expressed in ventral eye primordium and in anterior eye disc zones I and II. Suppression of eye specification in the ventral region of the eye primordium and anterior eye disc, inhibition of MF initiation; co-regulation with TSH, EY and WG.
hedgehog (hh)	DR, secreted morphogen	Expressed at posterior eye disc zone IV and lateral margins of the eye disc, together with DPP promotes MF initiation and propagation.
Notch (N)	DR, signal transduction	Pleiotropic roles during eye development, usually antagonistic to EGFR: initial promotion of eye identity; lateral inhibition for PR differentiation. Not antagonistic but integrated with EGFR upstream of *dpp* and *hh* for MF initiation.

epidermal growth factor receptor (EGFR)	DR, signal transduction	Pleiotropic roles during eye development, usually antagonistic to Notch: initial promotion of antennal identity. Not antagonistic but integrated with Notch upstream of *dpp* and *hh* for MF initiation. Involved in cell identity specification.
decapentaplegic (dpp)	DR, secreted morphogen of the TGFβ/ BMP family	Expressed in MF and lateral margins of the eye disc, together with HH promotes MF initiation and propagation.
wingless (wg)	DR, secreted morphogen	Expressed in anterior eye disc zones I and II, antagonises role of DPP.

TOY and EY, are referred to as the 'master' eye regulators and activate RDGN genes *eya* and *so* (Pappu and Mardon, 2002; Kumar, 2009b). Mutants of these genes show severe eye defects (i.e. reduced or absent eyes) as each is absolutely required for normal eye development and ectopic expression in other imaginal discs can lead to ectopic eye development (Halder *et al.*, 1995; Pappu and Mardon, 2002). In the anterior eye disc, within zones II and PPN, TOY and EY are expressed at a high level but are down-regulated within the MF and zone IV (Halder *et al.*, 1998; Czerny *et al.*, 1999, Jemc and Rebay, 2007a). During L2, *eya* and *so* are expressed in the eye disc but during L3, their expression is restricted zones PPN, MF and IV (Bonini *et al.*, 1993; Cheyette *et al.*, 1994; Pignoni *et al.*, 1997; Bonini *et al.*, 1997; Jemc and Rebay, 2007a).

TOY initially activates *ey* expression and TOY and EY then co-activate *eya* and *so*, and another RDGN factor *dachshund* (*dac*); EYA and SO dimerise to form the EYA-SO complex and can also interact with DAC individually and within a trimeric complex to drive retinal determination (Czerny *et al.*, 1999; Chen *et al.*, 1997; Halder *et al.*, 1998; Pignoni *et al.*, 1997; Bonini *et al.*, 1997; Punzo *et al.*, 2002; Hauck *et al.*, 1999). Among EYA-SO targets, positive feedback

that reinforces the network has been observed by activation of *ey*, *dac* (anterior zone IV only, see Figure 1.1) and auto-regulation of *so* itself (Pignoni *et al.*, 1997; Pauli *et al.*, 2005). The retinal determination targets of EYA-SO include the proneural gene *atonal*; the cell cycle regulator *string*; the cell fate determinant *lozenge*; and, *hedgehog* (*hh*), a secreted morphogen and a DR factor of eye development (see Table 1.1 for *hh*; Yan *et al.*, 2003; Pauli *et al.*, 2005; Zhang *et al.*, 2006; Jemc and Rebay, 2007). Regulation of *dac* changes dependent on the position of the cells. Activation by EYA-SO is only in the anterior of zone IV; in the posterior of zone IV, SO dimerises with the co-repressor GROUCHO to suppress *dac* expression.

1.1.3 Additional details of selected retinal development factors

1.1.3.1 TOY and EY

The *Pax* family of developmental regulators are highly conserved and contain a DNA-binding domain called a paired box; and several members also contain a homeobox (reviewed in Dahl *et al.*, 1997; Blake *et al.*, 2008). *Pax* factors all appear to be key embryonic regulators that are essential for the specification of CNS and other organs. *Pax-6* genes specify eye and other CNS regions in *Drosophila* (*toy* or *ey*), mouse, or human homologues (Czerny *et al.*, 1999; Punzo *et al.*, 2001; Kozmik, 2005). Viable mutations in the mouse and human homologues of *Pax-6* genes can cause a range of defects from mild anomalies to serious defects in the CNS; loss of eye; loss of olfaction; or loss of the external nasal structures (Hanson, 2001). Null mutants of *toy* or *ey* are embryonic lethal and the only viable mutants of *toy* and *ey* are eye-specific. The presence of two *Pax-6* genes in *Drosophila* arose due to a local duplication event as only a single orthologue of *Pax-6* is found in vertebrates though the homologues remain closely related (Czerny *et al.*, 1999). The homeodomain of both TOY and EY shares 90% sequence identity with vertebrate PAX-6 proteins, while the paired domain shows 91% (TOY) and 95% (EY) identity to vertebrate PAX-6. Despite their close relationship, only partial

co-expression is observed during embryonic development and, together with eyeless phenotypes of single mutants, indicates that they do not serve redundant functions to one another.

During larval and adult stages, *toy* and *ey* expression is evident in regions of the brain, ventral nerve cord (VNC) and eye tissue. The optic lobes and central brain, in particular the olfactory processing centres, show *toy* and *ey* signals that partially overlap. Whilst both are highly expressed in the olfactory centres, *toy* is expressed more broadly than *ey*.

Some of the spatial expression of *toy* within the central brain is now being resolved (Glossop *et al.,* unpublished results). Links to a subset of oscillator neurones of the central brain are indicated, this is discussed further in section 1.3.

1.1.3.2 EYA and SO

Throughout embryonic development, *eya* and *so* are expressed in the head and in a segmentally reiterated pattern within the ventral nerve cord (EYA and DAC, *so* data from lacZ enhancer trap; Kumar and Moses, 2001c). Optic lobe primordia, but not the embryonic anlagen of the eye disc, express *eya* and *so* – suggesting a function in CNS patterning at this stage of development (Bonini *et al.,* 1998; Halder *et al.,* 1998; Kumar and Moses, 2001c). Accordingly, null mutants of either of these genes causes lethality and the early mutants that were recovered, that defined the names of these genes, consisted of alleles containing deletions of eye-specific enhancers. Due to the availability of viable mutants of the eye phenotype and extensive data on eye development, research has been focused on the eye disc and there is little data about the other roles of *eya* and *so* during development or in the mature system. Non-ocular roles for *eya* and *so* are better described in vertebrates and indicate that mis-regulation of *Eya* or *Six* factors is tumorigenic (Jemc and Rebay, 2007a). In addition, it was recently shown that *Eya3* and *Six1* interact and form part of a pituitary endocrine response to photoperiod (Masumoto *et al.,* 2010; Dardente *et al.,* 2010).

The EYA protein has dual functions – transcriptional regulation (in conjunction with SO) and tyrosine phosphatase activity (reviewed in Jemc and Rebay, 2007a). A single *eya* gene is found in *Drosophila* whereas four homologues, *Eya1-4*, are present in mice and humans. Homologues of *eya* have also been implicated in development and disease in vertebrates. Pathologies observed in mice and humans include vision deficits, hearing defects, loss of the ears, branchial arch abnormalities and kidney defects (reviewed in Hanson, 2001). Expression of *Eya* homologues is thus essential for organogenesis in other tissues besides the eyes but it remains possible that there is partial compensation or redundancy. In eye development, *Eya1-3* has been observed in the mammalian eye but a myriad of *Eya1* phenotypes suggest that *Eya2* and *Eya3* can partially compensate for the loss of *Eya1*.

The *Six* gene family was founded by *so* and contains a homeobox DNA binding domain and the protein interaction six domain (reviewed in Kumar, 2009a). Two additional orthologues of *so* are present in *Drosophila, optix* and *D-six4*. Of these, *optix* is known as an RDGN factor that is expressed in anterior regions of the disc whereas *D-six4* functions in mesoderm-derived cells of the muscles, fat body and somatic gonadal cells. All three of these genes are conserved in vertebrates and appear to have duplicated to form three distinct gene families with two members in each. However, *optix* and *D-six4* homologues are expressed within the developing vertebrate eyes while *so* homologues are more restricted to the nasal and otic placodes, branchial arches, the kidney, craniofacial muscles and other muscular, skeletal and connective tissues. Pathologies involving *Six* family members are similar to those observed for *Eya1-4,* unsurprising given that factors of the *Eya* and *Six* families are expressed in similar tissues (Hanson, 2001; Kumar, 2009a).

1.1.3.3 A circadian regulator helps shape the eye

The basic leucine zipper (bZip) transcriptional factor *vrille* (*vri*) is a developmental regulator and, as mentioned about *toy, ey, eya* and *so*, is essential from embryonic stages as null or homozygous mutants are embryonic

lethal (George and Terracol, 1997). Mutant alleles are only recovered when enhancer/ promoter regions are disrupted and only in trans to wild-type or other mutant alleles. Several stages and tissues of the embryo require *vri*, and of particular relevance here, proliferating tissues, i.e. the imaginal epithelia of discs and gut. One of the roles of *vri* in the embryo appears to involve the DPP signal transduction pathway during dorsoventral patterning. In addition, *vri* also enhances DPP wing phenotypes and the phenotype of *vri* alleles on wing veins is similar to the *dpp shortvein* phenotype. During patterning and differentiation events of the eye disc in L3, expression of *vri* has been described and mis-regulation indicates that the function of *vri* affects eye development; however, the function is currently unknown (Szuplewski *et al.,* 2003). The majority of data on the control of *vri* expression and function comes from studies in the adult where it has been shown to be part of the core molecular oscillator mechanism, described further in section 1.2 (Blau and Young, 1999; Glossop *et al.,* 2003; Cyran *et al.,* 2003).

1.2 The circadian oscillator

The circadian (circa – about : diem – a day) oscillator is a timing mechanism that provides organisms with the ability to anticipate daily changes in the environment and thus co-ordinate physiological and behavioural events to the right time of day, or night. Plants, fungi, animals and prokaryotes show an anticipatory circadian rhythmicity in physiology, metabolism and behaviour (Vallone *et al.,* 2007; Hardin, 2005). The oscillator is adjusted by environmental cues, such as light or temperature (known as zeitgebers – time givers), to ensure that the internal clock is synchronised to the time of day (Devlin, 2002). This also ensures that the oscillator does not begin to 'free-run', a phenomenon observed when organisms are deprived of environmental cues that entrain the oscillator – as the period of the oscillator is not exactly 24 hours and can drift out of phase when deprived of synchronising cues. So, three features describe an oscillator: an environmental input pathway that is a zeitgeber; a pacemaker that uses the zeitgeber to synchronise circadian

rhythms; and an output pathway mediated by the pacemaker that modulates physiology, metabolism and behaviour accordingly. The behavioural rhythmicity of an animal is generally measured by examining periods of rest and activity, which are controlled by circadian pacemaker neurones in the brain. In addition to the central pacemaker neurones, many other peripheral tissues contain autonomous circadian oscillators (Plautz *et al.,* 1997). Outlined below are some of the molecular features of the oscillator and the organisation of the circadian system.

1.2.1 The molecular pacemaker of flies

An oscillator manifests as cycling of transcript and protein levels of circadian genes that interact in feedback loops and result in rhythmic output of the pacemaker (see Figure 1.2; Hardin, 2005; Glossop *et al.,* 1999; Glossop and Hardin, 2002; Cyran *et al.,* 2003). The interlocked-feedback loop model, originally shown by Glossop *et al.* (1999), was formed to illustrate the activation and repression of genes that drive rhythmicity. It consists of a negative loop (the *per*/*tim*/*cwo* loop) and a stabilising loop (the *vri*/*Pdp1ε* loop; Lee *et al.,* 1999; Blau and Young, 1999; Glossop *et al.,* 2003; Cyran *et al.,* 2003; Lim *et al.,* 2007; Matsumoto *et al.,* 2007; Richier *et al.,* 2008). Post-transcriptional and post-translational mechanisms operate on these loops to ensure that protein activity is tempero-spatially regulated. The core of the oscillator consists of seven proteins: three that act as transcriptional activators; three that act as repressors of transcription or protein function; and, one that has a context-dependent role. The transcriptional activators are CLOCK (CLK) and CYCLE (CYC) of the basic helix-loop-helix/ Per-Arnt-Sim (bHLH/PAS) domain transcription factor family, and PAR Domain Protein 1ε (PDP1ε), a PAR bZip transcription factor (Cyran *et al.,* 2003; Bae *et al.,* 1998; Benito *et al.,* 2007). The inhibitors are VRILLE (VRI), a bZip factor, TIMELESS (TIM) and the PAS domain protein PERIOD (PER) Glossop *et al.,* 2003; Cyran *et al.,* 2003; Lee *et al.,* 1999). CLOCKWORK ORANGE (CWO), a bHLH-Orange transcriptional repressor, has context-dependent roles (Lim *et al.,* 2007; Matsumoto *et al.,* 2007; Richier *et al.,* 2008). CWO appears to be a modulator

of the oscillator having a complex role that appears to have repression and activation elements that are also mediated via E-boxes. CYC is constitutively expressed (Bae *et al.*, 2000; Kilman and Allada, 2009), while *Clk* gene expression is rhythmic and CLK protein undergoes rhythmic phosphorylation/ de-phosphorylation (Kim *et al.*, 2002; Houl *et al.*, 2006; Houl *et al.*, 2008). The other five all show rhythmic mRNA and protein levels.

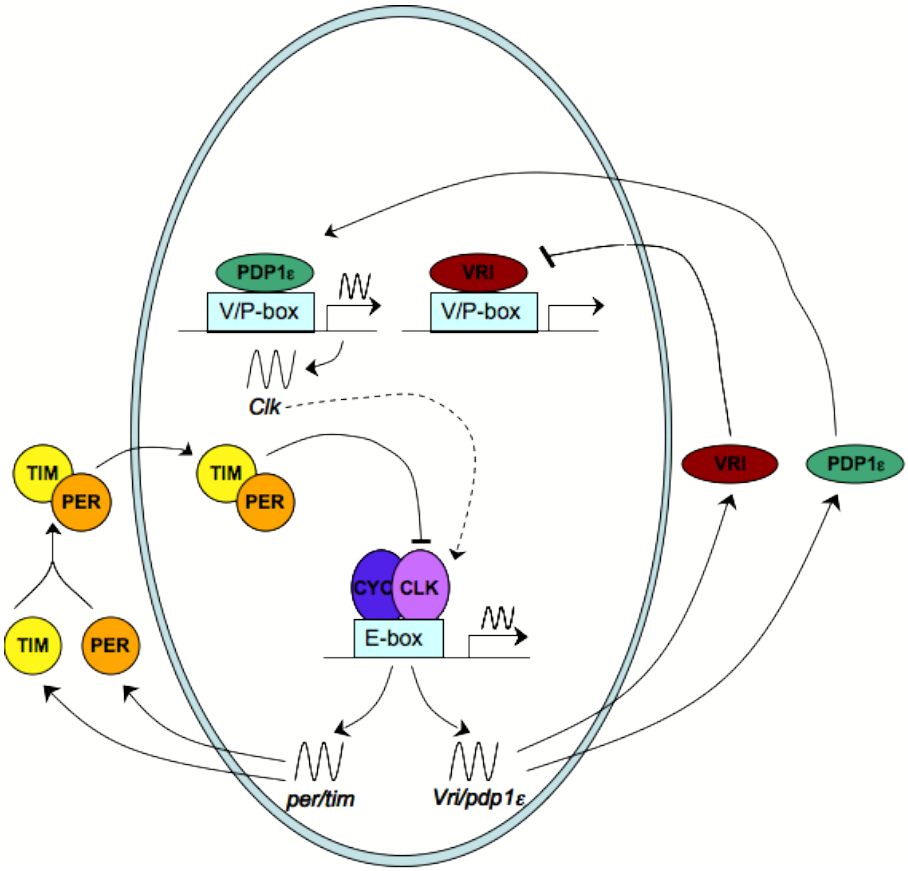

Figure 1.2 The core oscillator mechanism. The interlocked feedback loop model that generates rhythmic mRNA and protein levels, which in turn regulate rhythmic activity. CLK, CLOCK; CYC, CYCLE; VRI, VRILLE; PDP1ε, Par Domain Protein 1ε; TIM, TIMELESS; PER, PERIOD. Lines with a bar indicate inhibition/ repression; solid line arrows indicate activation; dashed line arrow indicates omitted process (of Clk mRNA export from nucleus, translation of CLK protein, dimerisation with CYC and re-entry into the nucleus to activate transcription); E-box, DNA sequence bound by CLK-CYC heterodimer; V/P-box, DNA sequence bound by VRI and PDP1ε; double line circle, nuclear envelope (Hardin, 2005).

CLK and CYC form heterodimers that bind to E-box regulatory elements to initiate transcription of *per*, *tim*, *cwo*, *Pdp1ε* and *vri* (and other clock-controlled genes) from the middle of the day into early night (see Figure 1.3;

reviewed in Hardin, 2005; Lim *et al.,* 2007; Richier *et al.,* 2008). Transcripts of *per, tim* and *cwo* accumulate to peak levels in the early night but post-translational mechanisms (kinase-driven phosphorylation and protein instability) delay accumulation of the proteins reaching peak levels late in the night. Following stabilisation of PER and TIM proteins, they feedback to regulate their own transcription by inhibiting the activity of CLK-CYC. This inhibition has not been fully resolved as yet but involves multiple components including inhibition by the binding of PER:PER and PER:TIM dimers directly to CLK-CYC and phosphorylation of CLK (Landskron *et al.,* 2009). The actions of CWO are also likely to contribute to the inhibition of CLK-CYC function. *In vitro* data suggest strong repression of E-box genes by CWO, an observation that is consistent *in vivo* with respect to auto-regulation – null mutants have elevated levels of *cwo* transcripts (Lim *et al.,* 2007; Matsumoto *et al.,* 2007; Richier *et al.*, 2008). Post-translational differences in CLK and PER phosphorylation are also seen in *cwo* null mutants. In addition, the transcript levels of other E-box genes, *per, tim*, *vri* and *pdp1*ε are reduced in the null mutant suggesting activation of these genes. It is possible, however, that some observations are the result of indirect effects.

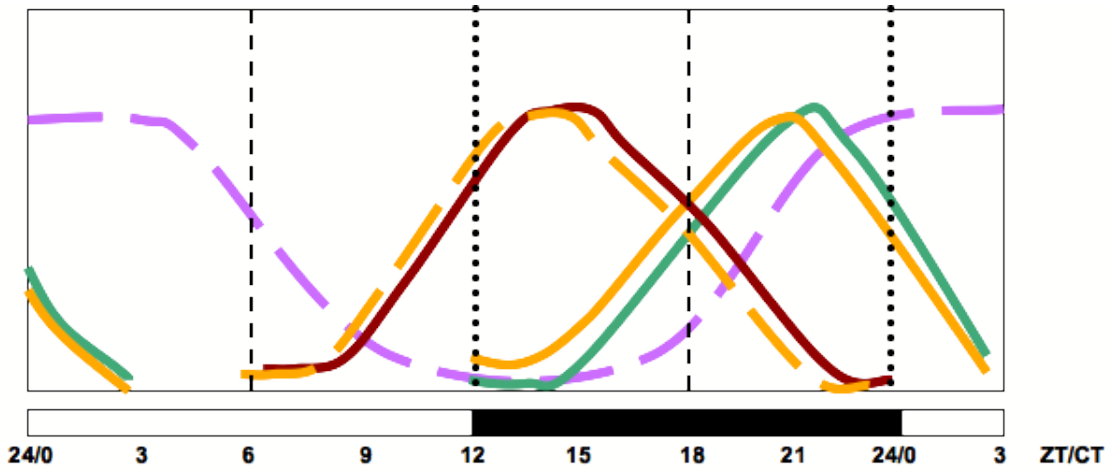

Figure 1.3 Protein and mRNA cycling over a 24 hour period. The relative levels of mRNA or protein at a given point over one light-dark cycle. Diagram is illustrative not quantitative. Purple dashed line, *Clk* mRNA; green solid line, PDP1ε protein; orange solid line, PER and TIM protein; orange dashed line, *per*, *tim* and *vri* mRNA levels; red solid line, VRI protein. Vertical lines on graph related to timeline shown below graph, time is in hours and black box indicates dark phase.

Translation of VRI protein is in phase with the accumulation of *vri* mRNA; the protein homodimerises, binds to VRI/PDP1ε box (V/P box) regulatory elements on the *Clk* gene and inhibits transcription of *Clk* (Glossop *et al.*, 2003; Hardin, 2005; Cyran *et al.*, 2003). *Clk* mRNA thus cycles in antiphase to CLK-CYC-driven, E-box regulated transcripts. PDP1ε accumulates with the same phase as PER and TIM though reasons for the lag between transcription and translation are not clear. PDP1ε recognises the same sites as VRI and is able to activate *Clk* transcription from the V/P box (Cyran *et al.*, 2003). Although PDP1ε can activate *Clk* expression, it is not required for rhythmic *Clk* expression, rather, it mediates rhythmic output locomotor activity (Benito *et al.*, 2007; Zheng *et al.*, 2009). PDP1ε is a conditional activator of *Clk* and is dependent on CLK-CYC itself for initial activation as observed by the lack of PDP1ε in the *Clk* and *cyc* mutants, Clk^{Jrk} and cyc^{01}. In addition, an isoform specific mutant of *Pdp1ε* exhibits arrhythmic behaviour and CLK protein levels are reduced but, crucially, present at low levels. Moreover, the mutant alleles Clk^{Jrk} and cyc^{01} produce non-functional proteins that are unable to mediate oscillator functions. Both mutants show constitutively high levels of *Clk* mRNA but low levels of the genes they activate (including *Pdp1ε*), which

indicates that *Clk* must also be activated by other factor/s (Cyran *et al.*, 2003). An analysis of *Clk* promoter and enhancer regions reveals heterogeneity in the regulation of *Clk* expression within subsets of oscillator neurones (Gummadova *et al.*, 2009). Gummadova *et al.*, (2009) examined various enhancer and promoter regions of *Clk* and identified subsets of the central brain oscillator neurones that are differentially controlled by these enhancers. These were designated as type-A and type-B. Type-A expression is mediated by a construct of the *Clk* promoter that lacks V/P boxes (see section 1.2.2 for information about neuronal subsets). Two interesting features to note about type-A expression are, (1) it is not mediated by PDP1ε and, (2) the neurones represented more closely resemble a subset that is expressed earlier in development. This suggests a subset of neurones in which *Clk* is activated by a different regulator or by PDP1ε either, indirectly or, via non-canonical binding sites. Type-B expression is observed in the remaining subsets of oscillator neurones, in addition to expression within the type-A subsets. The type-B enhancer is an extension of the type-A enhancer and contains one V/P box.

Recent data from Glossop *et al*. (unpublished results) indicate that TOY may regulate *Clk* expression. Several TOY/ EY binding sites were found in the *Clk* locus and over-expression of these proteins in a subset of the neurones (ventral lateral neurones, below) that drive locomotor behavioural rhythms shortens the period of behaviour – indicating an interaction with the oscillator. Furthermore, PRs and the central oscillator neurones also show endogenous *toy*/ TOY expression in wild-type adult brains (Glossop *et al.*, unpublished results), recently confirmed by Nagoshi *et al*. (2010). A preliminary study of whole head protein extracts show that TOY protein is modified over the 24hr period. In wild-type animals, however, this modification is dampened by a functioning oscillator mechanism. In the absence of the oscillator, it is hypothesised that feedback regulation to reduce the amount of modified TOY is removed (see Figure 1.4).

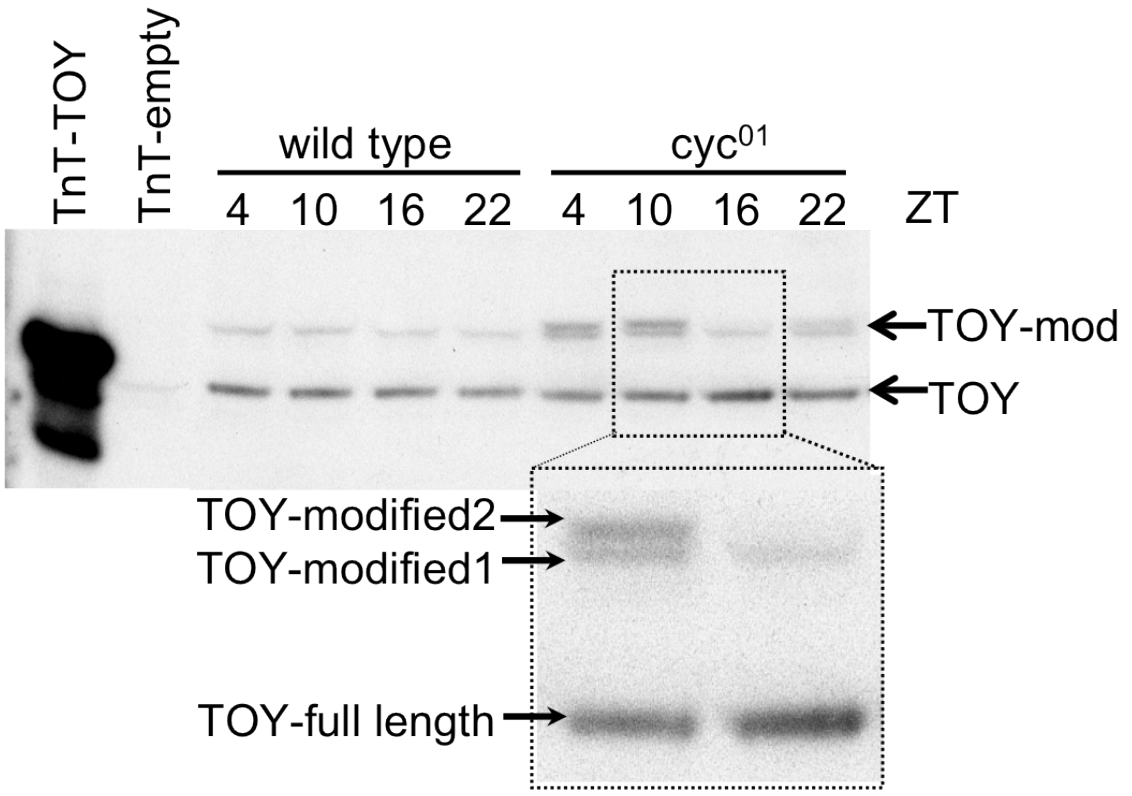

Figure 1.4 Western blot of TOY protein from wild-type and oscillator-deficient heads over a 24hr LD cycle, provided by Glossop (unpublished data). Heads from wild-type or *cyc*^{01} mutants were collected at ZT4, 10, 16 22 the proteins extracted and compared for TOY-immunoreactivity in a Western blot. *In vitro* synthesised TOY protein (TnT-TOY) and an unprimed negative control (TnT-empty) were used as a control for the TOY antiserum. In wild-type flies the modified TOY protein isoform is dampened whereas oscillator-deficient *cyc*^{01} mutants have elevated levels during the light phase. This suggests that in the presence of an intact oscillator mechanism, TOY protein levels are reduced during the light phase.

1.2.2 Organisation of the central brain circadian neurone network

The spatial distribution of oscillator cells in *Drosophila* is generally described as central and peripheral. The central components of the circadian system comprise seven neuronal clusters and glia in the central brain and optic lobes (Figure 1.5; Helfrich-Förster *et al.*, 2007; Hardin, 2005). The neuronal clusters may be placed in one of three categories, the lateral neurones – consisting of the dorsal lateral neurones (LNds), small ventral lateral neurones (s-LNvs) and large ventral lateral neurones (l-LNvs); the dorsal neurones – consisting of the

dorsal neurones (DN) 1s (DN1s), DN2s and DN3s; and the lateral posterior neurones (LPNs; Shafer *et al.,* 2006). Of these, the LNvs (and in particular the s-LNvs) regulate rhythmic locomotor output, as shown by arrhythmic locomotor behaviour when these neurones are electrically silenced or, ablated by pro-apoptotic gene expression (Nitabach *et al.,* 2002; Renn *et al.,* 1999; Stoleru *et al.,* 2004). The s-LNvs project to the ipsilateral accessory medulla area (aMe) and the dorsal protocerebrum in the vicinity of the DN2 and DN3 neurones and the Kenyon cells of the mushroom bodies, centres of olfactory learning (de Belle and Heisenberg, 1994; Helfrich-Förster *et al.,* 2007). The l-LNvs have been found to project mainly to the aMe and the medulla of the optic lobe ipsilaterally and contralaterally (via a ventral commisure). Helfrich-Förster *et al.* (2007) suggest that they mediate rhythmic signalling to the optic lobe, possibly to action cyclical sensitivity to visual perception and connect the aMe regions of the two hemispheres. The LNds project to the aMe and the dorsal protocerebrum, both ipsi- and contra-laterally (via a dorsal commisure) but input to their somata has not been deciphered. The DNs input to locomotor rhythm maintenance for crepuscular activity under light-dark conditions but not constant environmental conditions. Subsets of the DN1 and DN3 neurones project to the ipsilateral aMe, whereas DN2s do not. The remaining projections of the DN1-3 groups remain within the dorsal protocerebrum, of these DN1 and DN2 neurones cross to contralateral hemispheres via the dorsal commisure whereas the DN3 arborisations remain ipsilateral only. The LPN neurones express oscillator factors though their projection patterns remain elusive. It appears then that the aMe region is an organising centre receiving the input from several oscillator neurone classes and may be involved in the coordination of signals between these groups.

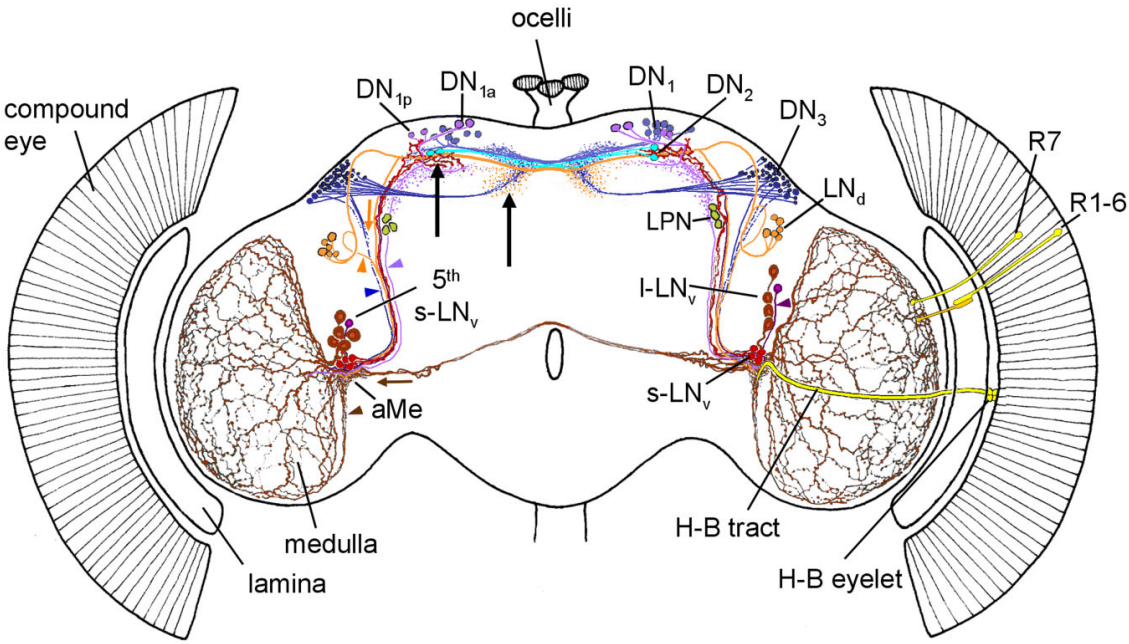

Figure 1.5 Central oscillator neurones. Figure from Helfrich-Förster *et al.* (2007), oscillator neurone groups of the central brain and their projections: aMe, accessory medulla; lateral neurons (LNd, l-LNv, s-LNvs and 5th s-LNv); dorsal neurons (DN1, DN2, DN3); lateral posterior neurones (LPN) R1-6, nuclei from photoreceptor cells 1 to 6; R7/8, nuclei from photoreceptor cells 7 and 8; H-B, Hofbauer-Buchner; H-B eyelet, extraretinal photoreceptor cluster; H-B tract, projection of H-B eyelet to the aMe.

The full context of projections is not, as yet, entirely clear due to resolution constraints, especially within the heavily innervated aMe and dorsal protocerebrum. What is apparent is that there appears to be cross-talk between the different clusters of oscillator neurones, this is postulated to be mediated largely by the neuropeptide pigment dispersing factor (PDF) secreted by the small and large LNvs (Peng *et al.*, 2003; Stoleru *et al.*, 2004; Im and Taghert, 2010). The PDF receptor, PDFR, a G-protein coupled receptor, is expressed in a large subset of the oscillator neurones, in the visual system and non-oscillator cells of the brain (Im and Taghert, 2010). Synchronicity between the oscillator neurones and the behavioural output rely heavily on this PDF signalling (Peng *et al.*, 2003; Stoleru *et al.*, 2004; Im and Taghert, 2010).

In the context of the *Clk* promoter analysis carried out by Gummadova *et al.*, (2009), the s- and l- LNvs, LNds, two DN1 neurones located anteriorly (DN1a)

and DN2 neurones exhibit type-A expression. Type-A expression is mediated by a promoter that lacks V/P boxes and, therefore, lacks binding sites for the only currently known activator of *Clk* – PDP1ε. A 122-base pair region is implicated primarily for the observed expression. The remaining oscillator neurones, posteriorly located DN1s (DN1p), DN3s and LPNs show type-B expression. The type-B promoter is an extension of the type-A region and all the oscillator neurones of type-A are also revealed by the type-B mediating promoter. The majority of cells of type-A expression develop during larval stages, namely the s-LNvs, DN1a and DN2 neurones; the remaining oscillator neurone subsets developing at later stages.

The locomotor activity patterns of *Drosophila* in a light-dark cycle show two peaks of activity, a morning and an evening peak that are controlled by subsets of the pacemaker neurones (Hardin, 2005). The LNvs and LNds are the controllers of locomotor activity with the LNvs mediating the morning activity peak and the LNds in control of the evening peak of activity (Stoleru *et al.*, 2004). The LNs have also been found to signal to the prothoracic gland to ensure that eclosion of adults from pupae occurs at dawn (Myers *et al.*, 2003).

The peripheral oscillators of *Drosophila* are found in several tissues, all are photoreceptive and are able to function autonomously (Plautz, 1997; Ivanchenko *et al.*, 2001; Tanoue *et al.*, 2004). Several sensory tissues have been shown to be oscillators, that is the photosensory compound eyes and ocelli; mechanosensors of the second antennal segment; and chemosensors of the third antennal segment, proboscis, maxillary palps, legs and wings. Rhythmic changes in membrane potential gate the responsiveness of the neurones and it has been suggested that such changes enable sensory neurones to have a dynamic range across which they can sample the environment, being most sensitive during periods when the stimulus is weakest (Mazzoni *et al.*, 2005; Nitabach *et al.*, 2005). Specific examples of circadian changes in peripheral organ function in *Drosophila* include: the observations by Tanoue *et al.* (2004) that the antennal neurones are both necessary and sufficient for maintaining olfactory response rhythms and are

truly autonomous as the rhythms persist despite ablation of LNvs. A circadian rhythm in visual sensitivity of larvae to maintain the photophobic response has also been documented (Mazzoni *et al.,* 2005). The larval photoreceptive organ, BO, connects directly to the LNs and together they form a circuit for light avoidance behaviour: BO transmits photic signals to the LNs and the LNs gate their sensitivity to this information to modulate the behavioural response over the course of the day. In addition, compound eye PR neurones show a 24hr rhythm in plasticity that is cell autonomous in order to maintain optimal perception and coding over the high amplitude changes in photic input over a 24hr period (Barth *et al.,* 2010).

1.3 Aims and outline

In the current study, I aim to investigate links between eye development and circadian oscillators. The molecular interactions are examined in order to learn more about the intricacies of both systems. I aim to reveal whether *eya* and *so* are primary targets of VRI during eye development. Immunohistochemistry, mis-expression of VRI and enhancer analysis in the developing eye disc, and *in vitro* techniques, are utilised to examine the influence of VRI on *eya* and *so* regulation in the eye disc. In addition, together with data from Glossop *et al*. (unpublished results), I hypothesise that molecular links between circadian and eye development factors enable tissue-specific circadian physiology in mature PRs. Furthermore, similar interactions may take place in the central oscillator neurones. Enhancer analysis, immunohistochemistry and *in situ* hybridisation are used to study expression in central brain and mature PRs.

Chapter 2 describes the protocols used in this study and results are shown in Chapters 3-5.

In Chapter 3, I examine the expression of VRI in developing eye discs in relation to developing PRs and EYA protein. VRI is highly expressed within zones I, II and PPN but down-regulated in the zones MF and IV, that is within

the PRs as they develop. Over-expression of VRI within the PRs results in cell-dependent phenotypes. These results suggest a role of attenuation rather than absolute regulation by VRI.

In vitro and *in vivo* studies of VRI binding sites within the *eya* and *so* genomic loci are described in Chapter 4. An *in vitro* binding assay shows that VRI binds potential regulatory sites within the *eya* and *so* loci at varying efficiencies. Crucially, two of the identified sites are located adjacent to a well-described *so* enhancer region. The most interesting finding here is that extension of the previously described enhancer of *so* appears to have epistatic effects on EYA expression, further reinforcing the close relationship of these two factors.

Chapter 5 shows preliminary data on the photo-dependent circadian regulation of *eya* and *so* transcripts within wild-type and oscillator-deficient adult brains and PRs. Circadian changes were observed in gene expression of the wild-type and oscillator-deficient genotypes, this may be a photo-response and, if so, suggest photoperiodic tracking as observed with vertebrate homologues of *eya* and *so*.

I conclude in Chapter 6 with a summary of all the results and discussion on the outlook and perspectives of this data on forging links between oscillator factors and tissue output.

Chapter 2 Materials and methods

2.1 Fly strains

Table 2.1 Fly strains. Genotypes of all fly strains used in the current study.

Type	Genotype	Other information
Wild type	*+; +; +*	Canton S strain
Wild type	*w; +; +*	standard reference wild type
Mutant	*w; +; Clk^{Jrk}*	non-functioning oscillator
Mutant	*w; +; cyc^{01}*	non-functioning oscillator
Transgenic	*w; GMR-Gal4/+; +*	*GMR-Gal4* driver
Transgenic	*w; +; UAS-vri-2b*	VRI responder
Transgenic	*w; +; UAS-vri-3*	VRI responder
Transgenic	*w; +; UAS-n-GFP*	GFP with nuclear localisation signal responder
Transgenic	*w; GMR-Gal4/+; UAS-n-GFP/+*	*GMR-Gal4* mediated nuclear GFP expression
Transgenic	*w; GMR-Gal4/+; UAS-vri-2b/+*	*GMR-Gal4* mediated VRI expression
Transgenic	*w; GMR-Gal4/+; UAS-vri-3/+*	*GMR-Gal4* mediated VRI expression
Transgenic	*w; GMR-Gal4/+; UAS-n-GFP/UAS-vri-2b*	*GMR-Gal4* mediated VRI and GFP expression
Transgenic	*w; GMR-Gal4/+; UAS-n-GFP/UAS-vri-3*	*GMR-Gal4* mediated VRI and GFP expression
Transgenic	*yw; +; so10-Gal4/+*	*so10* driver, courtesy of W. Gehring
Transgenic	*yw; +; so7-Gal4/+*	*so7* driver, courtesy of W. Gehring
Transgenic	*yw; so7+VP-Gal4[51C]/+; +*	*so7+VP* driver, produced for this study
Transgenic	*yw; so7+$VP^{[VP\text{-}mut]}$-Gal4[51C]/+; +*	*so7+$VP^{[VP\text{-}mut]}$* driver, produced for this study

2.2 In vitro protein synthesis

VRI protein was synthesised *in vitro* from pBSIIKS-*vri* (Glossop *et al.*, 2003) using a TnT T3 coupled rabbit reticulocyte lysate kit (Promega) that couples transcription and translation of a protein from a DNA template. Reactions were carried out according to kit guidelines as follows: 25μl lysate, 2μl TnT buffer, 1μl complete amino acid mix, 2μl RNasin (40 U/μl, Promega), 1μg cDNA plasmid, 1μl T3 RNA polymerase and made up to 50μl total reaction volume with ddH_2O; plasmid DNA was omitted for the un-primed negative control. Reactions were incubated at 30ºC for 90min.

2.3 Western blotting

Lysates were analysed on a western blot. 5μl of VRI or un-primed lysate (10%) samples or protein standards ladder (Bio-Rad) was mixed with 5μl ddH_2O and diluted 1:1 with 2x loading buffer (100mM Tris-Cl [pH 6.8], 4% SDS [v/v], 0.2% Bromophenol Blue [w/v], 20% glycerol [v/v], 200mM β-mercaptoethanol); incubated at 100ºC for 3min; centrifuged at 14000xg for 1min and placed on ice. 5% stacking gel (100mM Tris-Cl [pH 6.8] 0.1% SDS [v/v], 5% 29:1 acrylamide: bis-acrylamide [v/v] set with APS and TEMED) and 7.5% resolving gel (400mM Tris-Cl [pH 8.8], 0.1% SDS [v/v], 7.5% 29:1 acrylamide: bis-acrylamide [v/v] set with APS and TEMED) were used. Proteins were run in running buffer (25mM Tris, 190mM glycine) at 100V. Trans-Blot SD Semi-Dry Electrophoretic Transfer Cell (Bio-Rad) was used to transfer the proteins to Hybond-ECL nitrocellulose membrane (Amersham) in blot buffer (48mM Tris, 39mM glycine, 20% methanol [v/v], 0.0375% SDS [v/v]) at 20V for 1hr. For protein detection, the membrane was washed in TST buffer (140mM NaCl, 10mM Tris, 0.05% Tween 20 [v/v]); then, blocked in TBST buffer (5% skimmed milk powder [w/v], 5% thimerosol [v/v] in TST) for 1hr with agitation. Membrane was incubated overnight with agitation at 4ºC in guinea pig anti-VRI (GP-α-VRI), 1:2000 in TBST followed by several washes in TST. Membrane was then incubated with horseradish-peroxidase-conjugated goat anti-guinea pig

secondary antibody (Sigma-Aldrich), 1:1000 in TBST followed by several washes in TST. 1ml of ECL detection reagents A and B (GE Healthcare) were added to the membrane and agitated for 1min and autoradiographed to detect protein bands.

2.4 Immunohistochemistry (IHC) procedure

2.4.1 Protocol

Wandering L3 larvae CNS or 3-5 day old adult brains were dissected in phosphate buffered saline (PBS, 137mM NaCl, 2.7mM KCl, 10mM Na_2HPO_4, 1.8mM KH_2PO_4) and transferred to 4% paraformaldehyde (PFA [w/v]) in PBS. In the case of larvae, the CNS and attached discs were transferred; 5-6 larvae were dissected for *so* intron six enhancer analysis, in all other instances, 9-13 larvae were dissected. Males and females, 3-4 of each, were dissected for adult brains at each zeitgeber time (ZT), ZT3, 9, 15 and 21. Fixations proceeded for 20min followed by several washes with PBX (0.3% Triton X-100 [v/v] in PBS). Tissue was blocked in PXDN (0.3% sodium deoxycholate [v/v] and 5% normal donkey serum [v/v] in PBX) for 1hr, then incubated overnight with primary antibodies in PXDN at 4ºC. Samples were washed several times with PBX followed by secondary detection with fluorophore-conjugated antibodies in PXDN for 1-2hrs at room temperature in the dark. After several washes with PBX, samples were mounted in Mowiol 4-88 (Calbiochem) containing 2.5% diazabicyclo [2.2.2] octane (DABCO) [w/v] antifade reagent and stored at 4ºC in the dark.

2.4.2 Antibodies

Primary antibodies used were: GP-α-VRI (1:500, (Glossop *et al.*, 2003)); rat anti-ELAV (1:200); rabbit anti-PDP1 (1: 2500, (Reddy *et al.*, 2000)); mouse anti-EYA (1:10, eya10H6 by Benzer and Bonini from the Developmental Studies Hybridoma Bank); Guinea Pig 50 anti-CLK (CLK-GP50, 1:3000, (Houl *et al.*, 2008)).

For pre-absorption of antibody, *in vitro* synthesised VRI protein lysate, or unprimed control lysate (-ve) were mixed at 1:10 together with GP-α-VRI and incubated on ice for 15min prior to applying to tissue.

Secondary antibodies were all used at 1:200: donkey anti-guinea pig-Cy5; donkey anti-rat-FITC; donkey anti-rabbit-FITC; donkey anti-mouse-Cy3 (all from Jackson Immunoresearch from Stratech Scientific Limited, UK).

2.4.3 Confocal microscopy and image preparation

Images were collected on a Leica TCS SP5 AOBS upright confocal using a 63x/ 1.40 Plan Apo objective and confocal zoom was used. The following settings were always kept the same: pinhole – 1 airy unit; scan speed – 400Hz unidirectional; format 512 x 512. For GFP/ FITC detection, excitation (ex): 488nm, emission (em): 500-535nm; Cy3 detection, ex: 543nm, em: 556-610nm; Cy5 detection, ex: 633nm, em: 650-750nm; using the 488nm (20%), 594nm (100%) and 633nm (100%) laser lines, respectively. Individual channels were scanned sequentially and data is presented as single Z-sections or maximally projected stacks, refer to figure legend.

Basic functions included in the MBF ImageJ bundle were used for preparation and analysis of images.

2.5 Pharate adult preparation

2-4 day old pupae were collected, the pupal case was opened at the anterior and fixed in 4% PFA overnight. Fixed pharate adults were removed from the pupal case and imaged under PBS with a Leica MZ10 F microscope using a DFC 420C camera and processed with the Leica Application Suite, version 3.6.0, build 488.

2.6 Electrophoretic Mobility Shift Assays

2.6.1 Data mining

The consensus binding site for VRI has been previously described (Glossop *et al.*, 2003) using the optimal binding site of the bZip protein E4BP4/ NF-IL3A as a basis (Cowell *et al*, 1992): (G/A/T)T(T/G)A(T/C): GTAA(T/C). E4BP4/ NF-IL3A is the human homologue of VRI and shares 60% identity in 68 amino acids of the bZip domain, which translates to 93% similarity (George and Terracol, 1997). This similarity in identity in the bZip domain results in a similarity in consensus binding sites. There are some subtleties in binding site preference evident by the flanking and internal 'wobble' bases. For this reason, the core 8 bases of the consensus binding site, excluding bases -5 and +5, were used in data mining of genomic regions containing the *eya* and *so* loci (GenBank accession numbers, *eya*: AC092230 and AC011249; *so*: AC009739 and AC008258). Genomic and transcript sequences, obtained from FlyBase (Tweedie *et al.*, 2009), were aligned to demarcate the exon/ intron boundaries of genes by carrying out a transcript to genomic DNA alignment using the Spidey tool on NCBI. The core of the consensus sites was then mapped onto the genomic sequences.

Sites from each gene were selected for electrophoretic mobility shift assays (EMSA) to verify the ability of VRI to bind to these sequences. Sites that were non-consensus at bases -5 and/or +5 of the search site were included to determine whether VRI does recognise the selected sequences. Selected sites were also mutated to demonstrate specific sequence-dependent binding.

2.6.2 Probe preparation

The V/P box appearing in the *Clk* locus at -209 was previously shown to be recognised and bound well by VRI (Glossop *et al.*, 2003) and was therefore used as a positive control. Commercially synthesised (Sigma Aldrich, UK) sense

and corresponding anti-sense strands were used that contain the 10 bases of the VRI binding site flanked by 5 nucleotides on both, 5' and 3', ends (sense strands in Table 2.2).

Table 2.2 Oligonucleotides used for EMSA. Only the sense strand sequence is shown and given 5' to 3'. Consensus site is in uppercase, the core 8 bases used for data mining are italicised and mutated bases are underlined.

Name	Description	Sequence
C	*Clk*-209 (positive control)	attcaA*TTACATAA*Cctggc
e1	*eya* – upstream	cactgG*TTACATAA*Acagca
e2	*eya* – upstream	tagttA*TTACATAA*Cctcgc
e2M	mutated e2	tagttA*G*TACA*ATT*Actcgc
e3	*eya* – upstream	tctgtT*TTATGTAA*Acatgt
e4	*eya* – intronic	aaaaaT*TGATGTAA*Aacatt
e5	*eya* – intronic	tgcgaA*TTATGTAA*Aatttg
e5M	mutated e5	tgcga*TAATTGTAC*Aatttg
e6	*eya* – downstream	aataaT*TTACATCA*Aaaagc
s1	*so* – upstream	ttaatC*TTACATCA*Atcact
s2	*so* – upstream	ctgttA*TTATGTAA*Atttta
s3	*so* – intron 6	tttcgG*TTACATAA*Atatcc
s3M	mutated s3	tttcgG*G*TACA*ATT*Atatcc
s4	*so* – intron 6	tggggA*TTACATAA*Aagttg
s4M	mutated s4	tggggA*G*TACA*ATT*Aagttg

Clk-209 was labelled with digoxigenin (DIG) using the DIG Gel Shift Kit, 2nd Generation (Roche Applied Science) according to kit guidelines. Briefly, 2μM sense and anti-sense oligonucleotide strands were annealed in TEN buffer (10mM Tris, 1mM EDTA, 0.1M NaCl, [pH 8.0]) by heating to 95ºC for 10min and allowing to cool slowly to room temperature. Double-stranded probes are 3'-end labelled with DIG by terminal transferase in the presence of 0.05M DIG-ddUTP, 5mM $CoCl_2$ and labelling buffer (all reagents included in kit) at 37ºC for 15min; reaction was terminated by the addition of 2μl of 0.2M EDTA [pH 8.0] and volume increased to 25μl with ddH_2O.

Labelling was verified by spotting a dilution series of the reaction, together with a pre-labelled control included in the kit, onto positively charged Nylon membrane (Roche Applied Science) and UV cross-linked at 2000J. Membranes were washed in EMSA washing buffer (EWB, 0.1 M Maleic acid, 0.15 M NaCl, 0.3% (v/v) Tween 20; [pH 7.5]) and blocked for 30min in EMSA blocking buffer (EBB, 1% blocking reagent in EWB). Anti-digoxigenin conjugated with alkaline phosphatase (anti-DIG-AP) was added at 1:10000 in blocking buffer and the membrane incubated for 30min. The membrane was washed 2 x 15min with washing buffer and equilibrated in detection buffer (0.1 M Tris-HCl, 0.1 M NaCl; [pH 9.5]) for 5min. Membrane was incubated with chemiluminescent detection reagent CSPD at 1:100 in detection buffer in the dark for 5min at room temperature followed by 10min at 37ºC. Signal was detected by exposing photographic film (Kodak Biomax XR) to the membrane. Labelled probes were only used if labelling efficiency was equivalent or better than the pre-labelled control included in the kit, determined by qualitative comparison of the dilution series.

Labelled probes were used in a competition assay with sites selected from *eya* and *so* loci and compared to self-competition between labelled and unlabelled *Clk-209* probes. Individual sense and anti-sense strands of all unlabelled probes were used at 10μM, mixed and heated to 95ºC for 10min to denature and allowed to reach room temperature naturally to anneal.

2.6.3 Binding reaction

Reactions were carried out according to DIG Gel Shift Kit, 2nd Generation (Roche Applied Science) guidelines. 20μl reactions were prepared: 12.5% TnT reticulocyte lysate (VRI or control, [v/v]); binding buffer (10mM HEPES, 20mM KCl, 0.8mM EDTA, 0.4mM dithiothritiol (DTT), 4% glycerol); 1μg sheared salmon sperm DNA (Ambion Inc.); 1μl (0.156pmol) labelled probe and 1μl (10pmol) unlabelled competitor probe. Reactions were incubated at 30ºC for 20min, then run on 7% native polyacrylamide gels (0.5x Tris-borate-EDTA buffer [TBE, 1x is 90mM Tris-borate, 2μM EDTA], 7% 29:1 acrylamide: bis-

acrylamide set with APS and TEMED) in 0.5x TBE buffer at 100V for 1hr. A marker lane containing loading dye (0.25% Bromophenol Blue [v/v], 0.25% xylene cyanol [v/v], 4% glycerol [v/v]) was run alongside as an approximation of the position of the free, unbound probe. Probes were transferred from the gel onto positively charged nylon membrane using Trans-Blot SD Semi-Dry Electrophoretic Transfer Cell (Bio-Rad) in 0.5x TBE for 1hr at 20V followed by cross-linking at 2000J. Membrane was washed with EWB, blocked for 30min in EBB and incubated with anti-DIG-AP 1:10000 in EBB for 30min. Following washes, membrane was equilibrated in detection buffer for 5min, incubated for 5min at room temperature with CSPD 1:100 in detection buffer in the dark and further developed for 10min at 37ºC. Signal was detected by exposing the membrane to photographic film.

2.7 Production of transgenic animals

2.7.1 General methods for cloning

XL1-Blue (Stratagene) competent cells were used for all cloning steps and grown on agar plates or medium based on standard lysogeny broth (LB, 1% NaCl [w/v], 1% tryptone [w/v], 0.5% yeast extract [w/v]) with the selective antibiotic, 75μg/ml carbenicillin (an ampicillin analogue, Sigma Aldrich), when necessary. Heat shock transformation was used as standard and bacteria were grown at 37ºC as standard when used for cloning of the heat shock promoter or Gal4 in isolation. For all steps involving cloning of the enhancer from intron 6 of *so*, *so7+VP*, and any modifications or additions to this region, bacteria were grown at 30ºC for 20-24hrs. Sequences were examined using 4peaks (Mekentosj) or FinchTV (Geospiza) abi trace viewers and verified using BCM Search Launcher and ClustalW online software tools. Verified sequences were stored and processed in Microsoft Word or ApE plasmid software, ApE was also used to produce the plasmid map shown in Figure 2.1.

Plasmid purification from bacterial colonies was done with standard phenol, choloroform, isoamly alcohol, 25:24:1 (P:C:IAA) extraction or using Qiagen plasmid purification kits according to kit guidelines. Identity and orientation of cloned sequences was initially analysed by multiple restriction digests (restriction enzymes from New England Biolabs or Roche Applied Science), followed by sequence verification using Big Dye v3.1 Terminator kit (Applied Biosystems) and processed by the in-house DNA sequencing facility at the Faculty of Life Sciences. *so7+VP* contained some minor differences to those published for the *so* locus (GenBank accession numbers: AC009739 and AC008258), these were considered to be polymorphisms so were not mutated to the published sequence. None of the VRI, EY, TOY or SO sites were affected by the polymorphisms. No mutations were found in the attB site, hsp70 basal promoter or Gal4 coding region.

2.7.2 Amplification of so7+VP

Genomic DNA was extracted from wild type Canton S flies to use as the DNA template for amplifying 3947bp of intron 6 of *so*. 25 flies were homogenized on dry ice in solution A (0.1M Tris-HCl, [pH 9.0], 0.1M EDTA, 1% SDS [v/v]) and incubated at 70ºC for 30min. 8M KAc was gently mixed into the homogenate, incubated on ice for 30min and the homogenate centrifuged for 15min at 13000xg to remove chitinous solid matter. DNA suspended in the supernatant was extracted by 2x phenol: chloroform: isoamyl alcohol (P:C:IAA, 25:24:1, Sigma Aldrich) extractions according to standard methods, precipitated with isopropanol and resuspended in Tris-HCl EDTA (TE, 10mM Trish-HCl, 1mM EDTA, [pH 7.5]) buffer.

This purified genomic DNA was used as the template for amplification of the region of interest using PCR with the following primers (5'-3'): sense - atataa***TCTAGA***GCATTCTGGCATTCTGGGACTTTCG; anti-sense - aaaaa***ACCGGT***GAATTCCTGATCTTAGTAGCCATTC (lower case are extra bases for restriction digestion of the PCR fragment prior to cloning, bold and italicised are restriction sites for XbaI and AgeI, respectively). Phusion High-

Fidelity PCR kit (Finnzymes, distributed by Thermo Fisher Scientific) was used for amplification according to guidelines, cycling conditions are given in Table 2.3 (Eppendorf Thermocycler used for PCRs). 50ng genomic DNA was mixed with HF buffer, 200μM each dNTP, 0.5μM forward and reverse primers and 1U Phusion DNA polymerase.

Table 2.3 PCR settings for amplification of *so7+VP* from genomic DNA.

Step	Time (mm:ss)	Temp. (°C.)
1	00:30	98
2	00:10	98
3	00:30	65.3
4	02:00	72
5	Go to step 2 x5	
6	00:10	98
7	02:30	72
8	Go to step 6 x30	
9	10:00	72
10	END	

PCR product size and quality was checked on a 1.2% agarose gel in Tris-acetate-EDTA (TAE, 40mM Tris-acetate, 1mM EDTA, [pH 8.5]) buffer. The correct product was excised from the gel and purified using the Qiagen gel extraction kit according to kit guidelines. Phusion DNA polymerase produces blunt-ended products, A-tails were added to the PCR product by incubation with ThermoPol buffer (New England Biolabs), 300μM dATP (Bio-Rad), 2.5U Taq DNA polymerase (New England Biolabs) for 10min at 72°C. The product was purified using the Qiagen PCR purification kit according to kit guidelines and TA-cloned into pGEM-T Easy (pGEM-TE) plasmid vector (Promega) at a 1:3 vector:PCR product ratio with T4 DNA ligase (New England Biolabs) at 16°C overnight.

2.7.3 Amplification of basal promoter

A basal heat-shock promoter, hsp70, was amplified from pCaSpeR-hs (GenBank accession number U59056) using (5'-3'): sense - aaaa***ACCGGT***GAGCGCCGGAGTATAAATAG; anti-sense - ataa***GGATCC***TATTCAGAGTTCTCTTCTTGTATTC (lower case are extra bases for restriction digestion of the PCR fragment prior to cloning, bold and italicised are restriction sites for AgeI and BamHI, respectively) (Pelham and Bienz, 1982; McGarry and Lindquist, 1985). Similarly to the intron region, Taq DNA polymerase (New England Biolabs) was used for amplification followed by purification and TA-cloning into pGEM-TE vector (Promega), cycling conditions are described in Table 2.4.

Table 2.4 PCR settings for amplification of basal promoter of heat shock promoter hsp70 from pCaSpeR-hs.

Step	Time (mm:ss)	Temp. (°C.)
1	02:00	94
2	00:30	94
3	00:15	51.6
4	00:45	72
5	Go to step 2 x5	
6	00:30	94
7	00:15	61.8
8	00:45	72
9	Go to step 6 x24	
10	05:00	72
11	END	

2.7.4 Engineering of transgenic construct so7+VP

The multiple cloning site of pBSIIKS (GenBank accession number X52329) was modified for sub-cloning of enhancer and transgenes, restriction sites in the following order were used: XbaI, AgeI, BamHI and NotI, referred to as pBS-M. pBS-M and pGEM-TE-*so7+VP* were digested with XbaI (Roche Applied Science)

and AgeI (New England Biolabs) and ligated with T4 DNA ligase, to generate pBS-M-*so7+VP*. pBS-M-*so7+VP* and pGEM-TE-hsp70 were both digested with AgeI and BamHI (New England Biolabs) and ligated to make pBS-M-*so7+VP*+hsp70. pBS-M-*so7+VP*+hsp70 and pGaTB were digested with BamHI and NotI (Roche Applied Science) to excise Gal4 coding region (Brand and Perrimon, 1993) and ligated to make pBS-M-*so7+VP*+hsp70+Gal4. The driver transgene *so7+VP*+hsp70+Gal4 was excised using XbaI and ligated into pattB which contains the attB site for ϕC31 integrase-mediated site-directed insertion into genomic attB sites (Bischof *et al*., 2007).

2.7.5 Engineering of transgenic construct so7+VP[VP-mut]

VRI binding sites in the *so7+VP* transgenic construct, s3 and s4, were mutated to the same sequences that eliminated VRI binding in EMSA to make the *so7+VP[VP-mut]* construct. This was done sequentially using QuikChange Lightning Site Directed Mutagenesis kit (Stratagene) according to kit guidelines with some minor modifications: 150ng template DNA (plasmid) and 10μM primers were used. More extensive changes were made than suggested within the guidelines as previous reports have suggested the mutagenesis protocol can be successful under less stringent conditions than single base changes (Geiser *et al*., 2001). Primers used for mutagenesis were, site s3: gcatctagagcattctggcattctgggac**tttcgG*G*TACA*ATT*Atatcc**gattaatgac ctcaggttgaaagg. Site s4, gtaaacctcaaagtgctgaaaagact**tggggA*G*TACA*ATT*Aagttg**gattgccatcggc gggggggcctgggg. For both, direction is 5'-3'; only sense sequence is given; EMSA oligonucleotide primer is in bold, VRI binding site is uppercase, mutated bases are underlined and italicised. Cycling conditions are described in Table 2.5 and the final construct map shown in Figure 2.1.

Table 2.5 PCR settings for mutagenesis of sites s3 and s4 in *so7+VP* using QuikChange Lightning site directed mutagenesis.

Step	Time (mm:ss)	Temp. (°C.)
1	01:00	95
2	01:00	95
3	02:00	52
4	06:00	68
5	Go to step 2 x5	
6	01:00	94
7	02:00	58
8	06:00	68
9	Go to step 6 x13	
10	10:00	68
11	END	

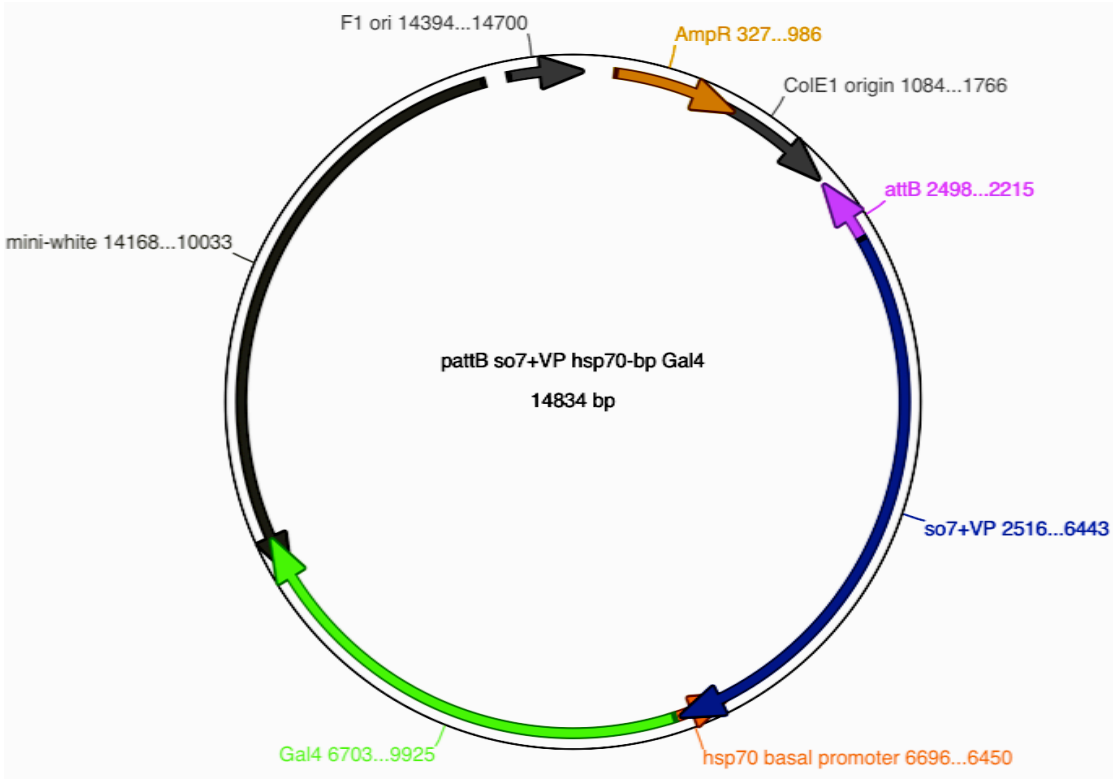

Figure 2.1 Map of final construct. Final construct showing the relative position of *so7+VP*, hsp70 basal promoter and Gal4 coding region in relation to transgenic (attB site, mini-white gene) and plasmid (ampicillin resistance, F1 and ColE1 origin gene) features.

2.7.6 Transgenesis

Site-directed transgenesis (Bischof *et al.*, 2007) at landing site 51C was used for production of transgenic animals. Integrase transposase enzyme ϕC31 is transgenically expressed within germline cells and mediates insertion of attB sequence (and adjacent DNA) within donor attP sites such that both sites are then eliminated. The attP cassette in this case is located within a single specific region of the genome (chromosome 2L, 51C) and plasmid pattB contains the transgene synthesised here and the mini-*white* gene for selection of successful transgene insertion. Sequence verified pattB plasmids containing either, *so7+VP* or *so7+VP*$^{[VP\text{-}mut]}$, followed by hsp70 basal promoter and Gal4 coding region, were sent to Best Gene Inc. (Chino Hills, California, U.S.A.) – a company dedicated for *Drosophila* embryo injection for transformation with transgenic constructs. Flies with eye colour (mediated by the mini-*white* gene for selection of successful insertions into the genome) were, thus, generated externally and the chromosome containing the transgenic integrase transposase was negatively selected.

2.8 In situ hybridisation

2.8.1 Probe synthesis

DIG-labelled mRNA probes were prepared for *in situ* hybridisation according to guidelines for the DIG-UTP RNA labelling mix. Briefly, single cutter restriction enzymes (New England Biolabs or Roche Applied Science) were used to linearise 10μg of plasmid DNA and, after verification of digestion, purified according to standard P:C:IAA protocols. DIG-UTP RNA labelling mix (Roche Applied Science) containing 10mM ATP, CTP, GTP (each), 6.5mM UTP and 3.5mM DIG-11-UTP was used for the synthesis of DIG labelled probes by Sp6 (for anti-sense) or T7 (for sense) RNA polymerase (Promega) to yield full length mRNA probes. A 3' UTR-specific probe for *so* was also tested but found

to be insufficient. BDGP DGC full length cDNA clones were used, *eya* – GH05272 (GenBank Accession number, AY047539); *so* – GH15741 (GenBank Accession number, AY060309). Template DNA was denatured at 55°C for 2min and transferred to ice prior to addition of 2µl NTP mix, 4µl 5x transcription buffer, 1µl RNasin (40U/µl), 1µl 100mM DTT, ddH2O to 18µl and 2µl RNA polymerase. The transcription reaction proceeded for 1hr at 37°C. Following transcription, the DNA template was eliminated using 2µl of DNase (RQ1, RNase-free; Promega) at 37°C for a further 30min and 2.5µl of 0.5M EDTA was added to end the DNase reaction. Probes were precipitated by incubation at -20°C overnight with 0.1x volume 4M LiCl and 3x volume 100% ethanol, followed by centrifugation at 4°C at 15000xg for 15min; and alcohol precipitated as standard. The RNA pellet was re-suspended in 99µl ddH_2O and 1µl RNasin was added before aliquoting and storage at -80°C. Probe concentration was determined prior to use for each aliquot (NanoVue, GE Lifesciences)

2.8.2 Preparation of tissue sections on slides

Male and female 3-5 day old adults of wild-type (*w; +; +*) and cyc^{01} mutants raised at 25ºC in a 12:12 L:D cycle were collected at ZT2, 6, 10, 14, 18 and 22. Light exposure to flies collected during the dark phase was minimised, flies were decapitated and immersed in TissueTek O.C.T. (Sakura) cryosectioning media prior to being set on dry ice. Heads were sectioned on an RNaseZap (Ambion Inc.) treated Leica CM3050S Cryostat, chamber temperature -20ºC, object temperature -18ºC and collected on Polysine coated slides (VWR International). Sections were 18µm thick and arranged such that two ZT collections of each genotype were on the same slide. Sections were dried at room temperature overnight.

2.8.3 Hybridisation and detection

Protocol is based on that described by Schaeren-Wiemers and Gerfin-Moser (1993) and adapted by Vosshall *et al.*, (1999). Tissue was fixed with 4% PFA for 10min, washed with PBS and acetylated for 10min in 1% triethanolamine solution containing 1:400 acetic anhydride. Pre-hybridisation was carried out at room temperature with hybridisation buffer to cover sections (50% formamide, 5x SSC [150mM NaCl, 15mM sodium citrate, pH adjusted to 7.0 with HCl], 5x Denhardts [Fisher Scientific; 1% Ficoll 400, 1% polyvinylpyrrolidone, 1% bovine serum albumin], 500µg/ml salmon sperm DNA [Ambion Inc.], 30µg/ml heparin [Sigma], 2.5mM EDTA, 0.1% Tween-20 and 0.25% CHAPS). Coverslips (Hybrislips, Sigma Aldrich) were gently placed on top of the slides to prevent dehydration and the chamber humidified with 5x SSC, sealed with parafilm to prevent evaporation, and incubated at 60°C for > 1hr. Probes, 200ng per ml in hybridisation buffer, were denatured prior to use and incubated at 60ºC for 16-24hr in a 5x SSC humidified chamber. Several post-hybridisation washes were carried out, firstly at 72ºC with 5x SSC, then with 0.2x SSC with a final wash with 0.2x SSC at room temperature.

For detection of probes, slides were washed with maleic acid buffer (0.1M maleic acid, 0.15M NaCl, 0.1% Triton X-100 [pH 7.5]) and blocked with maleic acid blocking buffer (0.1% blocking reagent [Roche Applied Science] in maleic acid buffer) for 1hr at room temperature. Anti-DIG- alkaline phosphatase (anti-DIG-AP; Roche Applied Science) was added 1:5000 in maleic acid blocking buffer and incubated at room temperature for 1hr. Following maleic acid buffer washes, and equilibration in detection buffer (100mM Tris-HCl, 100mM NaCl, 5mM $MgCl_2$, 0.1% Tween20, [pH 9.5]), NBT/ BCIP (18.75 µg/µl NBT, 9.4 µg/µl in 67% DMSO BCIP (v/v); Roche Applied Science) was applied and the slides allowed to develop overnight in a humidified chamber at room temperature in the dark. Chromogenic detection time was optimised to be overnight as 30min and 2hr colour development was insufficient. The reaction was stopped by immersion in ddH_2O and slides mounted in Mowiol 4-88 (Calbiochem) containing 2.5% DABCO [w/v] antifade reagent and stored at 4ºC in the dark. 3DHistech Panoramic Slide Scanner was used to collect images.

Chapter 3 Eye disc analysis

3.1 Introduction

3.1.1 Development and differentiation of photoreceptors

Differentiation of PRs commences during the third and final instar of larval development (L3). The eye disc is a valuable and extensively employed model system for the study of many processes that are reiterated throughout development – determination of tissue identity, patterning, axis and compartment specification, cell proliferation and apoptosis as well as fate specification and polarity. Retinal determination is dependent on highly co-ordinated convergence of several transcription factors and signal transduction pathways. The overall functional output of this convergence is seen as sequential development of ordered arrays of cells that form the adult eye units, the ommatidia. Cell fate is serially refined and this is observed as changes in the complement of transcription factors and signalling pathways operating within the cells. According to the progression of cells towards their final fate, they are categorised as a part of developmental stage zones within the eye disc (see Figure 1.1). Each zone has a different total complement of factors that pattern development and the relationships between them are dynamic within and between zones according to the entire profile of factors present. Thus, it is possible to observe a variety of different functions of retinal patterning factors at different positions within the developing eye disc. These dynamic functions are determined by the presence or absence of whole host of other patterning factors.

3.1.2 EYA and SO expression within the eye disc

Two factors, EYA and SO, that pattern the retina show position-dependent changes in function and are frequently mentioned with reference to one another as they form a heterodimeric transcriptional complex and their expression completely overlaps one another. Within the complex, SO has the DNA binding domain and EYA has a nuclear translocation signal and transactivation potential for gene regulation. Expression of *eya* and *so* genes is positively regulated by upstream factors EY and TOY just ahead of the MF, in the PPN zone, but negatively regulated in zone II cells ahead of the PPN zone despite the presence of the positive regulators (see Figure 1.1). Therefore, additional factors, or additional roles of currently known factors, must be contributing to the observed expression pattern. The transcription factor TSH is suggested to repress *eya* expression within zone II but promote expression within the PPN through its interactions with either HTH and EY (zone II) or EY alone (PPN).

3.1.3 VRI is proposed as a candidate eye development factor

VRI is a core factor of the molecular circadian oscillator mechanism in which it represses expression of the gene *Clk*. It is also an essential factor during several stages of development, though the precise role of VRI during development is yet to be determined. Expression of VRI in the developing eye disc was first documented by George and Terracol (1997). Szuplewski *et al.* (2003) further explored the eye disc function by disrupting the normal pattern of VRI expression in the eye disc and observed developmental phenotypes. These consisted of reduction of cell and eye size by creation of mosaic mutant cells or disruptions to pattern formation of the eye when VRI was over-expressed in the eye disc from embryonic stages. However, direct targets for VRI regulation during eye development were not determined. Some of the observed phenotypes are similar to those observed for established RDGN factors (Szuplewski *et al.*, 2003; Cheyette *et al.*, 1994; Bonini *et al.*, 1993)

and initial indications from oscillator cells are that that RDGN and oscillator factors may interact (Gummadova *et al.*, 2009 and Glossop *et al.*, unpublished results). I investigate here the spatio-temporal relationship between VRI and that of *eya* and *so* in the L3 eye disc.

It is important to note that in parallel to the results described here, *eya* and *so* genomic loci were examined for VRI binding sites. The preliminary analysis revealed several potential V/P boxes and advised the pursuit of determining the relationship between VRI/PDP1 and *eya*/*so* and are described within this chapter. The binding site analyses are elaborated in Chapter 4.

By co-labelling discs, I describe here that VRI is expressed in zones I, II and PPN and down-regulated within the MF. In addition, I have determined that VRI expression at this time is not dependent on *Clk* or *cyc* and that no PDP1 isoform is present in the L3 eye disc indicating VRI interactions within the eye disc are different to those described within the oscillator mechanism. By mis-expression of VRI in developed PRs, I have tried to determine whether VRI is a direct regulator of *eya*. It appears that a relationship between VRI and EYA is not binary but, rather, the data suggest that VRI may attenuate *eya* expression. It is unfortunate that SO antibody was not available to describe the relationship between VRI and *so* expression here. I also show here that mis-expression of VRI in the MF and zone IV leads to pupal lethality.

3.2 Results

3.2.1 VRI is down-regulated within the MF

I wanted to firstly to describe the region of VRI expression in the wild type eye disc in relation to the developing PRs. It was also of interest to determine whether CLK-CYC, the circadian oscillator activators of VRI (Blau and Young, 1999), also regulate *vri* expression during eye development by investigating L3 eye discs of Clk^{Jrk} and cyc^{01} mutants. Two groups of samples were prepared

and immuno-stained with GP-α-VRI. For the experiment, GP-α-VRI was pre-absorbed with unprimed TnT rabbit reticulocyte lysate while the negative control was pre-absorbed with TnT lysate primed to make VRI protein. Loss of immunoreactivity (IR) in the control would confirm VRI-positive signal observed in the experimental. Both lysates were first probed with GP-α-VRI on a western blot, two bands were revealed only in the *vri*-primed lysate as described previously (Figure 3.1; Glossop *et al.*, 2003).

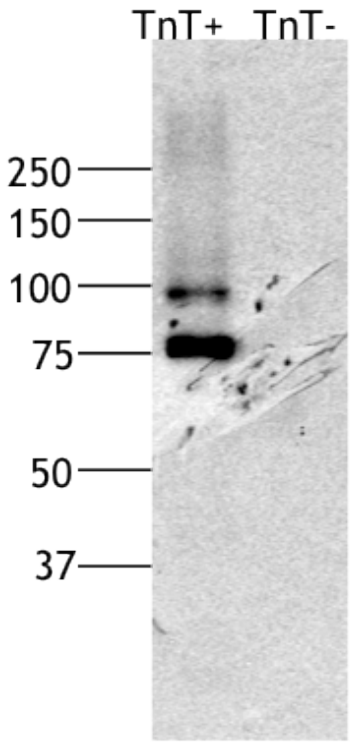

Figure 3.1 Western blot to show reactivity of unprimed and *vri*-primed lysate with GP-α-VRI. Rabbit reticulocyte lysate *in vitro* transcription/ translation system either, primed with a plasmid containing the *vri* coding region (TnT+), or, unprimed negative control (TnT-). Migration of protein standards is shown on the left of the image.

All eye disc images are oriented as shown in the schematic in Figure 1.1A. Figure 3.2 shows VRI immuno-labelling in an eye disc co-labelled for the pan-neuronal marker ELAV. The primary antibody mix was pre-absorbed with unprimed TnT lysate. VRI-IR is present in the anterior eye disc up to the MF in the PR epithelium (Figure 3.2A) and, at a reduced level, in a few rows of cells just posterior to the MF (close-up image shown in Figure 3.2B).

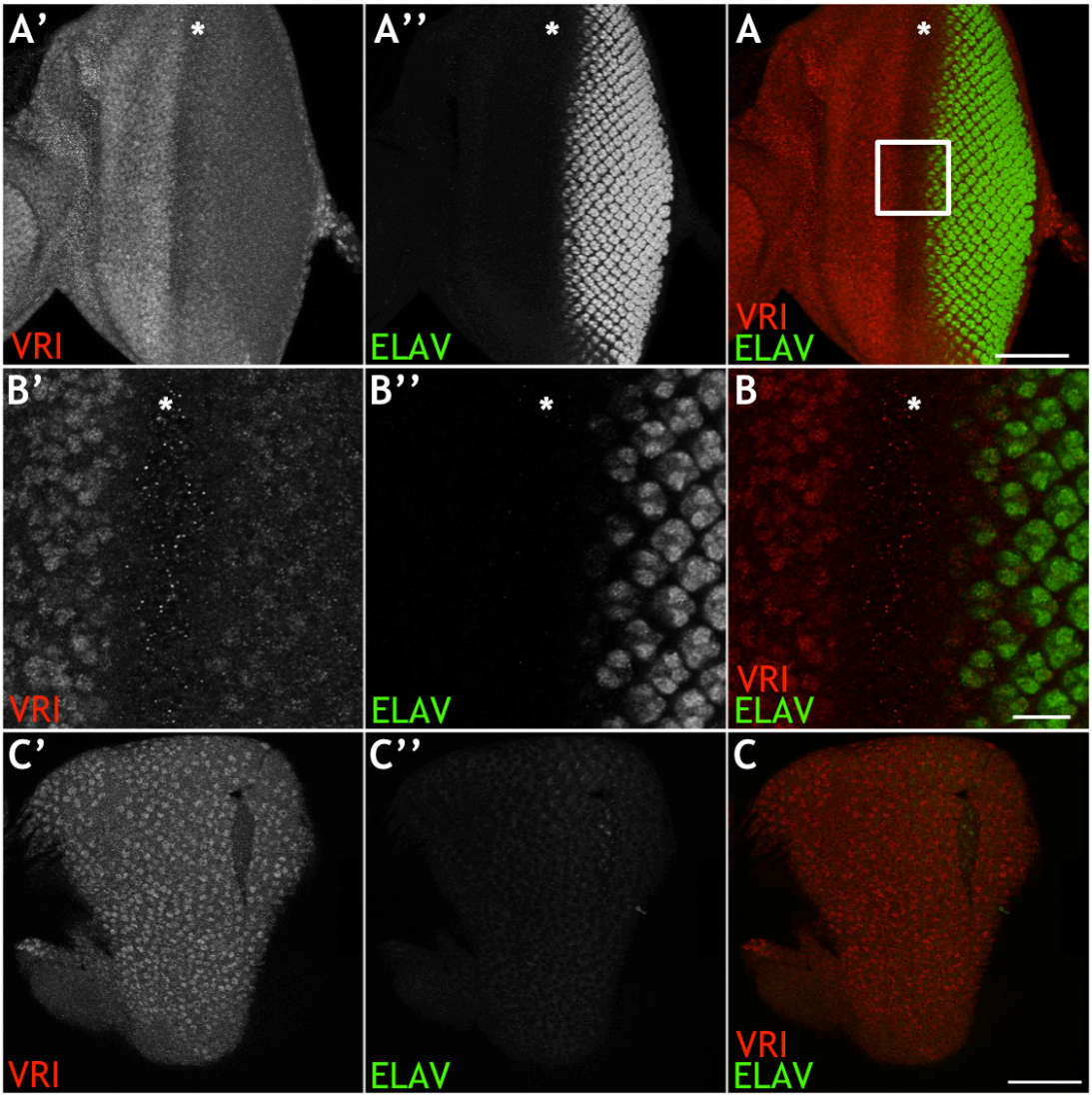

Figure 3.2 VRI is expressed in the anterior eye disc and the PE. *w;+;+* L3 eye disc, (A) VRI-ELAV merged image, flattened Z-sections through the photoreceptor epithelium; (B) VRI-ELAV merged image, single Z-section spanning the MF (white box in (A)); (C) VRI-ELAV merged image, flattened Z-sections through the PE; (A', B', C') VRI-IR (red on merged image); (A'', B'', C'') ELAV-IR (green on merged image) marks post-mitotic PRs. Key: anterior to the left; asterisk marks MF (A) scale bar = 50μm, (B) scale bar = 10μm, (C) scale bar = 50μm; minimum *n*=9.

Figure 3.2C shows the peripodial epithelium (PE) of the eye disc that forms cuticle, VRI-IR is strong within the large nuclei of the PE. Cells of the PE and the antennal disc (not shown) also express the *eya* and *so* activators EY (PE and antennal disc) and TOY (PE) but not EYA and SO (Czerny *et al.*, 1999; Halder *et al.*, 1995; Pappu and Mardon, 2002; Pignoni *et al.*, 1997; Bonini *et al.*, 1993; Bonini *et al.*, 1997; Punzo *et al.*, 2002;). This suggests that another

mechanism is necessary to prevent EYA and SO expression in those cells; be that in the form of a repressor in these tissues, or, that additional activators to EY and TOY are required in the PR epithelium. VRI expression is observed throughout the eye-antennal disc in L3 and appears only to be down-regulated ahead of the MF and hence, in the PRs as they differentiate.

Pre-absorption of GP-α-VRI with lysate primed to generate full-length VRI protein reduces the regional expression observed in the anterior of the disc, though a faint background signal is still evident (Figure 3.3A).

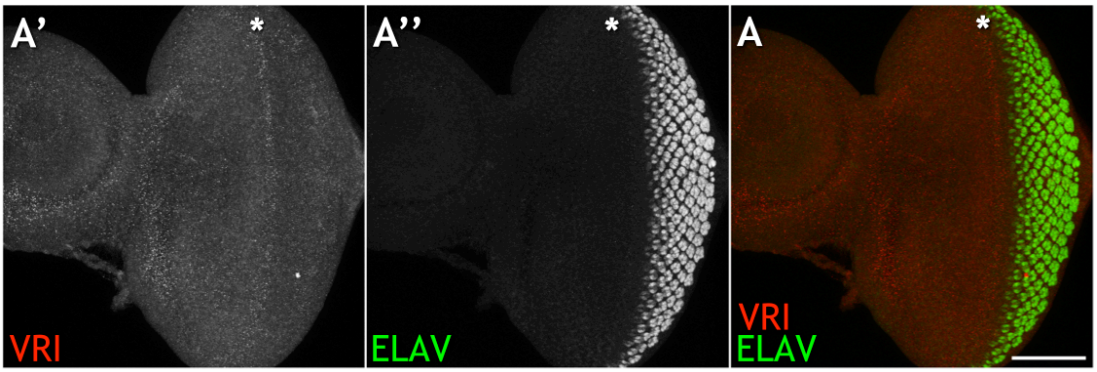

Figure 3.3 Pre-absorption of the primary antibody mix with *in vitro* synthesised VRI strongly reduces VRI-IR in the eye disc. *w*;+;+ L3 eye disc, flattened z-sections through entire disc, (A') faint background staining (red on merged image, right), (A'') ELAV-IR in PRs unaffected (green on merged image, right). Anterior to the left; asterisk marks MF; scale bar in = 50μm; minimum *n*=9.

VRI-IR is detected in Clk^{Jrk} and cyc^{01} mutants in the same spatial pattern as *w*;+;+ wild-type eye discs (Figure 3.4A and 3.4B, respectively) indicating that, in the context of the eye disc, *vri* expression is driven independently of CLK-CYC. Currently, the only known regulators of VRI are the CLK-CYC heterodimer (Blau and Young, 1999), this result implies that developmental activation of *vri* occurs via a CLK-CYC independent pathway.

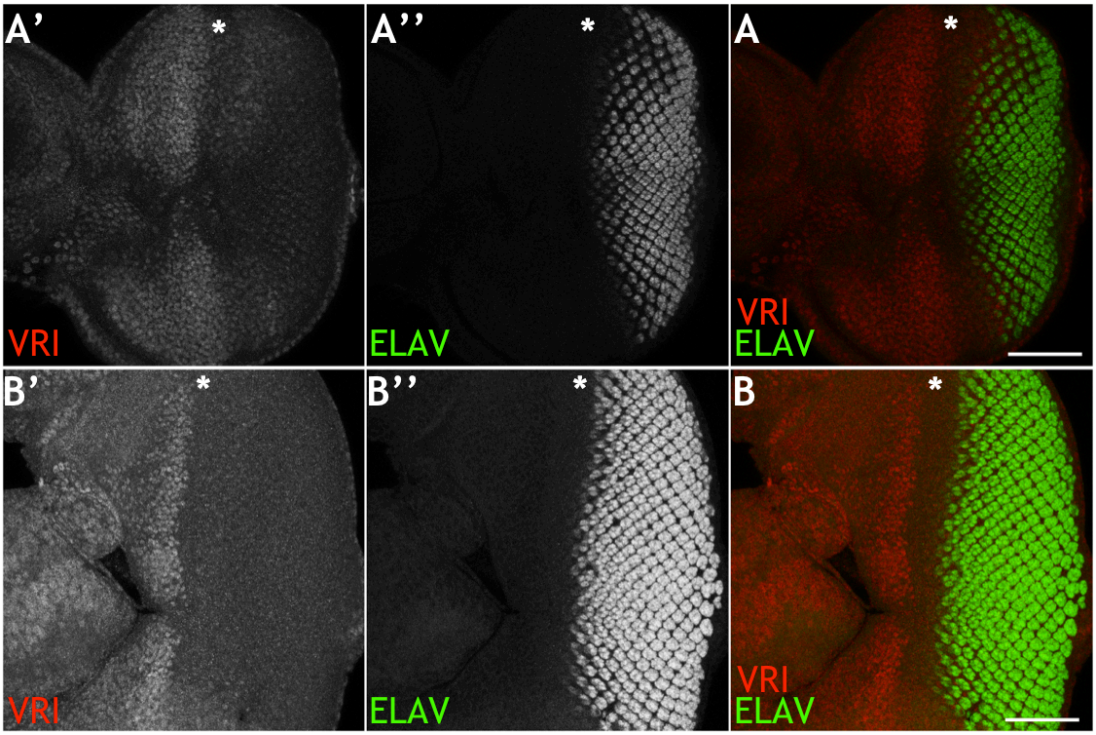

Figure 3.4 VRI-IR in the L3 eye disc appears wild-type in *Clk*^{Jrk} and *cyc*^{01} mutants. (A) *Clk*^{Jrk} eye disc VRI-ELAV merged image, flattened z-sections through the photoreceptor epithelium; (B) *cyc*^{01} eye disc VRI-ELAV merged image, flattened z-sections through the photoreceptor epithelium. (A', B') VRI-IR (red on merged image, right) in the anterior eye disc; (A'', B'') ELAV-IR (green on merged image, right) marks post-mitotic PRs. Key: anterior to the left; asterisk marks MF; scale bar = 50μm; minimum *n*=9.

Expression of *vri*, as revealed by VRI-IR, within the eye disc is dynamic and appears to be related to the progression of the MF. As the MF advances into anterior regions, VRI is down-regulated. This was best observed in discs from larvae of differing ages (by a matter of hours but still mid-L3 stage) and suggests that a reduction in VRI protein may be a cause or effect of furrow advancement and differentiation of PRs (Figure 3.5).

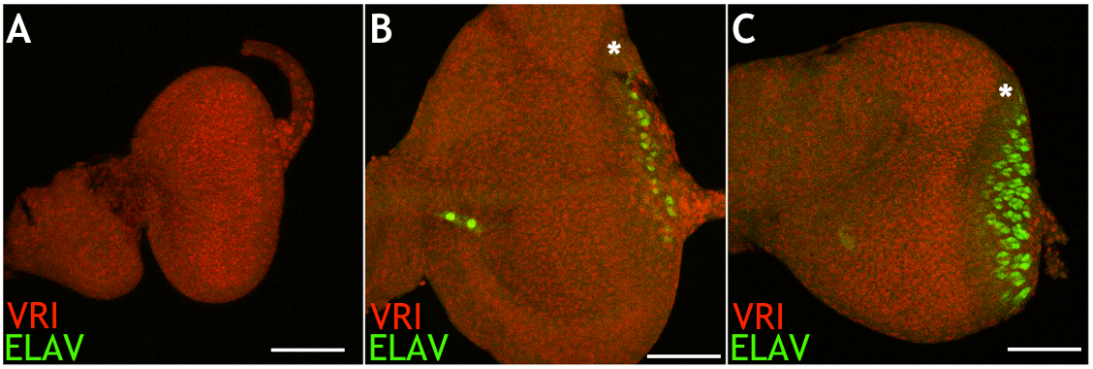

Figure 3.5 VRI is down-regulated ahead of the MF. Eye discs from L3 larvae at different stages of development, defined by the number of ELAV-positive PRs present. (A) youngest disc – no PRs present VRI-IR (red) throughout disc; (B) older than (A) – 1 row of PRs, VRI-IR down-regulated at the margin of the MF and some residual expression seen in photoreceptors; (C) older than (B) – 3 rows of PRs, VRI-IR further down-regulated as MF advances; ELAV-IR (green) marks differentiated PRs. Key: anterior to the left; asterisk marks MF; scale bar = 50μm; minimum *n*=9.

3.2.2 No PDP1 isoform is expressed in the L3 eye disc

As PDP1ε (activator) and VRI (repressor) have opposing roles in the regulation of *Clk* in the molecular oscillator mechanism (Cyran *et al.*, 2003), and V/P boxes are present in *eya* and *so* loci (Chapter 4), it was possible that PDP1ε may regulate *eya* and *so* expression during PR development. To determine if any of the PDP1 isoforms regulate PR development, I also checked for PDP1-IR in wild-type L3 eye discs. A triple immuno-labelling protocol was used and discs were stained for PDP1, VRI and EYA. A signal from the secondary fluorophore-conjugated antibody used for PDP1 labelling was apparent but signal distribution did not suggest cellular expression (Figure 3.6A, A'''). Examining this signal through the XZ and YZ planes confirmed that the signal was from secondary antibody accumulation within the lumen of the discs (Figure 3.6B, C). VRI and EYA signals were regional as described in this study (VRI) and in the literature (EYA; Bonini *et al.*, 1993) and overlap anterior to the MF within the PPN zone and in the ocelli precursors.

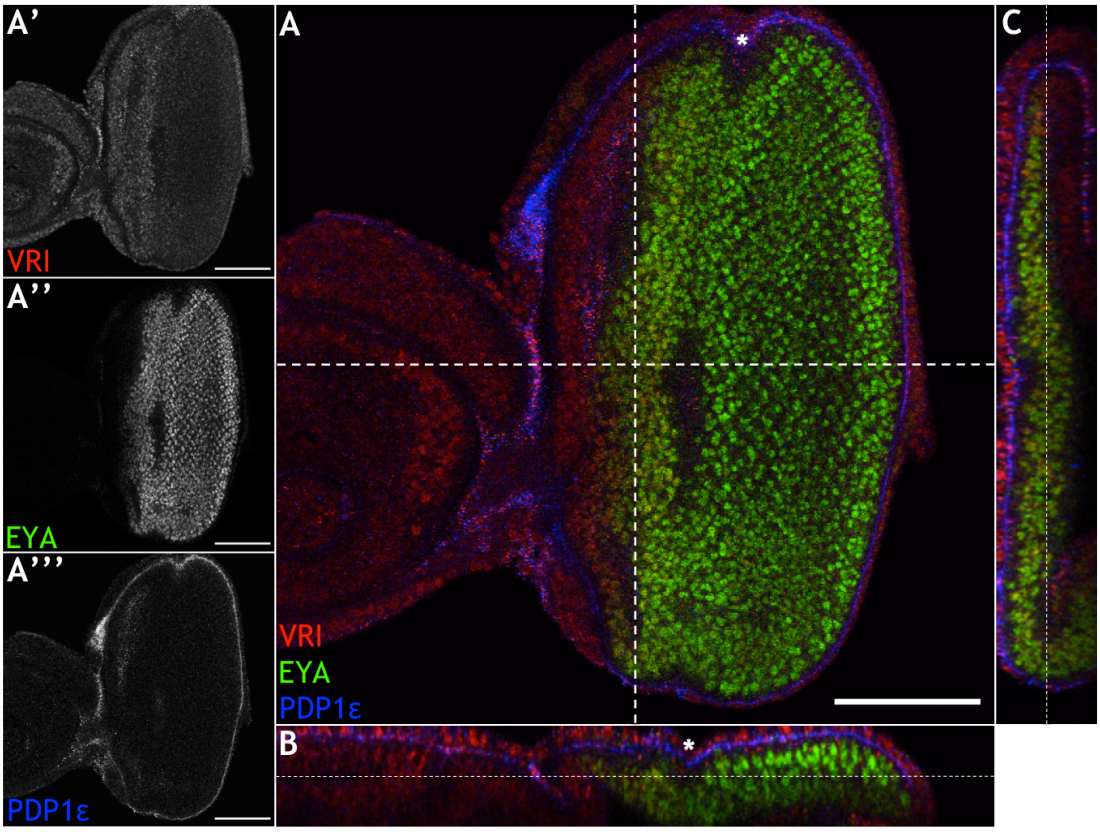

Figure 3.6 Orthogonal views of disc labelled for PDP1, VRI and EYA. (A) Single Z-section from *w*;+;+ eye disc XY plane; (A', A'', A''') VRI, EYA, PDP1, respectively, single channels in grayscale shown merged in (A). (B) single Y-section of XZ plane, apical to the top; (C) single X-section of YZ plane, apical to the left; (B & C) processed by Image J> Image> Stacks> Orthogonal views function. VRI (red) and EYA (green) labelling seen in nuclei whereas PDP1 (blue) signal is undefined and can be seen in the lumen of the disc between the peripodial and photoreceptor epithelial layers. Key: anterior to the left; asterisk marks MF; scale bar = 50μm; minimum *n*=9.

3.2.3 *VRI and EYA are expressed in partially overlapping regions in the L3 eye disc*

EYA has been described as being expressed throughout the differentiated photoreceptors and ahead of the furrow but not completely overlapping with the activators EY or TOY (Halder *et al.*, 1998). To explore whether VRI could be repressing *eya* and *so* expression to prevent the observed lack of co-expression with their activators EY and TOY, I initially immuno-labelled discs to see the expression of VRI and EYA in relation to one another. SO anti-serum is scarce and was unavailable to me therefore co-labelling of VRI and SO was

not carried out but EYA and SO have been reported to be expressed in the same cells of the developing eye disc (Pignoni *et al.*, 1997). Co-labelling of L3 eye discs for VRI and EYA reveals overlap in the distribution of the two proteins. Overlapping expression was observed in a few rows of cells anterior to the MF – PPN zone and in some cells of the ocellar region (Figure 3.6, Figure 3.7). Within the region anterior to the furrow and in the ocelli precursors, strong IR for both proteins was seen.

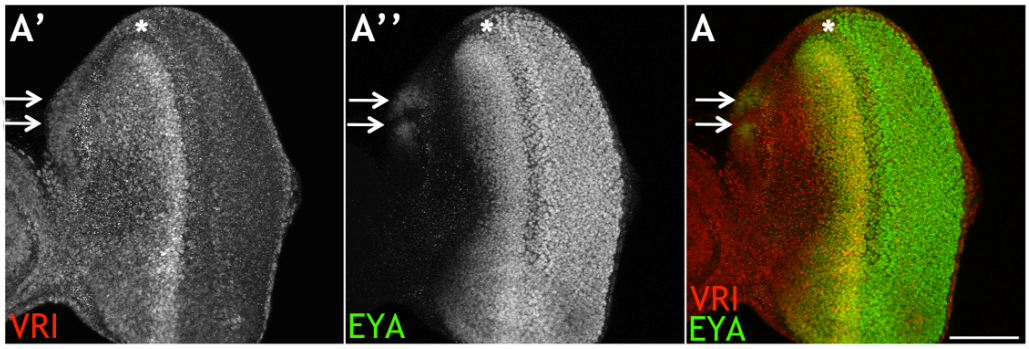

Figure 3.7 VRI- and EYA- IR in regions of the eye disc. (A) Flattened Z-sections through photoreceptor region of a CS L3 eye disc; (A', A'') VRI-IR, EYA-IR, respectively, single channels in grayscale shown merged in (A). Key: anterior to the left; dorsal is top; asterisks mark MF; arrows point to ocellar region; scale bar in = 50μm; minimum *n*=9.

3.2.4 Mis-expression of VRI in the photoreceptor epithelium

3.2.4.1 Eye disc phenotypes

Overlap in VRI and EYA expression suggests either, that VRI does not affect *eya* expression, or, that VRI may modulate *eya* expression but that multi-factorial rather than binary interactions are taking place within this tissue. I decided to over-express VRI in cells after it is normally down-regulated, specifically, cells posterior to the MF, to see whether this would disrupt *eya* expression in the eye disc. The GMR-Gal4 driver (Freeman, 1996; Ellis *et al.*, 1993) was used to mis-express VRI in cells within and posterior to the MF. The GMR (glass multimer reporter) driver consists of a pentameric repeat of a 29-bp region of an enhancer of the rhodopsin 1 gene (*rh1/ ninaE*; Ellis *et al.*, 1993; Moses and Rubin, 1991) bound by the GLASS transcription factor. In

developing eye discs, GLASS is expressed within the MF and all cells posterior to the MF. As EYA is also expressed in cells within and posterior to the MF, ectopic expression of VRI in these cells will indicate whether VRI can repress the expression of *eya*.

Two different UAS-*vri* transgenes (different insertions) were mis-expressed either, alone, or, in combination with UAS-nuclear-GFP (UAS-nGFP – GFP with nuclear translocation signal sequences) using GMR-Gal4. GFP was used to identify cells in which the driver was functional and the presence or absence of GFP did not appear to affect the over-expression of VRI. Figures 3.8-10 show representative eye discs in which GMR-Gal4 drives expression of UAS-nGFP alone (Figure 3.8), or, together with UAS-*vri-2b* (Figure 3.9) or UAS-*vri-3* (Figure 3.10). Single Z-sections of the disc are shown as individual channels for VRI, EYA and GFP (Figures 3.8-10, A', A'', A''', respectively) together with the merged image in Figures 3.8-10 A. Merged images of all pair-wise combinations of channels are also shown for comparison between the figures, Figures 3.8-10 B', B'', B'''. Although both transgenes are strongly induced by GMR-Gal4, expression from the UAS-*vri-3* insert is somewhat stronger than UAS-*vri-2b*.

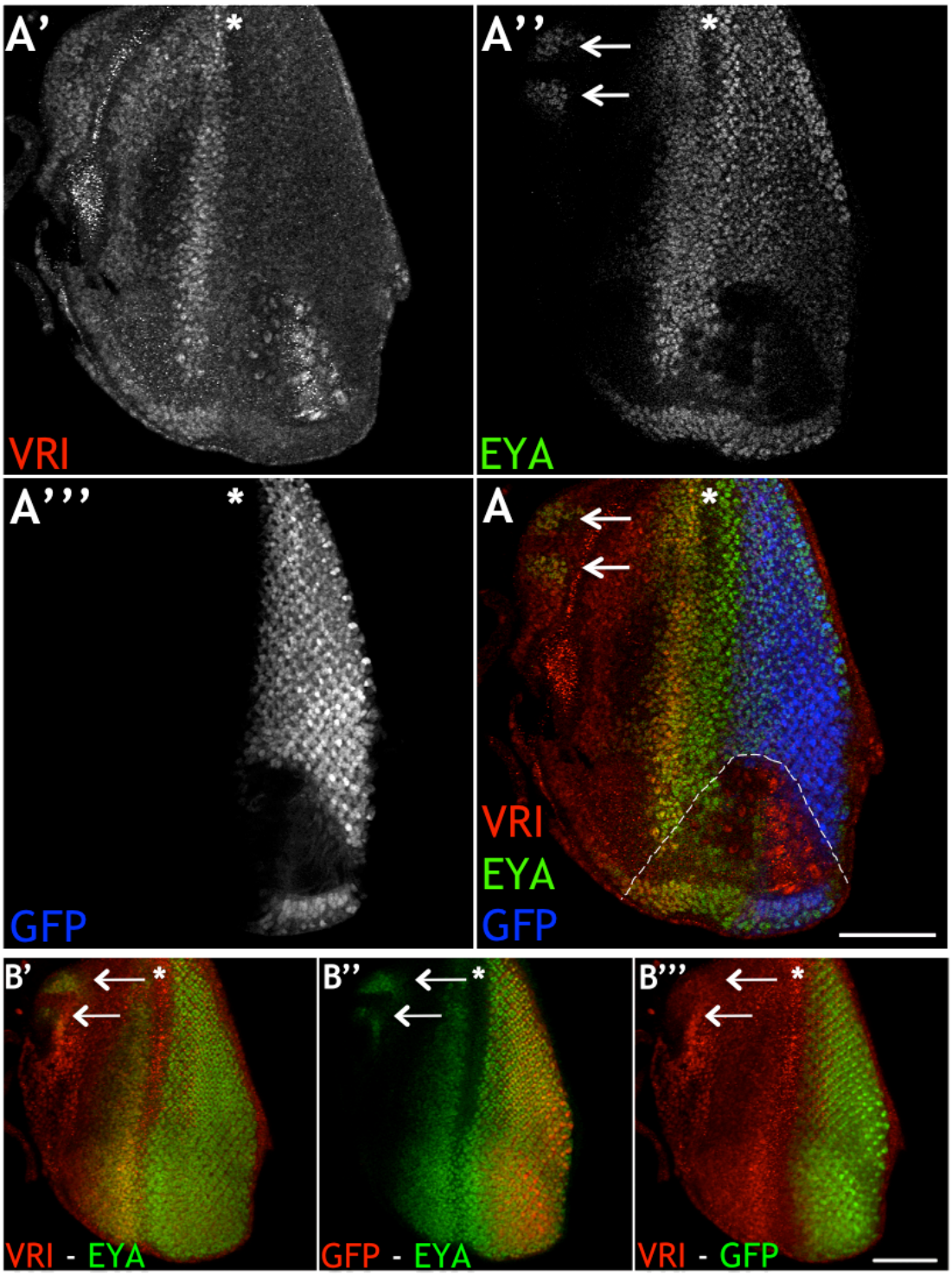

Figure 3.8 Activity of GMR-Gal4 highlighted by expression of UAS-nGFP transgene. (A) Single Z-section of disc immuno-labelled for VRI (A', red in A) and EYA (A'', green in A) with GFP expression (A''', blue in A) in cells in which GMR-Gal4 is active. (B', B'', B''') two channel merge images of individual channels shown in A'-A''', VRI-IR, red and EYA-IR, green (B'); EYA-IR, green and GFP, red(B''); VRI-IR, red and GFP, green (B'''). Key: anterior to the left; asterisk marks MF; arrows point to ocellar region; dotted line on (A) indicates edge of disc folded over; scale bar = 50μm; minimum *n*=9.

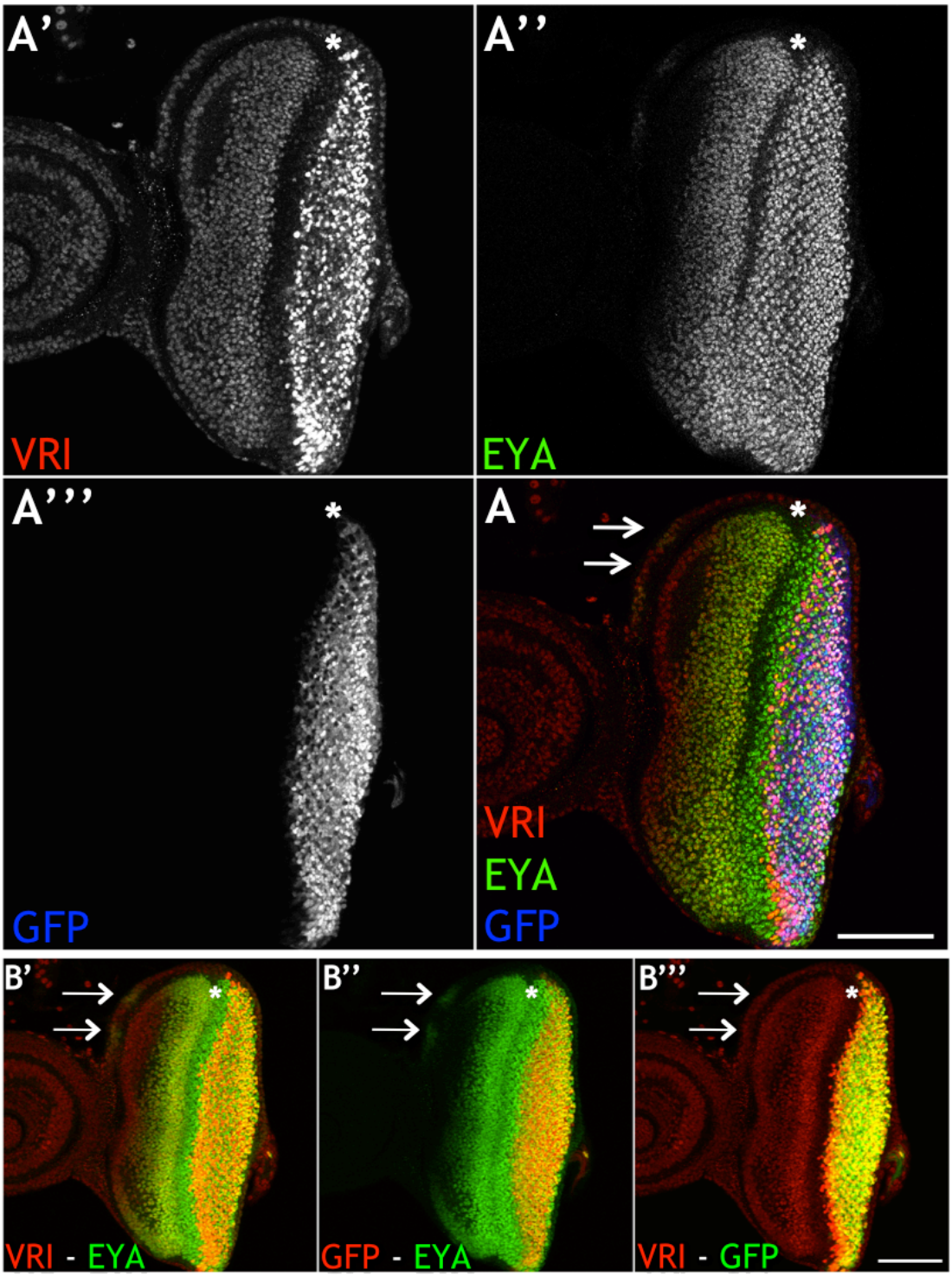

Figure 3.9 GMR-Gal4 driven expression of UAS-*vri-2b*. (A) Single Z-section of disc immuno-labelled for VRI (A', red in A) and EYA (A'', green in A) with GFP expression (A''', blue in A) in cells in which GMR-Gal4 is active. (B', B'', B''') two channel merge images of individual channels shown in A'-A''', VRI-IR, red and EYA-IR, green (B'); EYA-IR, green and GFP, red(B''); VRI-IR, red and GFP, green (B'''). Key: anterior to the left; asterisk marks MF; arrows point to ocellar region; scale bar = 50μm; minimum *n*=9.

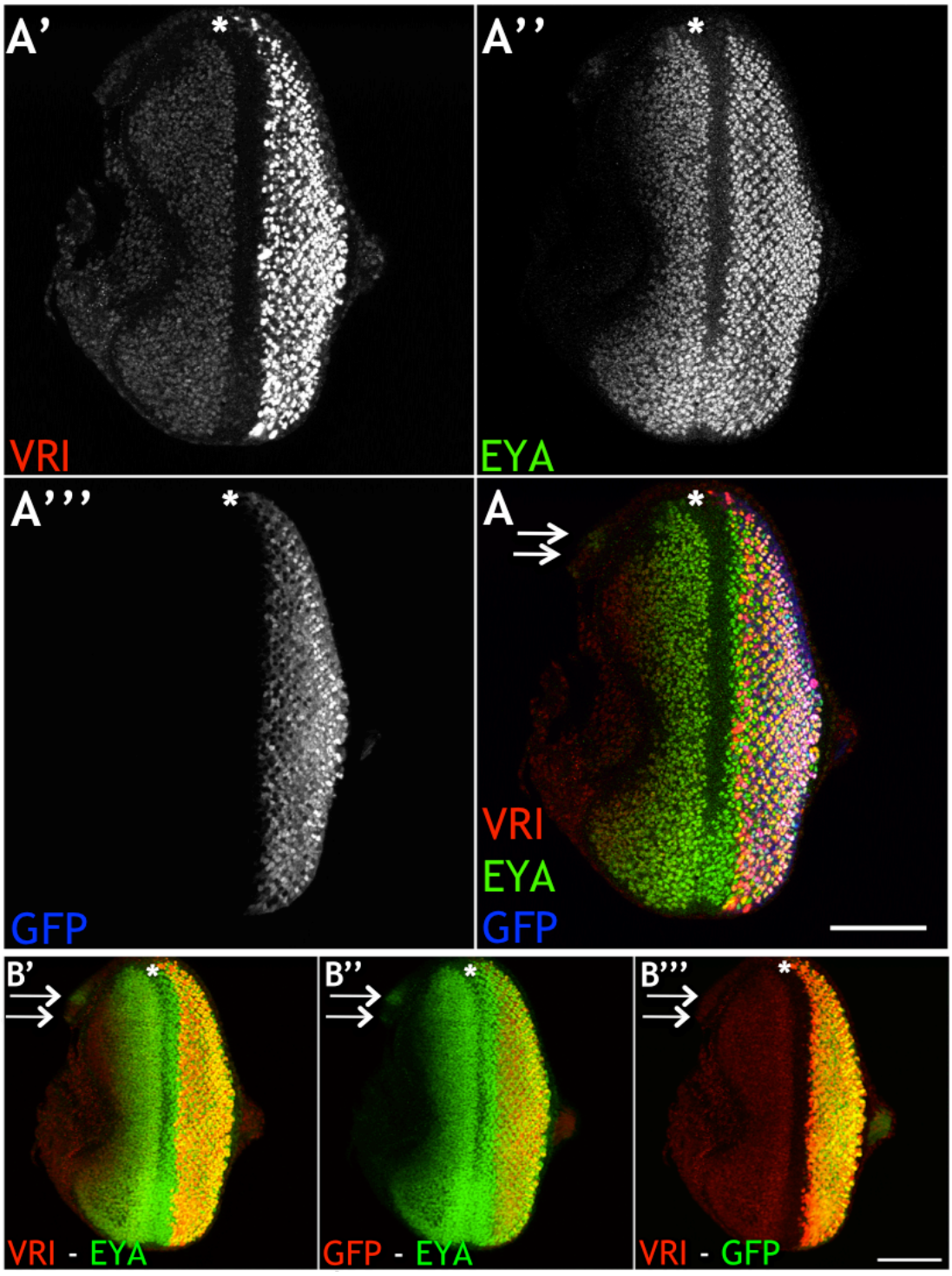

Figure 3.10 GMR-Gal4 driven expression of UAS-*vri-3*. (A) Single Z-section of disc immuno-labelled for VRI (A', red in A) and EYA (A'', green in A) with GFP expression (A''', blue in A) in cells in which GMR-Gal4 is active. (B', B'', B''') two channel merge images of individual channels shown in A'-A''', VRI-IR, red and EYA-IR, green (B'); EYA-IR, green and GFP, red(B''); VRI-IR, red and GFP, green (B'''). Key: anterior to the left; asterisk marks MF; arrows point to ocellar region; scale bar = 50μm; minimum *n*=9.

Although expressed at a high level within the differentiating cells, induction of VRI by the GMR driver does not completely reduce EYA-IR and expression of EYA remains at a high level. However, some heterogeneity was observed in the extent of co-localisation of VRI and EYA within post-mitotic neurones. As PRs differentiate, they move apically from the basal pool of cells and start to form clusters in the positions and orientations that they will assume in the developed ommatidia (Voas *et al.,* 2004). The PRs within each individual ommatidium are a heterogenous group and some of the cells of the cluster show both, VRI-IR and EYA-IR whilst others show only EYA-IR. Basal to the organised clusters, nuclear staining can be described to be of three types, (1) EYA-IR alone (green signal); (2) VRI- and EYA- IR at approximately equal levels (assessed subjectively – yellow signal); or, (3) have a greater amount of VRI-IR than EYA-IR (again, subjective assessment – orange signal). Finally the basal cell pool nuclei are predominantly of type 3 (VRI>EYA) with some nuclei of type 1 (EYA). These differences from apical to basal nuclei were observed for both UAS-vri transgenes although UAS-vri-3 was expressed in many more cells and at a higher level. For both transgenes, apically, large nuclei of type 3 (VRI>EYA) staining near the MF are observed that do not seem to follow any specific organisation. Next, basally to these, the position of type 2 (VRI=EYA) staining suggests nuclei of the PRs R3 and R4 interspersed with type 1 (EYA) stained nuclei. More basal layers consist of increasing numbers of type 3 (VRI>EYA) stained nuclei interspersed with more type 1 (EYA) than type 2 (VRI=EYA) stained nuclei. VRI is more widely expressed in apical nuclei when induced from the UAS-vri-3 transgene with an increase in the number of type 2 (VRI=EYA) staining nuclei to more PRs of the cluster and pre-cluster.

3.2.4.2 Pupal phenotypes

Szuplewski *et al.*, (2003) found that over-expression of VRI using *ey*-Gal4 in the eye disc from embryonic stages caused eye deformities of varying severity depending on the UAS-vri transgene used. The most severe of these eye phenotypes was loss of the compound eye and CNS. Similarly, I have found that mis-expression of VRI within the PR epithelium using GMR-Gal4 caused

deformities of the eye of varying severity depending on whether UAS-vri-2b or UAS-vri-3 was used.

GLASS protein is expressed within the CNS in addition to pre- and post-mitotic cells of the eye disc (Ellis *et al.*, 1993). The GMR-Gal4 driver contains a pentameric repeat of a 29bp element of an enhancer of *rh1* that is recognised by GLASS (Freeman, 1996; Ellis *et al.*, 1993; Moses and Rubin, 1991). Wernet *et al* (2003) generated a "long" version of GMR-Gal4 – a pentameric repeat of a 38bp element of the *rh1* enhancer that is also recognised by GLASS. The long-GMR construct exhibits a higher PR specificity and, therefore, presumably also contains repression sites. The long-GMR construct, hereafter referred to as G-long, was also used to reduce non-eye-specific VRI expression, compared to GMR-Gal4, in an attempt to rescue the lethal phenotype observed with GMR-Gal4. Despite spatially restricted expression of VRI by G-long-Gal4, eye phenotypes and pupal lethality were observed; however, eye phenotypes are weaker compared to those observed with GMR-Gal4.

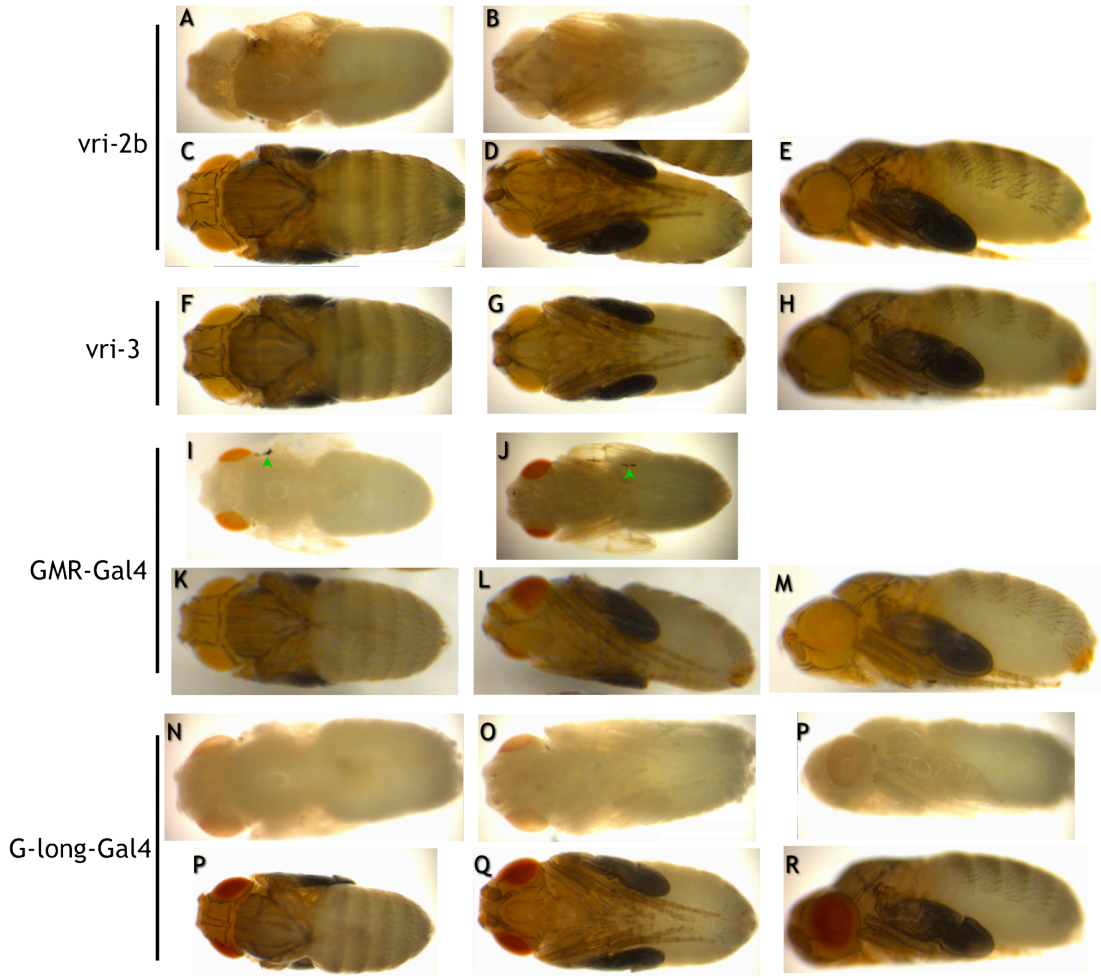

Figure 3.11 Normally developing control animals. Pupae containing a single copy of the transgene indicated on the left. (A, B, I, J, N-P) 2 day old pupae; (C-H, K-M, P-R) 3-4 day old pupae. (I, J) green arrowheads indicate background phenotypes of GMR-Gal4 flies, necrosis can be seen at the wing hinge (I), or, ventral wing blade (J). Key: left panels show dorsal view; middle panels show ventral view; right panels show lateral view; anterior to the left.

Control pupae, containing a single copy of either, Gal4 driver or UAS-vri responder, are shown in Figure 3.11 and appear wild-type apart from variation in eye colour (due to variation in the *mini-white* transgenic selection gene and normal sex differences) and some GMR-Gal4 wing phenotypes (see Figure legend). Control flies developed and emerged normally; experimental animals, however, were only observed as pharate adults extracted from pupae as VRI mis-expression resulted in 100% pupal lethality, irrespective of driver or responder line used. Similar eye phenotypes, though less severe, accompanied by 100% pupal lethality also resulted by raising animals at 18ºC to slow development. Experimental pupae of a Gal4 driver expressing UAS-vri-

2b or UAS-vri-3 are shown in Figures 3.12 and 3.13, respectively; phenotypes were similar although UAS-vri-3 caused more potent and severe phenotypes. Black necrotic tissue within the compound eye field is observed; this ranged from weaker phenotypes of individual scattered ommatidia (black spots within a developed compound eye, Figure 3.12I), to the most severe GMR-Gal4 mediated UAS-vri-3 phenotype causing more wide-spread necrosis and collapse of the cephalic region. Severity of phenotypes ranged thus: GMR-vri-3 > GMR-vri-2b > G-long-vri-3 > G-long-vri-2b.

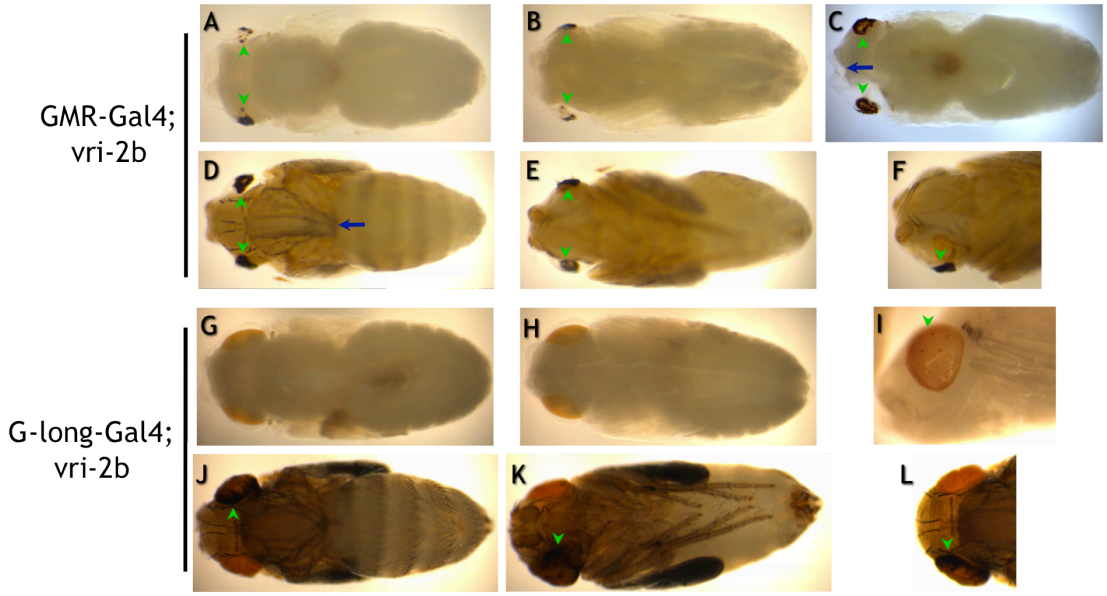

Figure 3.12 Mis-expression of the vri-2b transgene. Shorthand of genotype is indicated on the left. (A-C, G-I) 2 day old pupae; (D-F, J-L) 3-4 day old pupae. (A-F, I-L) Green arrowheads indicate necrotic eye tissue; (C) blue arrow points to collapse of cephalic region; (D) blue arrow points to thorax phenotype (non-eye phenotype of GMR-Gal4 widespread expression). Right panels, (C) dorsal view; (F) ventral view, head and upper thorax; (I) lateral view, head and upper thorax; (L) dorsal view, head and upper thorax. Key: left panels show dorsal view; middle panels show ventral view; anterior to the left.

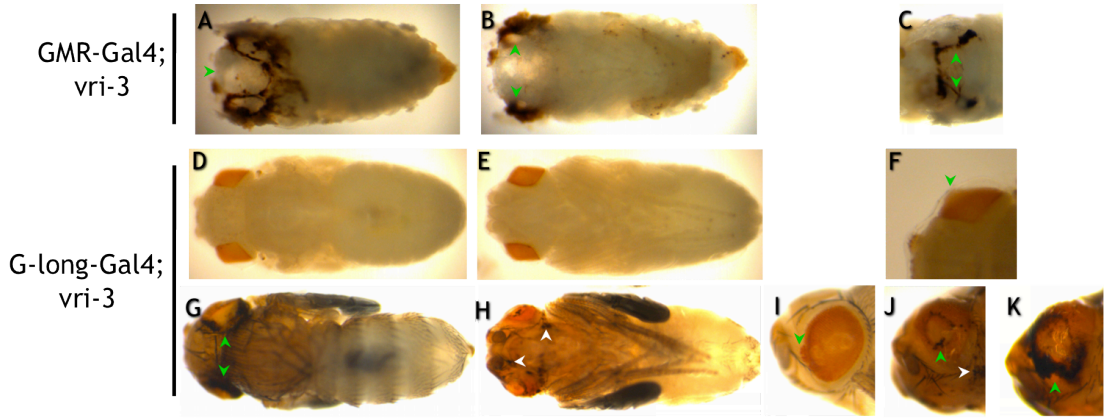

Figure 3.13 Mis-expression of the vri-3 transgene. Shorthand of genotype is indicated on the left. (A-F) 2 day old pupae; (G-K) 3-4 day old pupae. (A-C, F, G, I-K) Green arrowheads indicate necrotic eye tissue; (H, J) white arrowheads indicate non-eye necrotic tissue. Right panels, (C) dorsal view, head; (F) dorsal view, right compound eye; (I-K) lateral view of eye increasing in severity of phenotype. Key: left panels show dorsal view; middle panels show ventral view; anterior to the left.

3.3 Discussion

3.3.1 VRI is required in the eye disc

3.3.1.1 VRI as a modulator of eye development

VRI expression was examined here in relation to the developing photoreceptors. Although a requirement for VRI in the eye disc had already been demonstrated (George and Terracol, 1997; Szuplewski *et al.,* 2003), it has not been shown what function is served by VRI during eye disc development. I have reinforced here that VRI has a role in eye development that is independent of the oscillator factors CLK-CYC. In addition, it appears that no PDP1 isoforms are expressed within the eye disc – a further difference between VRI interactions as described within the oscillator mechanism, where VRI and PDP1 bind the same regulatory sites within the *Clk* gene but have opposing effects on gene transcription. The regional expression of VRI, which is expressed anterior to the MF and not within the developed PRs, appears to be dynamic and negatively associated with MF progression, i.e. VRI is down-regulated ahead of MF – indicative of an acute function in MF progression and subsequent events. VRI is also expressed in the apposing epithelium forming the other side of the disc to the PR epithelium, the peripodial epithelium (PE). Cells of the PE form part of the cuticle and body wall and provide essential regulatory patterning and cell proliferation signals to the PR epithelium (Gibson and Schubiger, 2000; Cho *et al.,* 2000). Cell movements and cell death within the PE cause contraction that eventually leads to disc eversion during metamorphosis (Milner *et al.,*1983). EY is expressed in the PE but EYA is not observed, either due to lack of other activators of EYA, or, because VRI is repressing or modulating EYA expression here.

Overlap in expression of EYA and VRI ahead of the MF, in the PPN determination zone and the ocelli precursors, suggests that VRI does not repress expression of *eya*. However, the PPN zone ahead of the furrow shows convergence of many different signalling pathways – Notch, EGFR, HH, TGFβ

(DPP), WG and the RDGN. Within this zone, convergence of signals are integrated and gene regulation cannot be described as ON/ OFF. If VRI is regulating expression of *eya* and *so* within the eye disc, it is likely that it is acting as a modulator.

VRI as a modulator, rather than absolute repressor, is further indicated from the mis-expression data as VRI induction in the PRs does not act as a binary switch on EYA expression. Furthermore, it remains possible that there is perdurance of EYA protein in cells of the PR epithelium and that VRI can modulate the regulation of these genes even though it does not appear to be an absolute determinant of their expression. Alternatively, it is also possible that VRI induction in cells posterior to the MF cannot overcome the positive feedback loops established between RD genes within this region. In addition, evidence of different immuno-labelling types, 1 (EYA), 2 (VRI=EYA) and 3 (VRI>EYA), suggests that VRI mis-expression in the developing PR epithelium does not have the same effect in all cells. The cell pool within the PR epithelium is heterogenous and it follows that response to mis-expression of VRI is heterogenous. Type 1 (EYA) cells may retain the factors that clear VRI protein from cells as the MF advances; type 2 (VRI=EYA) cells may have a more well-established positive feedback circuit for RD factors that prevent VRI influencing EYA expression; while type 3 (VRI>EYA) cells may represent cells in which VRI is able to modulate EYA moderately but not absolutely. Heterogeneity in VRI expression and function is also indicated by comparing GFP and VRI expression in the posterior eye disc. GMR-Gal4 simultaneously induced expression of UAS-nGFP and UAS-vri transgenes yet only partial co-expression of GFP and VRI signals was observed – indicating uneven induction of these two UAS constructs. However, as similar results were observed with two independent inserts of UAS-vri, it is possible that cell autonomous mechanisms influence expression of the UAS constructs. Ultimately however, as *in situ* hybridisation data for *eya* and *so* is lacking here, suggestions of the action of VRI within the eye disc still require further analysis.

Pupal lethality resulting from mis-expression of VRI posterior to the MF with either, GMR-Gal4 to direct expression in all cells, or, with G-long to restrict expression to PRs, reiterates observations by Blau and Young (1999). Szuplewski *et al*. (2003) used *ey*-Gal4 to mis-express VRI within the eye disc from embryonic stages and observed eye phenotypes ranging in severity dependent on temperature and UAS-vri transgene. The most severe of these was absence of the eye-antennal disc in L3 larvae resulting in an absence of eye and other eye-antennal disc derived head structures in adult flies. Despite this, adult flies emerged from pupae as adults (Terracol, personal communication). However, there must be some remnants of eye-antennal disc as the organ that enables emergence from the pupal case originates from this disc (Cavodeassi *et al.,* 2000). The ptilinum is an organ with a single function – it consists of a sac that is everted by blood pressure during eclosion to push open the pupal case. Following opening of the pupal case, the sac collapses and cuticle hardens around the area leaving the ptilinal suture (Ferris, 1994). That extensive damage to the eye-antennal disc using *ey*-Gal4 does not compromise viability while mis-expression of either UAS-vri transgene with either GMR- or G-long- Gal4 drivers causes 100% lethality during pupal stages suggests that off-target VRI expression causes lethality.

3.3.1.2 VRI as a generic developmental factor

Rather than be specifically a factor of eye development, it is possible that VRI is a developmental factor and has a generic function that is reiterated in all imaginal discs. VRI is expressed in wing and leg imaginal discs in addition to the eye-antennal disc (George and Terracol, 1997). Disruptions to VRI protein expression within the wing or eye-antennal discs by creating mutant clones causes decreases in cell size and atrophy of some cells (Szuplewski *et al.,* 2003). Over-expression of VRI causes atrophy in embryonic epidermis, wing disc and eye-antennal disc, which is attributed to an anti-proliferative influence as well as disrupted cytoskeletal regulation. In addition, they noted that similar eye phenotypes were observed by over-expressing an inhibitor of proliferation (Rbf) or a GTPase involved in actin cytoskeleton regulation (Rho1). The authors suggest that the anti-proliferative phenotype is related to

cytoskeletal integrity but this has not been qualified with evidence of *cis*-regulatory interactions with other factors of the actin cytoskeleton network.

Observations of similar phenotypes by alterations in normal VRI function during development raise the possibility that VRI may have a generic developmental role, partly in regulation of the actin cytoskeleton as suggested by Szuplewski *et al*. (2003). In such a scenario, during development, the primary function of VRI may be to influence general targets found in many cell types. In addition, VRI may also have tissue-specific targets that it modulates. This condition is true of several other signalling pathways found converging on eye development. Notch, EGFR, HH, TGFβ (DPP) and WG all function within other imaginal discs for functions such as establishment of axis boundaries and antagonistic interactions, e.g. Notch and EGFR or DPP and WG, to act as developmental timers. It is possible that VRI is a part of this group of eye development factors that generate the appropriate environment within the tissue in order for the specific developmental factors to differentiate into specialized tissue.

Chapter 4 Binding sites and enhancer analysis

4.1 Introduction

4.1.1 Molecular function of VRI

The bZip transcription factor protein monomers are α-helical and function as dimers (reviewed in Cowell, 2002; Deppmann *et al.*, 2006). These α-helices bind DNA at the N-terminal and dimerise with other bZip monomers via repeated hydrophobic residues, particularly leucine, at the C-terminal. Currently, the only known function of VRI is as a homodimer in circadian oscillator regulation (Glossop *et al.*, 2003). The basic DNA binding domain of VRI is closely related to the proline and acidic amino rich (PAR) family of bZip proteins but, crucially, lacks a PAR domain (Cowell, 2002). The PAR domain is located at the C-terminal and appears to regulate activation of genes.

The 68 amino acids of the basic DNA binding domain of VRI and its human homologue, E4BP4/ NF-IL3A, share 60% identity and 93% similarity (George and Terracol, 1997). This suggested that the consensus DNA binding sequence for E4BP4 might assist VRI binding site searches. Indeed, the E4BP4 consensus sequence was used by Glossop *et al.* (2003) to find VRI binding sites within the *Clk* locus that were bound by VRI protein. The similarity between the DNA binding domains of PDP1 and VRI suggested that they may co-regulate (Cowell, 2002). Indeed, these sites were also shown to complex with PDP1ε and came to be known as V/P boxes that are targeted alternatively by VRI and PDP1ε regulation in the second feedback loop within the oscillator mechanism (Cyran *et al.*, 2003).

4.1.2 Regulation of eya and so loci and expression at other developmental stages

Currently the only known direct transcriptional regulator of *eya* is EY, initially identified via microarray analysis and confirmed with *in silico* analysis of EY binding sites followed by *in vitro* and *in vivo* experiments (Ostrin *et al.,* 2006). Regulation of *so* has been shown *in vitro* and *in vivo* by activtors TOY, EY, EYA-SO and ORTHODENTICLE (OTD; Niimi *et al.,* 1999; Punzo *et al.,* 2002; Pauli *et al.,* 2005; Blanco *et al.,* 2010). The majority of these interactions have been shown to be via an enhancer located in the sixth intron of *so* and interactions occur in a complex manner to regulate *so* expression during L3 eye disc development.

Embryonic expression of *eya* and *so* is observed in the developing head and larval CNS as well as being segmentally reiterated throughout the germ band as it extends and retracts (Kumar and Moses, 2001c). Only in the antero-dorsal region and brain lobes are *eya* and *so* co-expressed whilst germ band expression is in abutting domains. During larval development, EYA-IR was observed in the larval central brain and VNC as well as the precursors of the adult lamina of the compound eye (Bonini *et al.,* 1998). In addition, expression was observed in the follicle cells of the ovary. Data on *eya* expression within the adult CNS is limited and EYA-IR cell clusters are described as functional, rather than anatomical, subsets of neurones (Bonini *et al.,* 1998). Both, *eya* and *so,* are expressed within the developed adult PRs (Bonini *et al.,* 1998; Serikaku and O'Tousa, 1994). There is currently no data on the expression of *so* outside of the visual system.

The finding by Glossop *et al.,* (unpublished results) that TOY is expressed in adult central brain oscillator cells, and enrichment of *toy* in oscillator cells (Nagoshi *et al.,* 2010) are preliminary indications that RDGN factors have a role in the oscillator. *eya* and *so* expression has not been characterised with respect to circadian rhythms and central brain oscillator cells. Due to the

relationship with *toy*, I wanted to examine whether these genes are expressed within the central brain oscillator network.

I show here that several potential VRI binding sites are present in *eya* and *so* loci. A selection of the identified sites were tested *in vitro* and showed different affinities for VRI binding, highlighting the need for validation of *in silico* analysis and revealing sites that had a high affinity for VRI protein. Two of these high affinity sites are located adjacent to the well-characterised enhancer in intron six of *so* and were further studied *in vivo* by transgenic reporter analysis. Further analysis revealed a modulatory role of the VRI sites for the enhancer. More intriguing and surprising were epistatic effects of the *so* enhancer transgene on *eya* expression. Larval CNS were also imaged to better describe the epistatic effects of the *so* enhancer transgene on *eya* expression.

4.2 Results

4.2.1 VRI binds multiple sites in the eya and so genomic loci in vitro

Within the *eya* locus, 27 upstream, 2 intronic and 24 downstream V/P boxes were found, this equates to 53 sites within 278.5kb of DNA (exons span 19.5kb). Contained within the *so* locus are 26 upstream, 2 intronic and 14 downstream V/P boxes equating to 42 sites in 326.2kb of DNA (exons span 15.8kb). Of these, three proximal upstream, two intronic and one downstream sites from *eya,* and two proximal and two intronic sites from *so* were selected for *in vitro* analysis in an electrophoretic mobility shift assay (EMSA).

Figure 4.1 shows representative blots of the *eya* and *so* sites in EMSA. Lanes 1, 2 and 3 of both the blots show identical negative (lane 1) and positive (lanes 2 and 3) control conditions repeated in each blot. Lane 1: negative control – labelled probe, *Clk*-209, was combined with an unprimed control protein

synthesis lysate. Some minor background binding to lysate proteins (low intensity signal smear below VRI-shift position) is observed but VRI-shift is absent. Lane 2: positive control where labelled *Clk*-209 probe was combined with VRI-primed protein synthesis lysate, a large amount of probe is bound by VRI protein and is retarded higher in the gel seen as a prominent band of staining in the blot (VRI-shift position is indicated). Lane 3: positive control for competition assay represents maximal competition, unlabelled positive control probe was used in addition to the components used for lane 2. Used at an excess, the unlabelled probe displaces the labelled probe for VRI binding, consequently reducing the VRI shift signal. For all other lanes of the image, a reduction of signal at the VRI-shift position indicates that the site is bound by VRI. The reduction in VRI-shift is to varying degrees and is a qualitative indicator of affinity of VRI for the tested probe. Presence of a VRI-shift signal comparable to that observed in lane 2 indicates that the tested probe is not recognised by VRI protein.

All sites from *eya* and *so* were used in a competition assay against *Clk*-209 and were named as e*[x]* for sites from *eya* or s*[x]* for sites from *so*. Figure 4.1 shows that sites e1, e2 and e5 (lanes 4, 5 and) are able to bind VRI at an affinity comparable to *Clk*-209; site e3 shows incomplete displacement of labelled *Clk*-209 (lane 7); whilst sites e4 and e6 appear to be weak, or unable to, compete with *Clk*-209 for VRI occupancy (lanes 8 and 11). Mutation of the core bases of the VRI recognition site greatly reduces, or eliminates, competition with *Clk-209* for VRI binding. Sites that were bound well by VRI, e2 and e5, were thus used as mutated versions (compare lanes 5 and 6, and 9 and 10, respectively). This demonstrates that it is the specific sequence of the core 8 bases of the binding site that mediates the VRI-shift.

Figure 4.1 shows that sites s2, s3 and s4 (lanes 5, 6 and 8) bind VRI at an affinity comparable to *Clk*-209 whereas site s1 (lane 4) only partially displaces *Clk*-209 from the VRI binding site. As observed for probes from the *eya* locus, mutation of the sequence of the core eight bases of the VRI binding site to non-consensus renders the probes unable to displace *Clk*-209 from VRI. This

was carried out for sites s3 and s4, (compare lanes 6 and 7, and 8 and 9, respectively) demonstrating again that the specific sequence of those eight bases of the oligonucleotide probes determines affinity for VRI.

In summary, VRI has high affinity for six of the ten tested sites, reduced affinity for two of the sites and, very low to no affinity for two sites in the order: *Clk-209* = e1 = e2 = e5 > e3 > e4 = e6; and *Clk-209* = s2 = s3 = s4 > s1. Mutating bases within the binding site to form a non-consensus sequence abolishes binding, demonstrating that the specific sequence of a double-stranded oligonucleotide probe is necessary for binding. Furthermore, a trend can be seen with regards to binding site affinity, summarised in Table 4.1. Sites e3-e6, s1 and s2 all contain non-consensus bases. Of these, e5 and s2 (that compete for VRI binding comparable to control) have an identical sequence where the bases that can differ, or 'wobble', of the site are A–T–T––––**A**, the terminal A being non-consensus (emboldened and underlined). Wobble bases of e3 are T–T–T––––**A**, and of s1 are T–G–T––––**G**, both sites that show reduced competition with the positive control, s1 being the weaker competitor of the two. The wobble bases of sites that were not bound by VRI, e4 and e6, were T–G–T––––**A**. The affinity for VRI binding to this selection of sites may be described: *Clk-209* = e5 = s2 > e3 > s1 > e4 = e6. Sites with non-consensus nucleotide A at the +5 position retain high affinity binding to VRI in combination with nucleotide T (consensus) at the -5 position (e5, s2). Combination of non-consensus A at the +5 position with consensus T at the -5 position reduces affinity for VRI (e3). Further changing the e3 binding site to incorporate consensus nucleotide G at position -3 results in an apparent loss of VRI binding (e4, e6). The loss of DNA-VRI complex formation observed for sites e4 and e6 can be recovered to a small extent by changing the +5 position nucleotide to non-consensus G (s1). As single nucleotide changes of wobble bases of the binding site sequence changed the affinity of VRI for the site, the approach used here is supported. Searching for the core eight bases of the E4BP4/ NF-IL3A consensus binding site provides a large number of candidates but these require validation in EMSA.

Table 4.1 Summary of VRI binding to sites from *eya* and *so*. Sites for EMSA were short-listed by searching for the core 8 bases of the consensus binding site (combinations of consensus sequence possible for nucleotides at position -4 to +4). Also described is competition of these sites in comparison to the positive control; > indicates somewhat reduced competition; >> indicates considerably reduced/ absent competition.

Probe	Site sequence < - > < + > 5 4321:1234 5	Binding compared to *Clk-209* (C)
Consensus site	**G** **T** *T T* *T A :GTAA* **T** **A** *G C* **C**	
C	**G** *TTAT:GTAA* **T**	Self-competition shows highest reduction in VRI-shift
e1	**T** *TTAT:GTAA* **C**	Equivalent to C
e2	**G** *TTAT:GTAA* **T**	Equivalent to C
e3	**T** *TTAT:GTAA* **A**	C > e3
e4	**T** *TGAT:GTAA* **A**	C >> e4 ➔ *no binding*
e5	**A** *TTAT:GTAA* **A**	Equivalent to C
e6	**T** *TGAT:GTAA* **A**	C >> e6 ➔ *no binding*
s1	**T** *TGAT:GTAA* **G**	C > s1
s2	**A** *TTAT:GTAA* **A**	Equivalent to C
s3	**T** *TTAT:GTAA* **C**	Equivalent to C
s4	**T** *TTAT:GTAA* **T**	Equivalent to C

eya EMSA

Lane		1	2	3	4	5	6	7	8	9	10	11
TnT protein lysate		-	V	V	V	V	V	V	V	V	V	V
Labelled probe		C	C	C	C	C	C	C	C	C	C	C
Competitor probes	Wild type	-	-	C	e1	e2	-	e3	e4	e5	-	e6
	Mutant	-	-	-	-	-	e2	-	-	-	e5	-

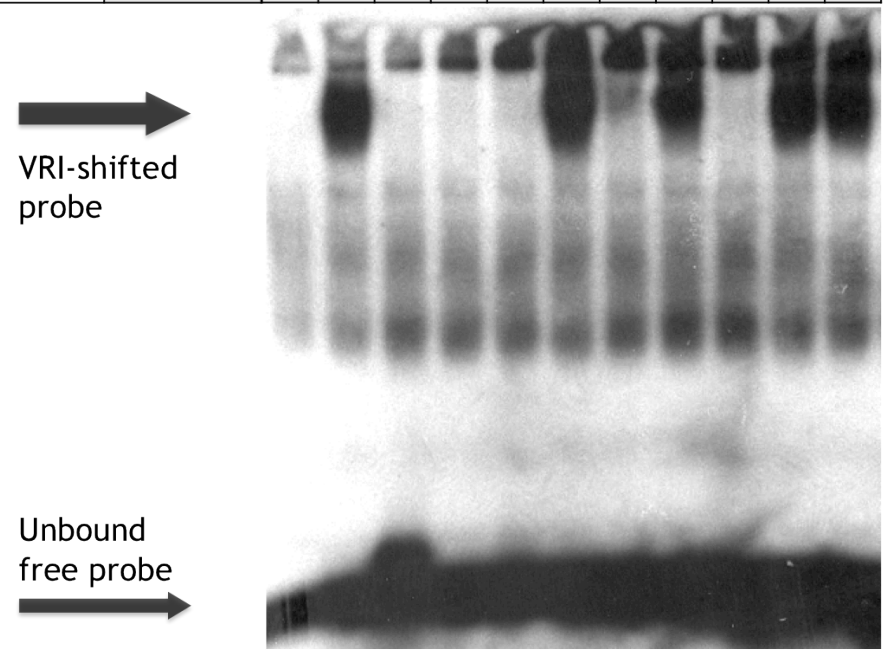

so EMSA

Lane		1	2	3	4	5	6	7	8	9
TnT protein lysate		-	V	V	V	V	V	V	V	V
Labelled probe		C	C	C	C	C	C	C	C	C
Competitor probes	Wild type	-	-	C	s1	s2	s3	-	s4	-
	Mutant	-	-	-	-	-	-	s3	-	s4

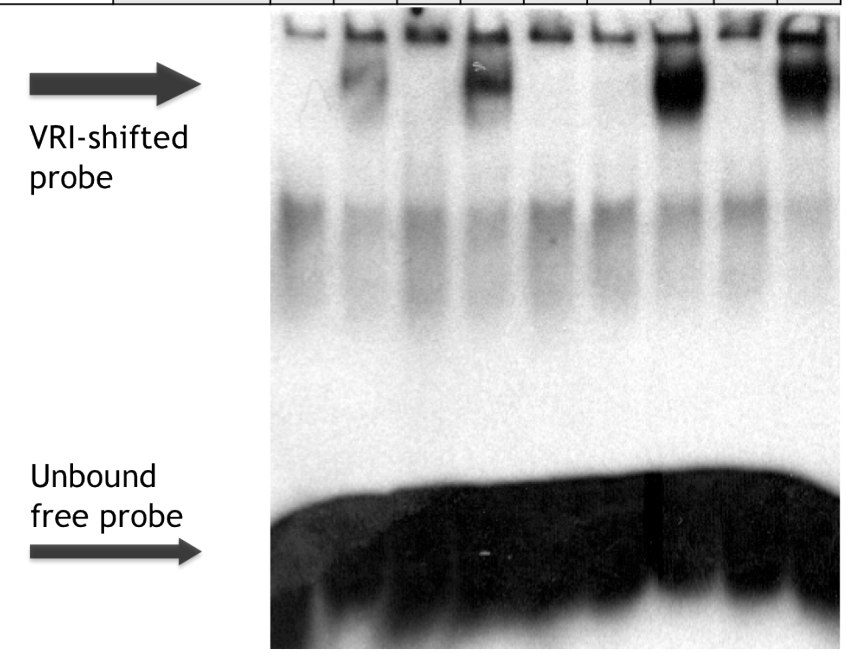

Figure 4.1 EMSA results summary. TnT lysate used in binding experiments was either VRI (V in VRILLE row) or unprimed control lysate (- in VRILLE row). The positive control labelled probe used in all instances was from the *Clk* locus (C), also used unlabelled in competition assay. Competitor probes are described within the text.

4.2.2 Construction of a transgenic reporter for intron 6 of so

The two VRI binding sites in the sixth intron of *so* were of particular interest as an enhancer of *so* has been described within this intron (Niimi *et al.*, 1999; Punzo *et al.*, 2002; Pauli *et al.*, 2005). Since VRI is known to repress transcription, study of putative enhancers bearing VRI-target sites poses a challenge. It is possible to study such repressive enhancers either, *in vitro*, by the addition of an activation domain to VRI protein, as done by Cyran *et al* (2003); or, alternatively, by appending activatory enhancers. However, as I have already demonstrated that sites selected from *eya* and *so* are bound by VRI *in vitro*, I wanted to examine VRI function *in vivo* - and this required endogenous activation sites.

Intron 6 of *so* has previously been shown to contain an enhancer element (Niimi *et al.*, 1999; Punzo *et al.*, 2002; Pauli *et al.*, 2005) with six activation sites: one autoregulatory, two bound by TOY and three bound by EY and TOY. The enhancers bearing these sites were named as follows: *so10* – a 425bp region containing the five PAX6 sites bound by either TOY alone or EY and TOY; *so9* – adjacent to *so10, a* 1192bp region containing the autoregulatory site; collectively these two regions (approx. 1.6kb) were named *so7*. In addition, a recessive mutant allele of *so*, so^1 is an eye-specific null that results in loss of the compound eyes and ocelli but does not affect embryonic *so* expression (Cheyette *et al.*, 1994). This mutant results from a deletion of 1.3kb within intron 6 that includes *so10* and most of *so9* (Cheyette *et al.*, 1994; Niimi *et al.*, 1999). The necessity of *so7* was shown by rescue of the eyeless, and partial rescue of the ocelli-less, phenotype by *so* expression driven by the *so7* enhancer in a so^1 mutant background (Punzo *et al.*, 2002). In the same study partial rescue of the eyeless and ocelli-less phenotypes was also shown using the *so10* enhancer to drive *so* expression in the so^1 mutant background. Site s3 from the current study is 2300bp upstream of *so7* and site s4 is 750bp upstream of *so7*, see schematic (Figure 4.2).

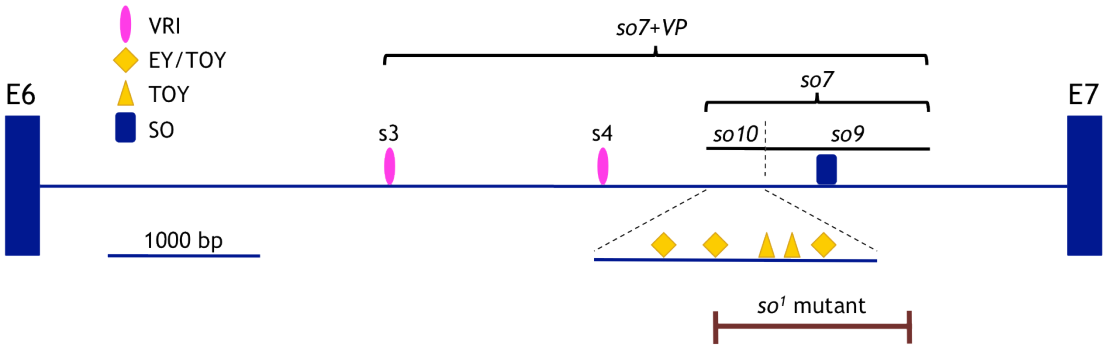

Figure 4.2 Schematic of intron 6 of *so*. Relative positions of the various enhancers studied here are shown with the positions of transcription factor binding sites indicated. The position of the deletion in *so*^{1} mutants is also shown. The driver lines of the *so10* and *so7* enhancers were kindly donated by W. Gehring (Niimi *et al.*, 1999; Punzo *et al.*, 2002; Pauli *et al.*, 2005). The *so7+VP* enhancer driver line was generated in the current study.

A region including the 2330bp (including primer upstream of s3 for cloning start site) upstream of *so7* containing sites s3 and s4 and *so7* was cloned upstream of Gal4 and used to make transgenic flies, henceforth referred to as *so7+VP-Gal4*. VRI binding sites within *so7+VP-Gal4* were mutated to the same mutant sequences used for EMSA to produce the *so7+VP*$^{[VP\text{-}mut]}$*-Gal4* construct for a direct comparison of VRI input to this enhancer. The ϕC31-mediated site-directed transgenesis system (Bischof *et al.*, 2007) was employed for the production of transgenic flies containing *so7+VP-Gal4* and *so7+VP*$^{[VP\text{-}mut]}$*-Gal4*. Site 51C located on the right arm of the second chromosome was used for insertion of both cloned constructs for faithful comparison. This position is intergenic and the neighbouring genes are 18894bp (*M-spondin*) upstream and 5971bp (*CG12865*) downstream. *CG12865* is yet to be characterised. *M-spondin* is an extra-cellular matrix protein (Umemiya *et al.*, 1997) and is expressed in the lamina and R7 PR (Mollereau *et al.*, 2000). Currently, there are no documented background effects due to the use of this landing site for transgenesis.

The contribution of the VRI binding sites to the intron 6 enhancer of *so* was assessed by comparison of GFP expression mediated by *so7+VP-Gal4* and *so7+VP*$^{[VP\text{-}mut]}$*-Gal4* with *so7-Gal4* and *so10-Gal4* lines.

4.2.3 Comparison of so intron 6 transgenic lines

GFP reporter and antibody labelling observed for the driver lines was compared to that observed in negative control animals of the genotype *w; +; UAS-nGFP*, referred to only as control animals, below. Antibody labelling observed in control animals is identical to that observed for wild-type animals apart from ectopic GFP expression within the lamina of adult CNS (Figure 4.12, plates 1 and 2). This ectopic expression was at basal level and did not impact on expression observed in the presence of the drivers.

4.2.3.1 Larval eye discs

Pauli *et al*. (2005) described *so10* as controlling expression within the compound eye precursor field of the eye disc but not in the ocelli precursor field. Meanwhile *so9* was only expressed at the posterior margin of the eye disc. Combination of the two regions into the *so7* fragment resulted in an expansion of *so10*-mediated expression into the ocelli precursor cells. However, *so10* and *so7* expression appeared to extend further past the MF and into anterior regions than was reported by immuno-staining protocols for SO (Cheyette *et al.,* 1994; Halder *et al.,* 1998). VRI is expressed in anterior regions where *so7* appears to drive ectopic expression. I was interested in studying the differences in expression mediated by *so7*-Gal4 and *so7+VP-Gal4* particularly in these cells of the eye disc and PE. Together with this comparative analysis, it was important to assess the specific contribution of the VRI sites with the use of *so7+VP*$^{[VP\text{-}mut]}$. EYA and SO function as a heterodimeric transactivation complex during development of the eye disc and their expression is described to entirely overlap one another (Bonini *et al.*, 1993; Cheyette *et al.,* 1994; Serikaku and O'Tousa, 1994). To compare GFP expression to endogenous regional expression and in relation to VRI expression, larval tissues were co-labelled with EYA and VRI antibodies.

I show that *so10-Gal4* expresses GFP in several groups of cells: (1) PE; (2) minimally within PRs although highest expression was seen in cells adjacent to

the MF; (3) strong expression in cells anterior to the MF. Expression in cells anterior to the MF extends into the lateral margins of the eye disc, this includes a subset of the ocelli precursors (outlined in Figure 4.3B) – medial cells of the dorsal group of precursors. Co-labelling for EYA whilst examining the expression mediated by the enhancer revealed that the *so10* enhancer drives expression within a subset of the cells comprising the dorsal ocelli precursors. This explains why only partial rescue of the ocelli-less phenotype is observed when *so10* drives *so* expression in a so^1 mutant background (Punzo *et al.*, 2002; Pauli *et al.*, 2005).

so7-Gal4 drives GFP expression in the same groups of cells but is up-regulated. Additionally, GFP expression extends into both dorsal and ventral ocelli precursor cell groups but the expression in the lateral margin of the eye disc leading to the ocelli is down-regulated such that there is an interruption in GFP expression between cells just anterior the MF and the ocelli precursor cells. These results are consistent with earlier descriptions of *so10* and *so7* enhancer activities, both of which rescued the eyeless phenotype of so^1 mutants, with *so7* also partially rescuing the ocelli-less phenotype as result of driver activity in an increased number of cells of the lateral margin, including the precursors.

Expression of GFP mediated by *so7+VP* and $so7+VP^{[VP\text{-}mut]}$ shows similar localisation but an up-regulation of GFP signal intensity mediated by $so7+VP^{[VP\text{-}mut]}$. Compared to *so7*, expression within the dorso-lateral margin of the eye disc is increased and a greater number of the ocelli precursors show GFP expression.

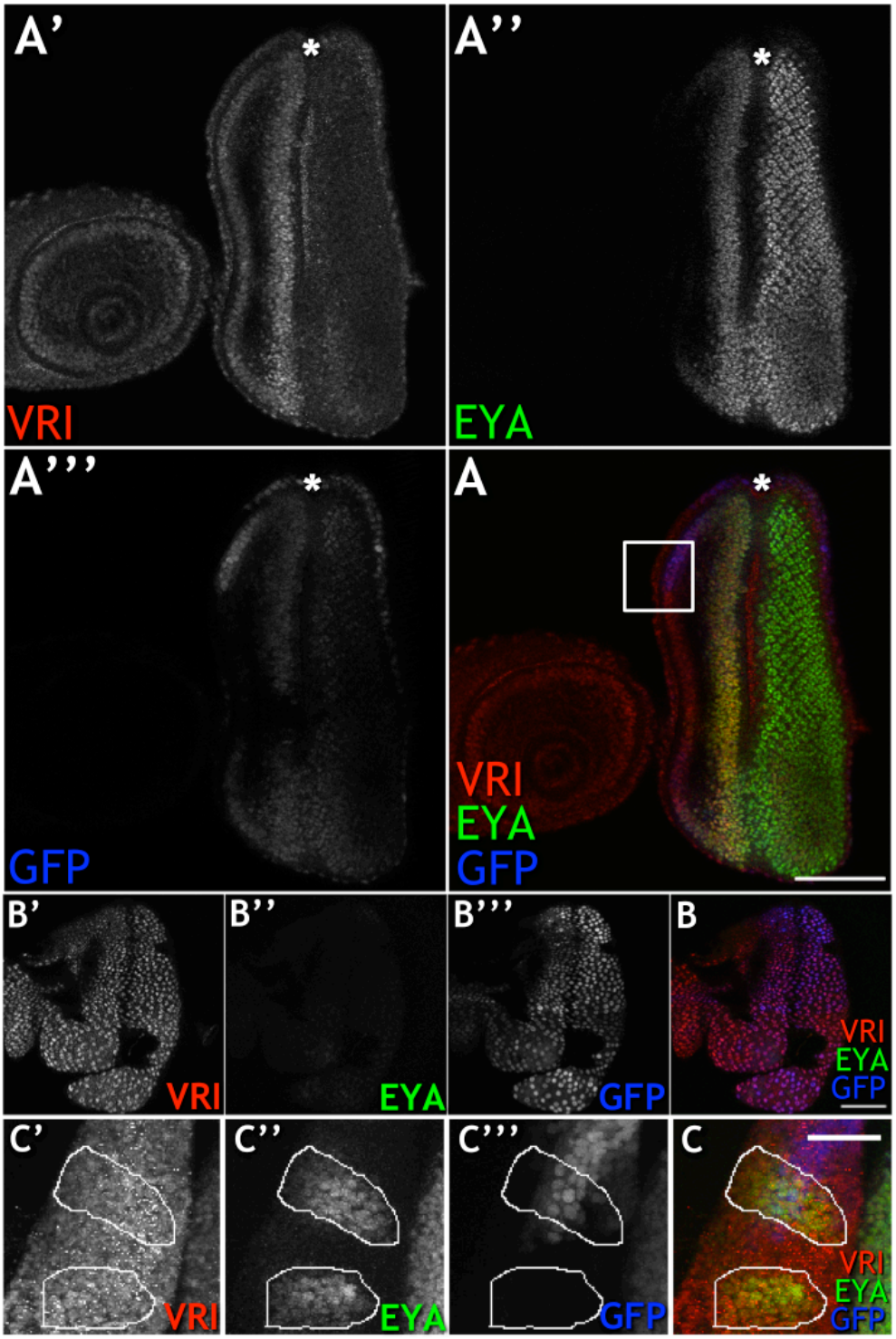

Figure 4.3 Activity of *so10*-Gal4 in L3 eye disc reported by GFP co-labelled for VRI and EYA. (A) Single Z-section of PR epithelium of disc immuno-labelled for VRI (A', red in A) and EYA (A'', green in A) with GFP expression (A''', blue in A). (B) Single Z-section of PE of disc immuno-labelled for VRI (B', red in B) and EYA (B'', green in B) with GFP expression (B''', blue in B). (C) Flattened Z-sections of ocelli precursors (white box on A) immuno-labelled for VRI (C', red in C) and EYA (C'', green in C) with GFP expression (C''', blue in C). Key: anterior to the left; asterisk marks MF; white box on (A) shown expaned in (C); scale bar = 50μm; minimum *n=5*.

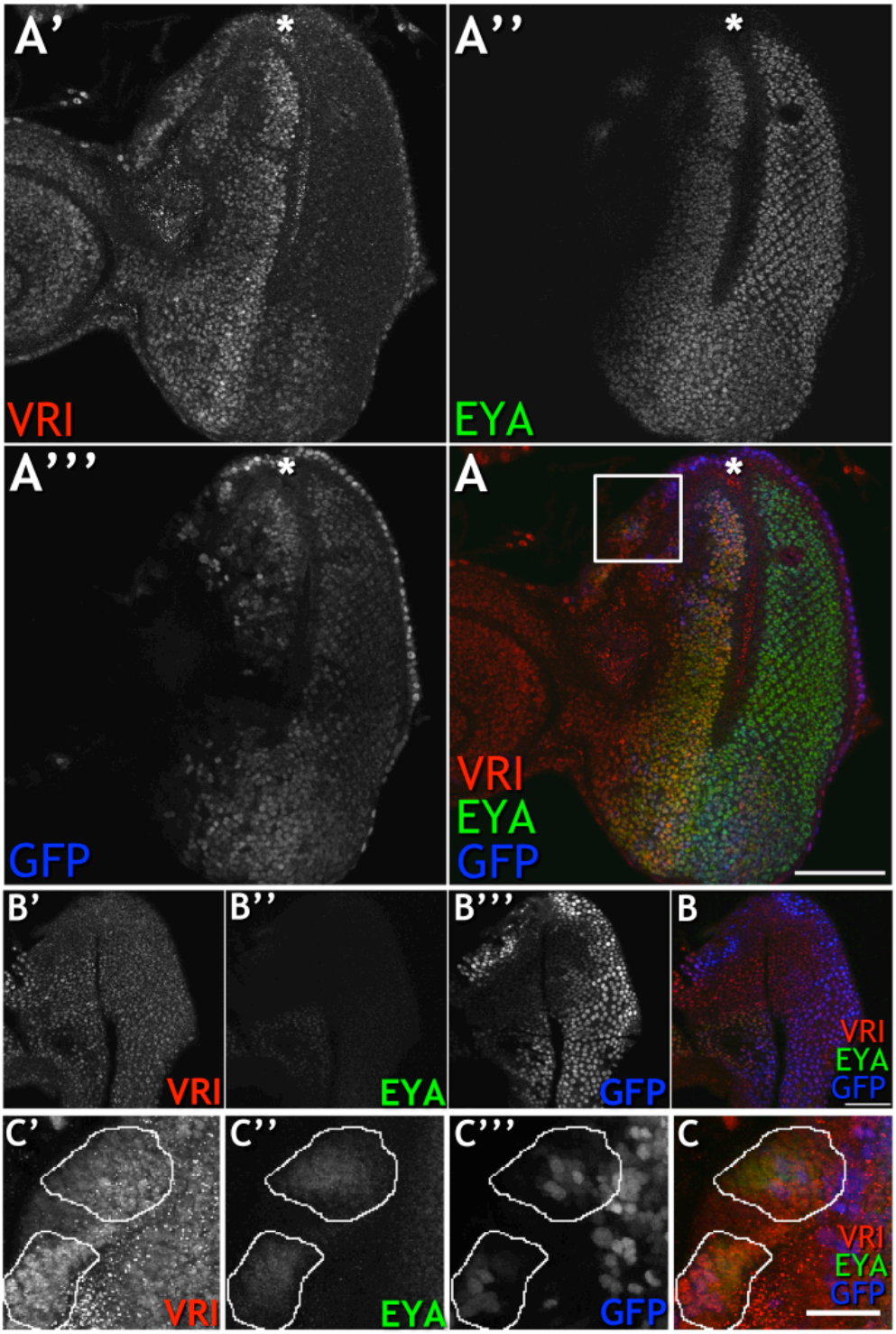

Figure 4.4 Activity of *so7*-Gal4 in L3 eye disc reported by GFP co-labelled for VRI and EYA. (A) Single Z-section of PR epithelium of disc immuno-labelled for VRI (A', red in A) and EYA (A'', green in A) with GFP expression (A''', blue in A). (B) Single Z-section of PE of disc immuno-labelled for VRI (B', red in B) and EYA (B'', green in B) with GFP expression (B''', blue in B). (C) Flattened Z-sections of ocelli precursors (white box on A) immuno-labelled for VRI (C', red in C) and EYA (C'', green in C) with GFP expression (C''', blue in C). Key: anterior to the left; asterisk marks MF; white box on (A) shown expaned in (C); scale bar = 50μm; minimum *n=5*.

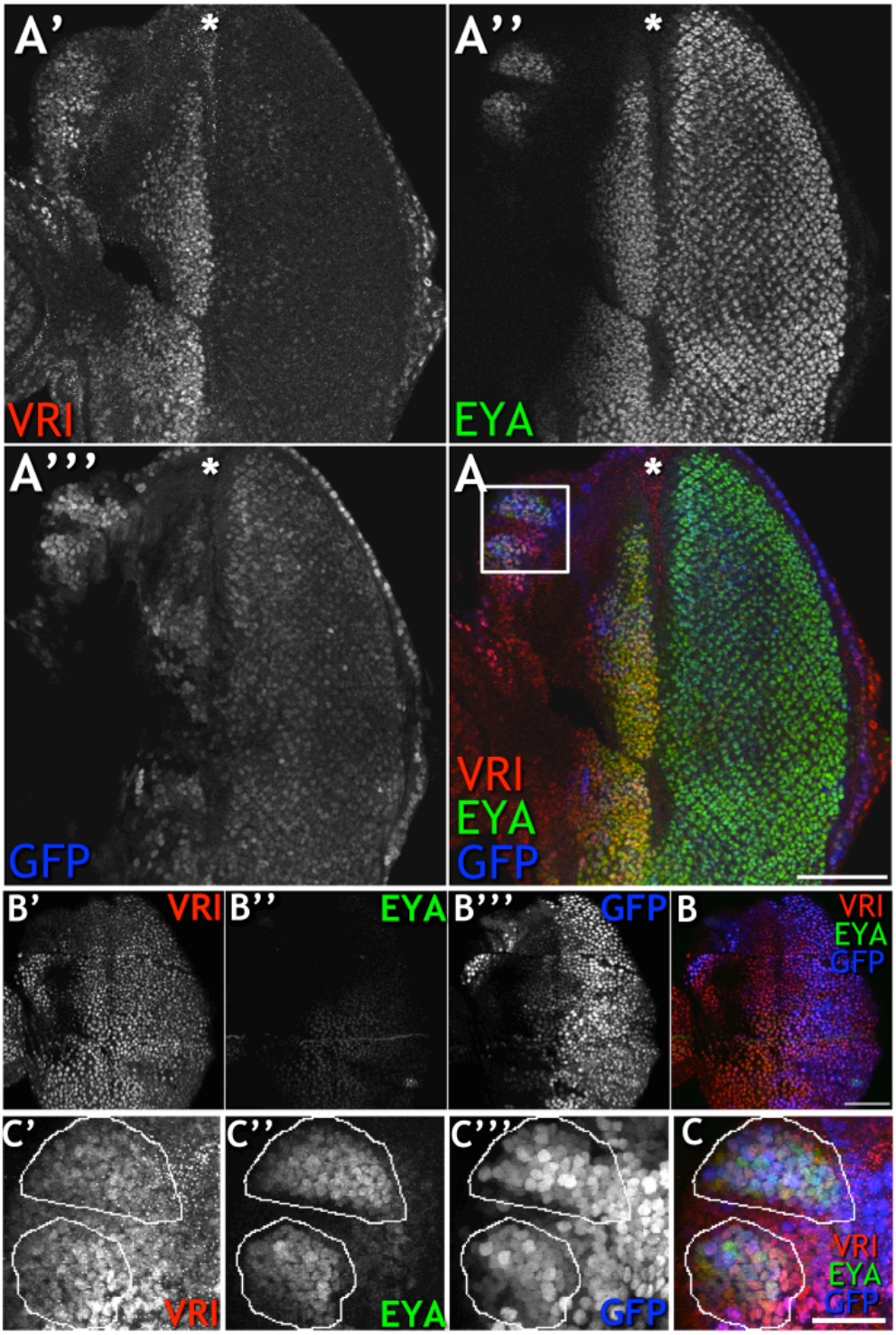

Figure 4.5 Activity of *so7+VP*-Gal4 in L3 eye disc reported by GFP co-labelled for VRI and EYA. (A) Single Z-section of PR epithelium of disc immuno-labelled for VRI (A', red in A) and EYA (A'', green in A) with GFP expression (A''', blue in A). (B) Single Z-section of PE of disc immuno-labelled for VRI (B', red in B) and EYA (B'', green in B) with GFP expression (B''', blue in B). (C) Flattened Z-sections of ocelli precursors (white box on A) immuno-labelled for VRI (C', red in C) and EYA (C'', green in C) with GFP expression (C''', blue in C). Key: anterior to the left; asterisk marks MF; white box on (A) shown expanded in (C); scale bar = 50μm; minimum *n=5*.

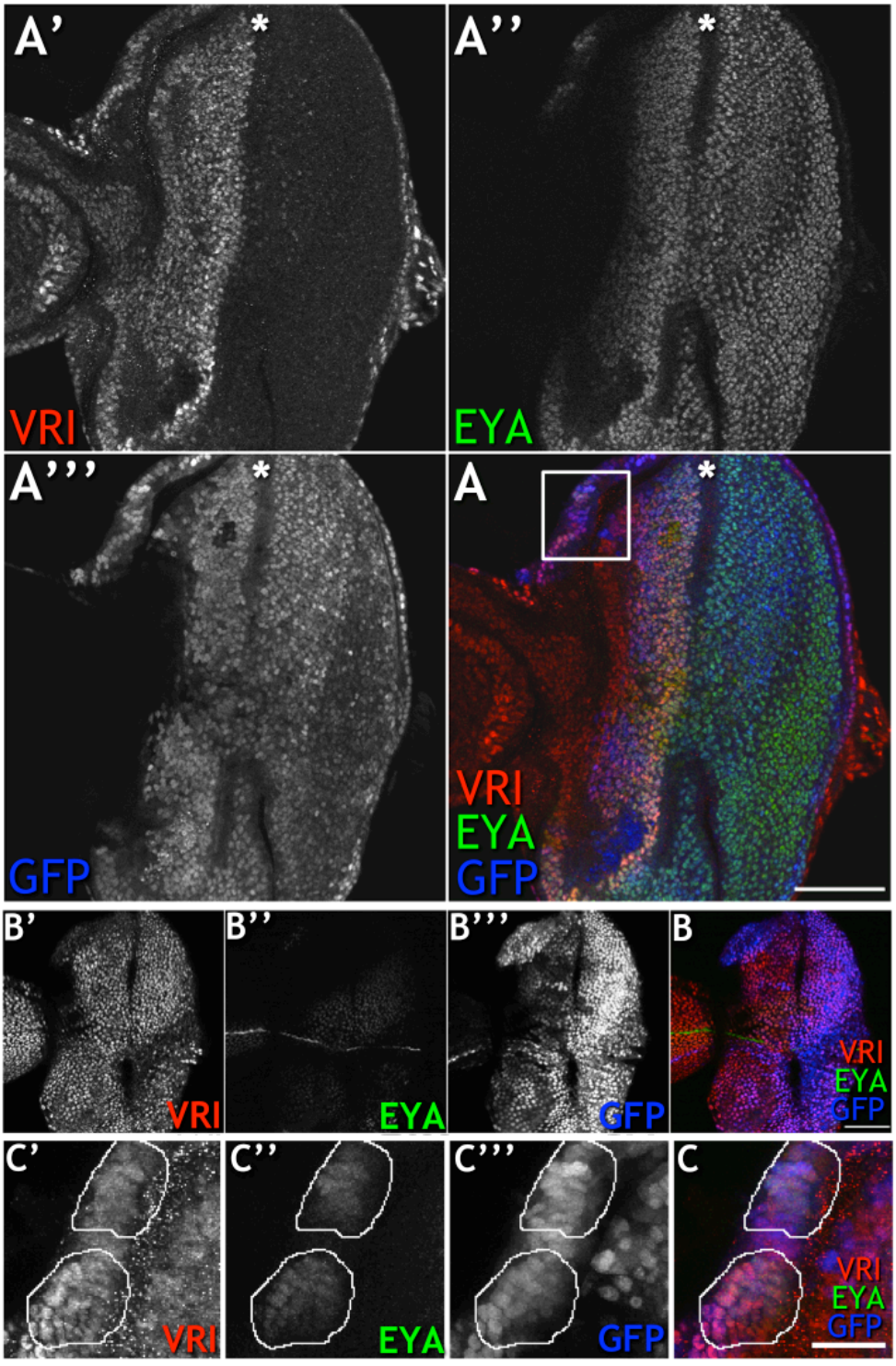

Figure 4.6 Activity of *so7+VP[VP-mut]*-Gal4 in L3 eye disc reported by GFP co-labelled for VRI and EYA. (A) Single Z-section of PR epithelium of disc immuno-labelled for VRI (A', red in A) and EYA (A'', green in A) with GFP expression (A''', blue in A). (B) Single Z-section of PE of disc immuno-labelled for VRI (B', red in B) and EYA (B'', green in B) with GFP expression (B''', blue in B). (C) Flattened Z-sections of ocelli precursors (white box on A) immuno-labelled for VRI (C', red in C) and EYA (C'', green in C) with GFP expression (C''', blue in C). Key: anterior to the left; asterisk marks MF; white box on (A) shown expanded in (C); scale bar = 50μm; minimum *n=5*.

4.2.3.2 Larval CNS, antennal and leg discs

Within antennal discs, no GFP expression is observed in discs from the *so10*-Gal4 driver (Figure 4.7B), as seen for discs from control animals (Figure 4.7A), whereas 2 or 3 cells express GFP in antennal discs from *so7-Gal4* (Figure 4.7C). For the *so7+VP*- and *so7+VP*$^{[VP\text{-}mut]}$- Gal4 drivers (Figures 4.7D and 4.7E, respectively), cells at the attachment site of the antennal discs to the mouth hooks contain GFP and the number of cells and intensity of the signal increases in discs from *so7+VP*$^{[VP\text{-}mut]}$*-Gal4*.

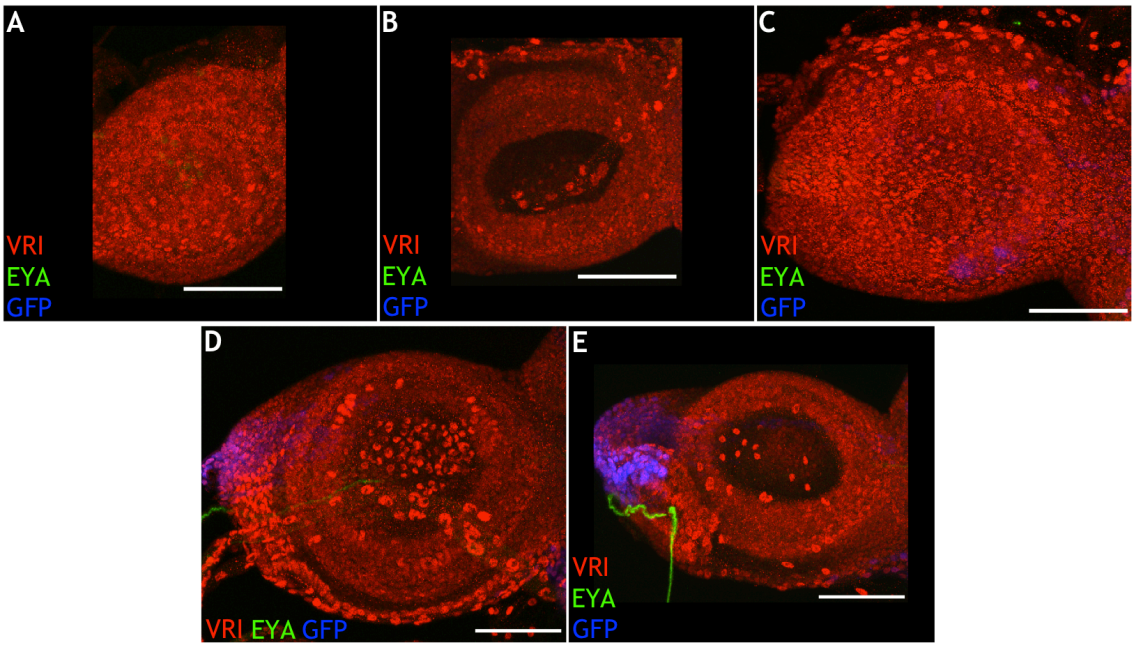

Figure 4.7 Activity of *so* intron 6 drivers in L3 antennal disc reported by GFP and co-labelled for VRI and EYA. Flattened Z-sections of the antennal discs of (A) control (genotype: *w; +; UAS-nGFP*); (B) *so10*-Gal4; (C) *so7*-Gal4; (D) *so7+VP*-Gal4; (E) *so7+VP*$^{[VP\text{-}mut]}$-Gal4. Key: anterior to the left; VRI-IR (red), EYA-IR (green), GFP (blue); scale bar = 50μm; minimum *n=5*.

Leg discs (attached to CNS, see Figures 4.8-10 of L3 CNS) of the different driver lines show a similar relationship compared to the antennal discs. The *so10-Gal4* driver does not show any reporter signal whereas, GFP is expressed in a small number of individual cells scattered throughout the leg discs of the *so7-Gal4* driver. For the *so7+VP* and *so7+VP*$^{[VP\text{-}mut]}$ drivers, the GFP expression is regionalised to the thoracic body wall attachment site and distal leg regions, once again at a higher intensity in discs from *so7+VP*$^{[VP\text{-}mut]}$ compared to *so7+VP*.

The most pronounced difference between transgenic constructs from this study and those that they were based on is that seen within the CNS of L3 larvae. Reports on EYA expression did not describe which cells within the developing CNS were positive for EYA (Bonini *et al.,* 1998) and expression mediated by the various so intron 6 enhancers was not described for the CNS (Punzo *et al.,* 2002; Pauli *et al.,* 2005). I found that in control L3 larval CNS, EYA expression is seen in cells of the outer optic anlagen; in 11 pairs of cells either side of the midline in the ventral nerve cord (VNC) and some cell groups lateral to these in the anterior VNC; and, in medial cell clusters of the central brain (Figure 4.8A and A'''). EYA-IR is also observed in leg discs (still attached to the CNS) near the thoracic attachment and regions that form distal leg. This expression pattern is also observed in L3 CNS from *so10*- and *so7*- Gal4 driver lines (Figure 4.9A and A''' and 4.9C and C''', respectively). In the CNS from *so7+VP-Gal4* (Figure 4.10A and A'''), there is a clear up-regulation of EYA expression in several additional cell groups. These include cells in the VNC and central brain as well as in an axonal projection extending into the inner optic anlagen, likely to be Bolwig's nerve – the projection from the larval photoreceptive organ of the same name. An identical pattern of expression is observed in CNS of *so7+VP$^{[VP\text{-}mut]}$-Gal4* but EYA staining intensity is increased (Figure 4.10C and C'''). This suggests that either, the insertion site used for the transgenics generated here has a *trans*-activation effect on *eya* expression; or, that the additional region of the *so* intron used for the driver lines is altering epistasis of *eya*.

Meanwhile, GFP expression mediated by the driver lines is always observed in the outer optic anlagen with intensity and region size increasing such that *so10* < *so7* < *so7+VP* < *so7+VP$^{[VP\text{-}mut]}$*. Within the central brain, a small number of cells express GFP driven by the *so10* driver, this number increases with the *so7* driver (compare Figure 4.9A' and 9C') but is suppressed by both, *so7+VP* and *so7+VP$^{[VP\text{-}mut]}$* drivers (compare Figure 4.10A' and C' with Figure 4.9C'). Similarly, expression within the VNC is evident in a few disparate cells when driven by *so10* (Figure 4.9A'). The number of cells increases and pattern of

expression of GFP extends into bilaterally symmetrical longitudinal axonal tracts with the *so7* driver (Figure 4.9C'), reminiscent of the longitudinal connectives and some commissural projections are observed, but not within every segment. The *so7+VP* and *so7+VP*$^{[VP\text{-}mut]}$ drivers do not show any VNC expression of GFP (Figure 4.10A' and C').

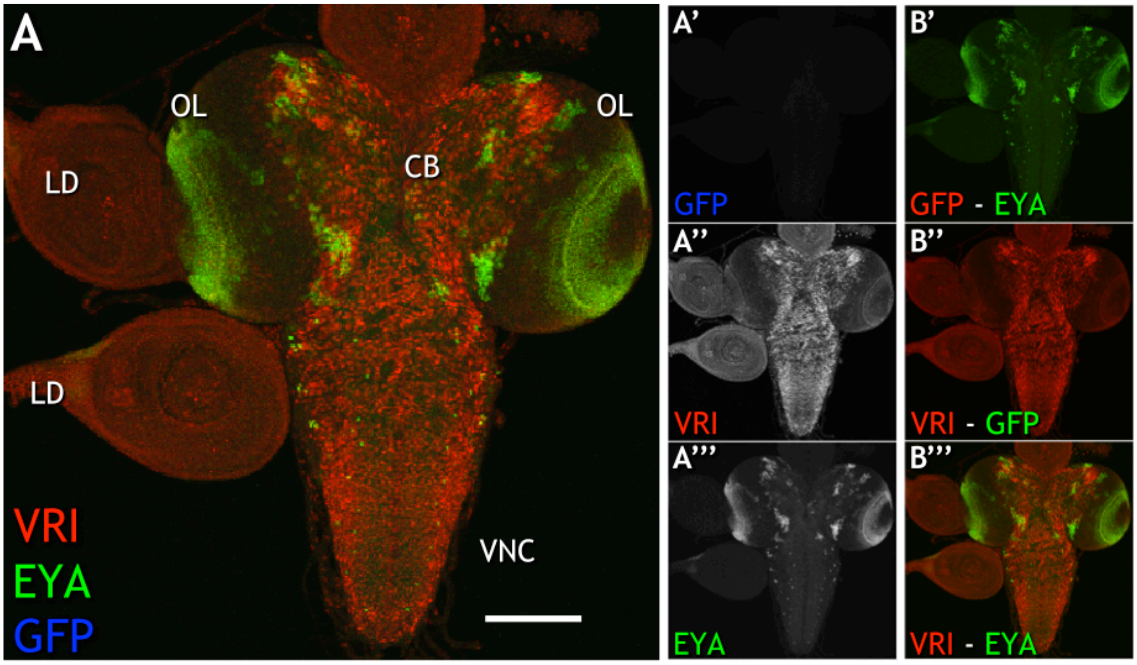

Figure 4.8 Control L3 CNS labelled for VRI and EYA. (A) Flattened Z-sections showing GFP expression (A', blue in A) and immuno-labelled for VRI (A'', red in A) and EYA (A''', green in A). (B', B'', B''') two channel merge images of individual channels shown in A'-A''': GFP, red and EYA-IR, green (B'); VRI-IR, red and GFP, red (B''); VRI-IR, red and EYA-IR, green (B'''). Key: dorsal to the top; OL, optic lobe; LD, leg disc; CB, central brain; VNC, ventral nerve cord; scale bar = 100μm; minimum *n=5*.

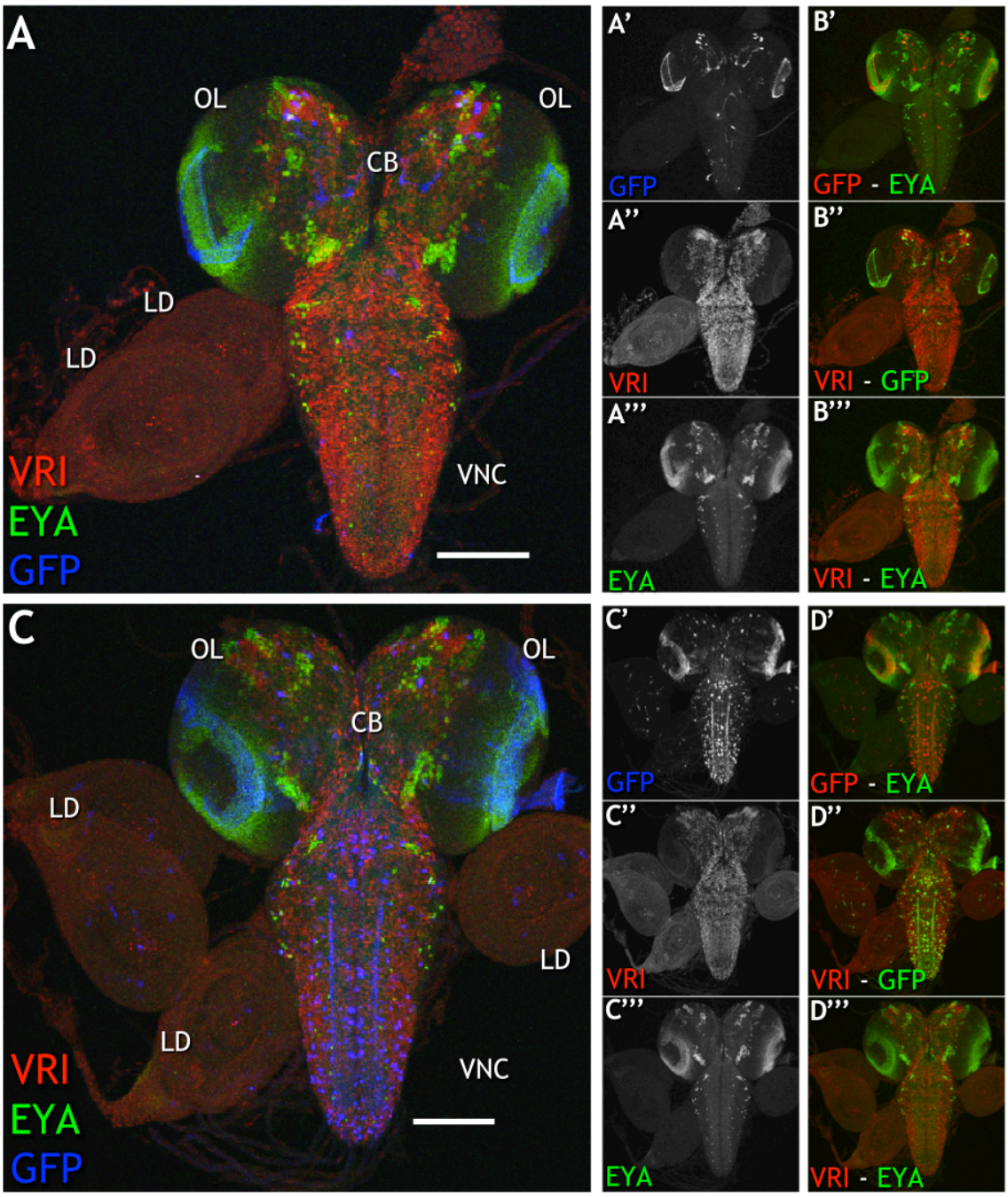

Figure 4.9 L3 CNS of *so10*-Gal4 and *so7*-Gal4 labelled for VRI and EYA. (A) Flattened Z-sections showing GFP expression mediated by *so10*-Gal4 (A', blue in A) and immuno-labelled for VRI (A'', red in A) and EYA (A''', green in A). (B', B'', B''') two channel merge images of individual channels shown in A'-A''': GFP, red and EYA-IR, green (B'); VRI-IR, red and GFP, red (B''); VRI-IR, red and EYA-IR, green (B'''). (C) Flattened Z-sections showing GFP expression mediated by *so7*-Gal4 (C', blue in C) and immuno-labelled for VRI (C'', red in C) and EYA (C''', green in C). (D', D'', D''') two channel merge images of individual channels shown in C'-C''': GFP, red and EYA-IR, green (D'); VRI-IR, red and GFP, red (D''); VRI-IR, red and EYA-IR, green (D'''). Key: dorsal to the top; OL, optic lobe; LD, leg disc; CB, central brain; VNC, ventral nerve cord; scale bar = 100μm; minimum *n=5*.

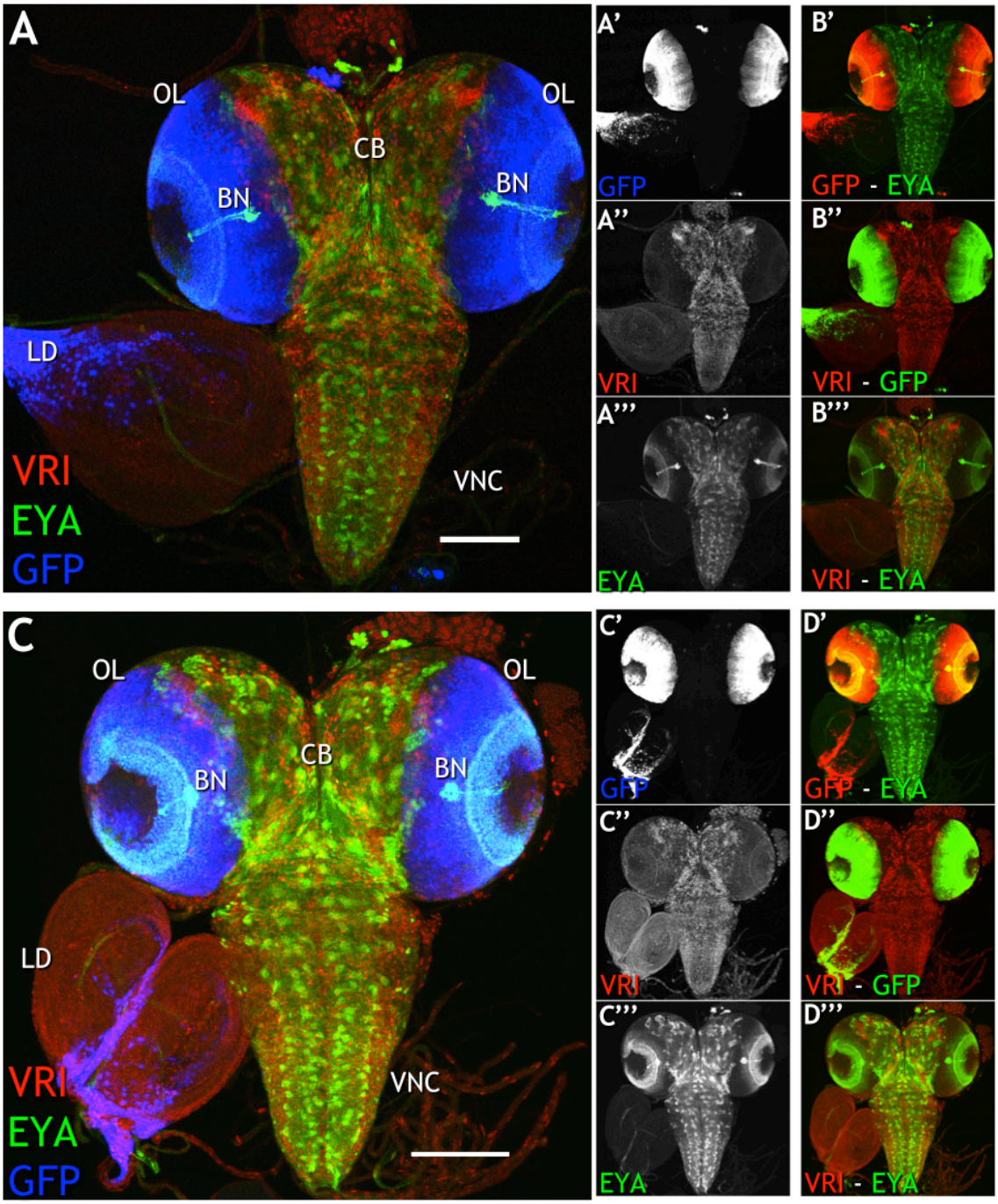

Figure 4.10 L3 CNS of *so7+VP*-Gal4 and *so7+VP*$^{[VP\text{-}mut]}$-Gal4 labelled for VRI and EYA. (A) Flattened Z-sections showing GFP expression mediated by *so7+VP*-Gal4 (A', blue in A) and immuno-labelled for VRI (A'', red in A) and EYA (A''', green in A). (B', B'', B''') two channel merge images of individual channels shown in A'-A''': GFP, red and EYA-IR, green (B'); VRI-IR, red and GFP, red (B''); VRI-IR, red and EYA-IR, green (B'''). (C) Flattened Z-sections showing GFP expression mediated by *so7+VP*$^{[VP\text{-}mut]}$-Gal4 (C', blue in C) and immuno-labelled for VRI (C'', red in C) and EYA (C''', green in C). (D', D'', D''') two channel merge images of individual channels shown in C'-C''': GFP, red and EYA-IR, green (D'); VRI-IR, red and GFP, red (D''); VRI-IR, red and EYA-IR, green (D'''). Key: dorsal to the top; OL, optic lobe; LD, leg disc; CB, central brain; VNC, ventral nerve cord; scale bar = 100μm; minimum *n=5*.

4.2.3.3 Adult CNS at different times of the day

The *so* intron 6 driver lines were also used to examine whether these enhancers mediate expression in the mature central brain clock cells and, if so, whether reporter expression changes over the course of the day. Adult brains were dissected at ZT3, 9, 15 and 21 and co-labelled for CLK and EYA. EYA has previously been reported to be expressed in the nuclei of several cells in the adult CNS but were not ascribed to be part of any previously described anatomical nuclei (Bonini *et al.*, 1998). Rather, the distribution of EYA-positive cells was considered to be as functional clusters that spanned anatomical brain regions. In addition to learning the positions of EYA-positive cells in relation to oscillator neurones, I was also interested to know whether EYA is rhythmically regulated. That there may be rhythmic regulation of EYA is suggested by data that indicate an involvement of TOY, an activator of EYA in developing eye discs, in regulation of *Clk* (Glossop *et al.*, unpublished data).

Oscillator neurones were marked using CLK-GP50 antiserum (Houl *et al.*, 2008). Houl *et al.* (2008) describe CLK-IR to be constitutive and indeed, I found that CLK signal is identical for all the tested genotypes and is also constitutively present during all four tested ZT times (Figures 4.12 and 4.14-16, plates 1 and 2 and Figure 4.13, plate 2, A, A'', B, B'', D, D'', E, E''; Figure 4.13, plate 1 A, A'', B, B'', D, D'', F, F'', G, G''). CLK was also detected in nuclei of glial cells that ensheathe the entire CNS, nuclei of the lamina monopolar neurones and the ocellar interneurones.

so10>GFP was expressed in a small number of cells that had a scattered distribution throughout the CNS and did not co-localise with CLK- or EYA-positive cells (Figure 4.13, plate 1 A, A', B, B', D, D', F, F', G, G'; plate 2 A, A', B, B', D, D', E, E'). GFP remained in the cytoplasm of some of these cells and spread through the processes, though morphology could not be accurately traced.

so7>GFP was present in cell bodies that lie between the lamina and the optic lobe (Figure 4.14, plates 1 and 2 A, A', B, B', D, D', E, E'). Expression was robust and seen as concentrated GFP between the lamina and optic lobe. Within the central brain, expression was apparent in numerous cells with a scattered distribution, as for *so10*>GFP. Again, co-expression with CLK or EYA was not observed either.

so7+*VP*>GFP and *so7*+*VP*$^{[VP\text{-}mut]}$>GFP show identical results for GFP expression within the adult CNS (Figures 4.15 and 4.16, plates 1 and 2, A, A', B, B', D, D', E, E'). Compared to *so7*>GFP, GFP is down-regulated in the central brain and up-regulated in the lamina monopolar cells and their processes.

In addition, as in the larval CNS, ectopic expression of EYA is seen in scattered neurones of the central brain (similar to *so7*>GFP expression); in the ocellar interneuronal nuclei and axons; and, in axons of the visual system (Figures 4.12 and 4.14-16, plates 1 and 2 and Figure 4.13, plate 2, A, A''', B, B''', D, D''', E, E'''; Figure 4.13, plate 1 A, A''', B, B''', D, D''', F, F''', G, G'''). Visual system axons include the Hofbauer-Buchner tract and other photoreceptor axons from, either, lamina interneurones between R1-R6 and the medulla, R7 and R8 direct projections to the medulla, or both.

The Hofbauer-Buchner tract (H-B tract) contains the axonal projection from the Hofbauer-Buchner eyelet (H-B eyelet), which is an extra-retinal, extra-ocular 'eyelet' that lies below the posterior margin of the compound eye and is formed during metamorphosis from the remnant of Bolwig's organ, the larval photoreceptive organ (Helfrich-Förster *et al.,* 2002). The H-B eyelet retains the photopigment Rhodopsin 6 (Rh6) and projection pattern of Bolwig's organ which has arborisations near the sLNvs. During metamorphosis, the l-LNvs differentiate and the H-B eyelet also arborises with these. Bolwig's organ is the only opsin-mediated photoreceptor in larvae and (Xiang *et al.,* 2010), together with cryptochrome, provides photic information to sLNvs for circadian rhythmicity in larvae (Malpel *et al.,* 2002). The eyelet's contribution in the adult is more complex as photic information for entrainment of the

LNvs for circadian rhythmicity is also provided by the compound eyes in addition to eyelet and cryptochrome (Helfrich-Förster *et al.*, 2001).

Endogenous EYA expression was not observed in afferent innervations to the optic lobes of control, *so10*>GFP or *so7*>GFP adult brains at any of the time points analysed. This was confirmed by increasing the laser power to maximum in order to reveal whether the extra EYA signal seen in *so7*+*VP*>GFP and *so7*+*VP*$^{[VP\text{-}mut]}$>GFP was an up-regulation of normal protein distribution that is usually below analysis threshold (data not shown). The normal distribution of EYA was nuclear and observed in control, *so10*>GFP and *so7*>GFP CNS, and which persisted in *so7*+*VP*>GFP and *so7*+*VP*$^{[VP\text{-}mut]}$>GFP lines; cells are categorised into five clusters within the central brain according to their anatomical location. I have labelled these clusters EYA+ve 1-5 and their positions relative to oscillator neurones are shown on Figure 4.12. EYA+ve 1, a large cluster of >40 cells in the posterior dorsal superior protocerebrum distributed amongst the DN1s and DN2s. EYA+ve 2, a large cluster of >40 cells in the lateral dorsal brain ventral to DN3s. EYA+ve 3, a large cluster of 20-30 cells in the anterior lateral ventral brain clustered from the LNds to the LNvs. EYA+ve 4, 3-5 cells close to the midline in the posterior dorso-medial superior protocerebrum. EYA+ve 5, 6 cells in the posterior ventro-medial brain. The EYA+ve 1 and 2 clusters were also described by Bonini *et al*. (1998). The central body neuropiles of fan-shaped body, ellipsoid body and noduli appeared to show EYA-IR although signal is not nuclear and does not show cell shape definition, rather, it is suggestive of background staining.

Two cells of the EYA+ve 1 group are co-labelled for CLK in all genotypes at all tested times of the day and their position indicates that they are the DN2s. In addition, one of the EYA+ve 2 cells sometimes co-labels for CLK and appears to be a large DN3. The heterogeneous DN3 oscillator neurone group consists of large and small cells that extend from posterior into anterior regions. Although this co-labelled EYA+ve 2 cell was seen within each genotype at each time-point, there was some inconsistency. The position of this cell within the DN3 group was always lateral but seen variously in an anterior or

posterior position and sometimes could not be distinguished from the surrounding cells.

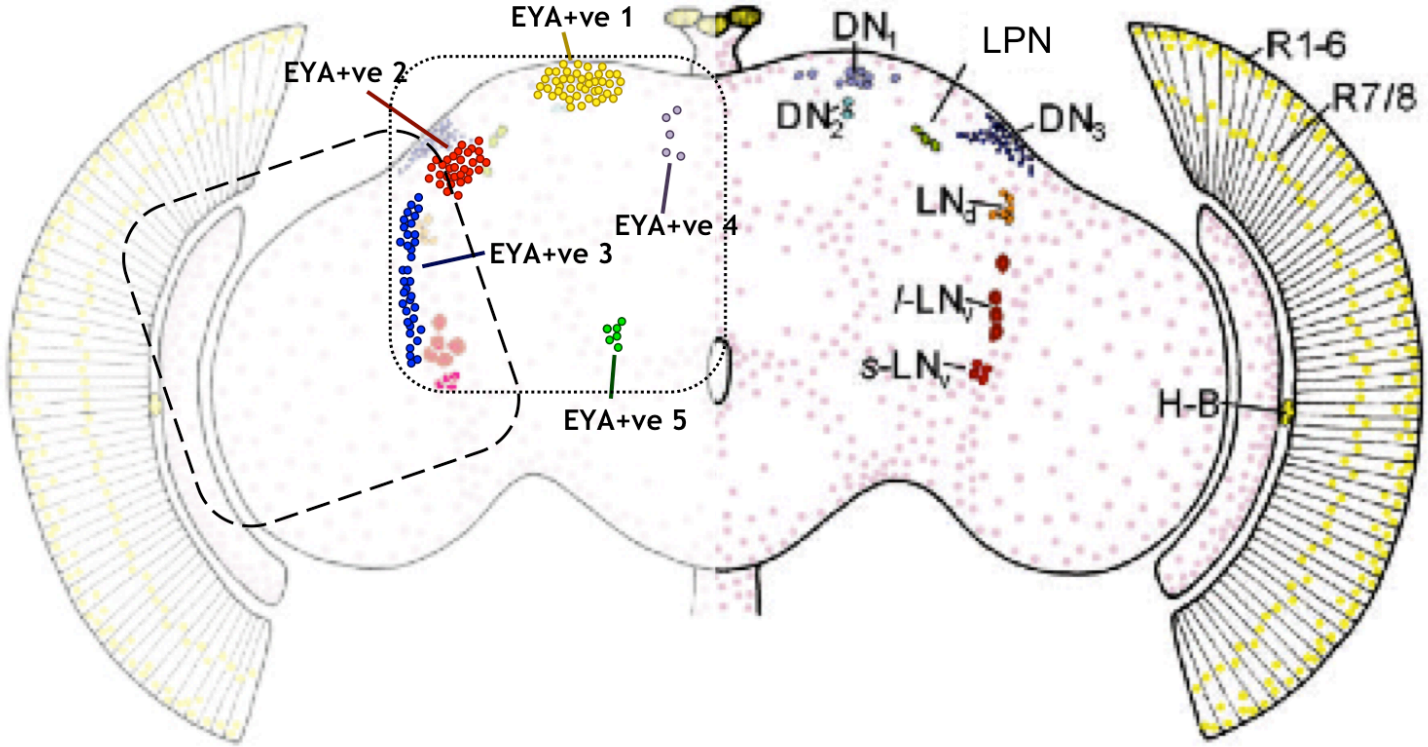

Figure 4.11 EYA and oscillator gene expressing cells in the adult *Drosophila* brain. Figure adapted from Helfrich-Förster (2003), left hemisphere of image has been faded in order to superimpose groups of cells showing EYA-IR from the current study (EYA+ve 1-5, represented by different colours for cells comprising individual groups). Dashed line box indicates optic lobe region shown in figures 4.12, 4.13 plate 2 and 4.14-4.16 A and D, figure 4.13 plate 1 A and F. Dotted line box indicates central brain region shown in figures 4.12, 4.13 plate 2 and 4.14-4.16 B and E, figure 4.13 plate 1 B, D and G. Original image maintained for the right hemisphere showing the oscillator neurone groups of the central brain: lateral neurons (LNd, LPN, l-LNv, s-LNv); dorsal neurons (DN1, DN2, DN3); R1-6: nuclei from photoreceptor cells 1 to 6, R7/8: nuclei from photoreceptor cells 7 and 8; H-B: photoreceptor cells of the Hofbauer-Buchner eyelets); glia shown as distributed pink cells.

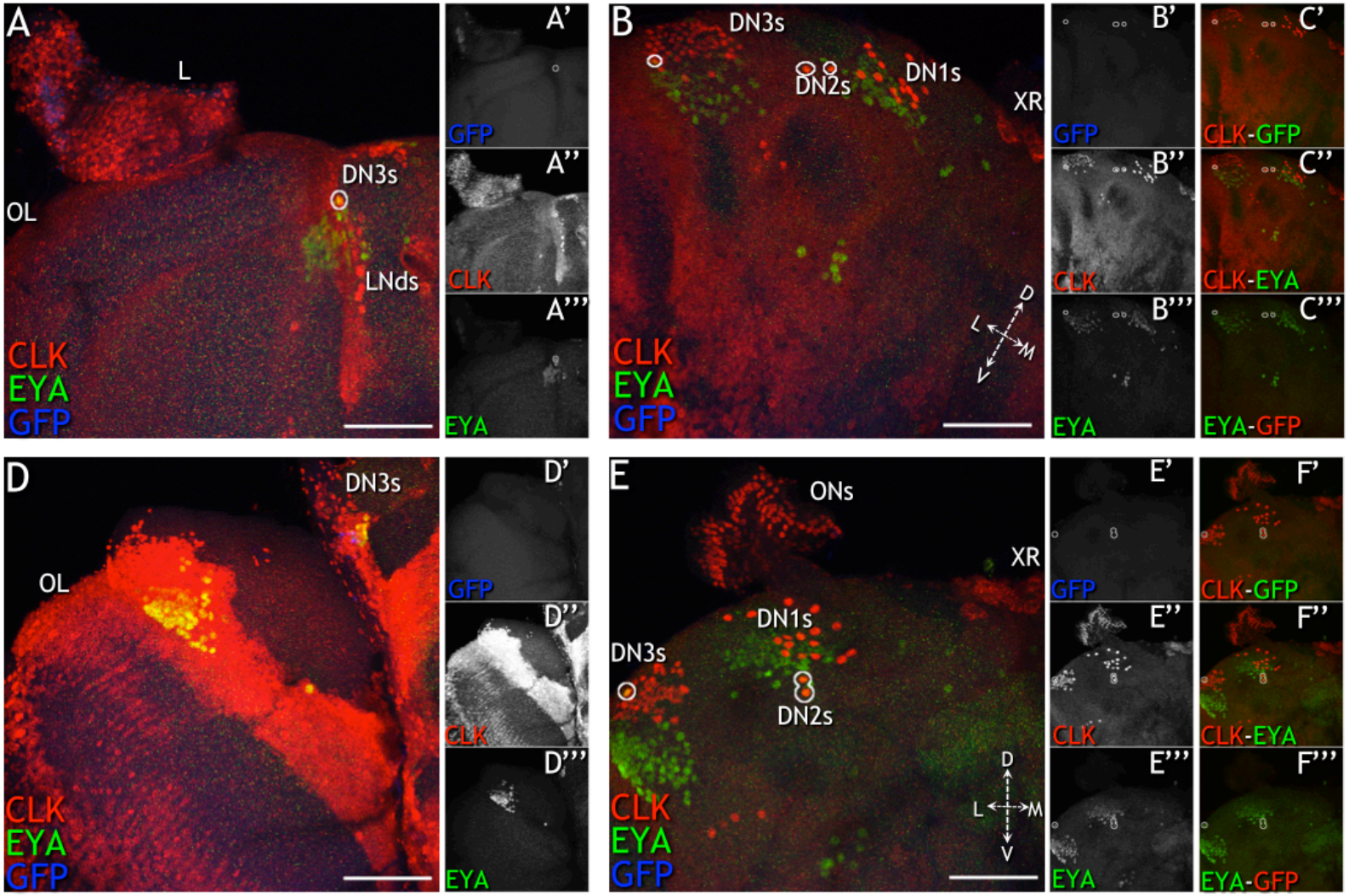

Figure 4.12, Plate 1 Wild-type control (*w*;+;+/*UAS-nGFP)* adult CNS at ZT3 and ZT9. Minimum *n=3* each, male and female; full legend on page 116.

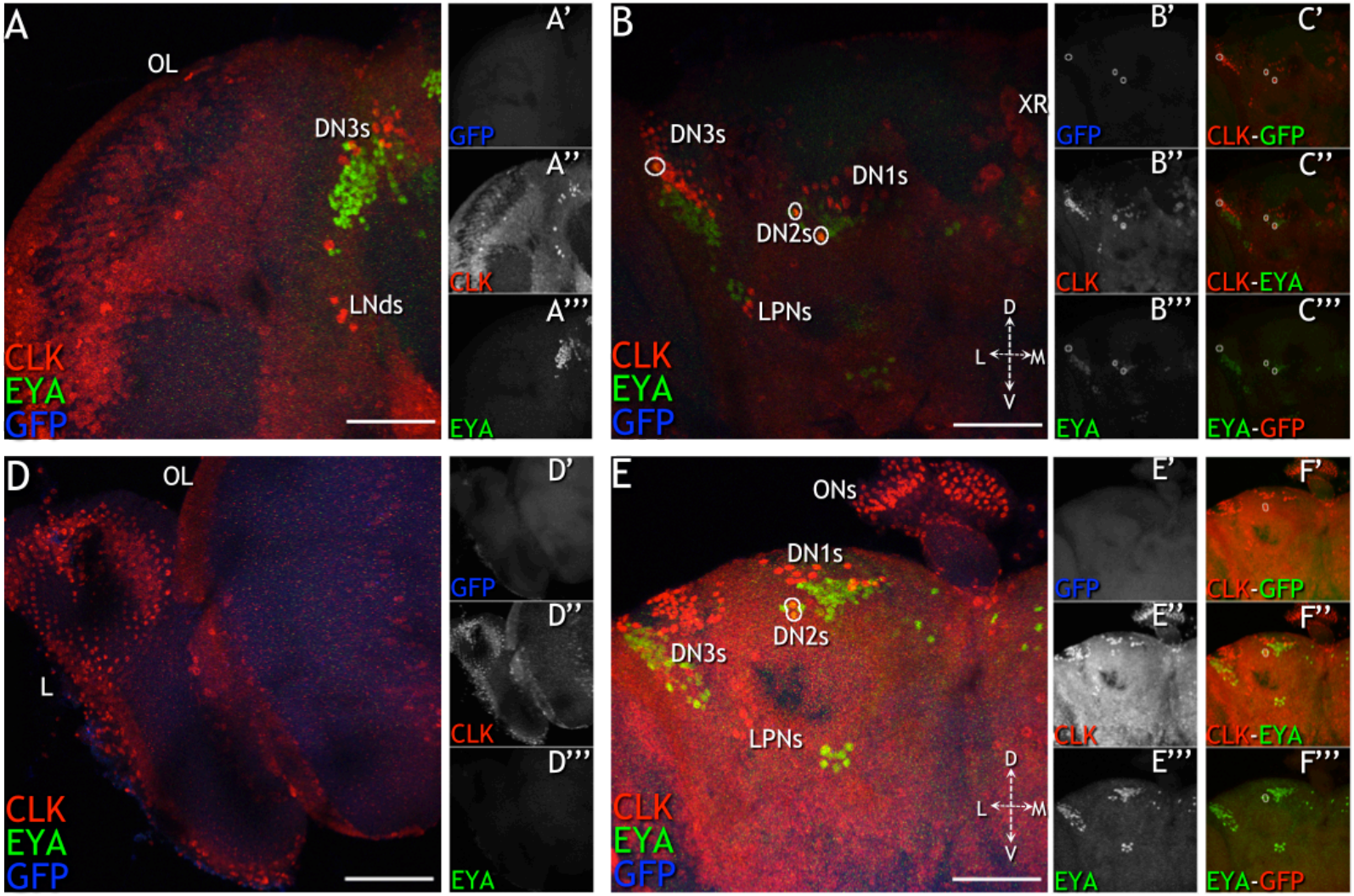

Figure 4.12, Plate 2 Wild-type control (*w;+;+/UAS-nGFP)* adult CNS at ZT15 and ZT21. Minimum *n=3* each, male and female; full legend on page 116.

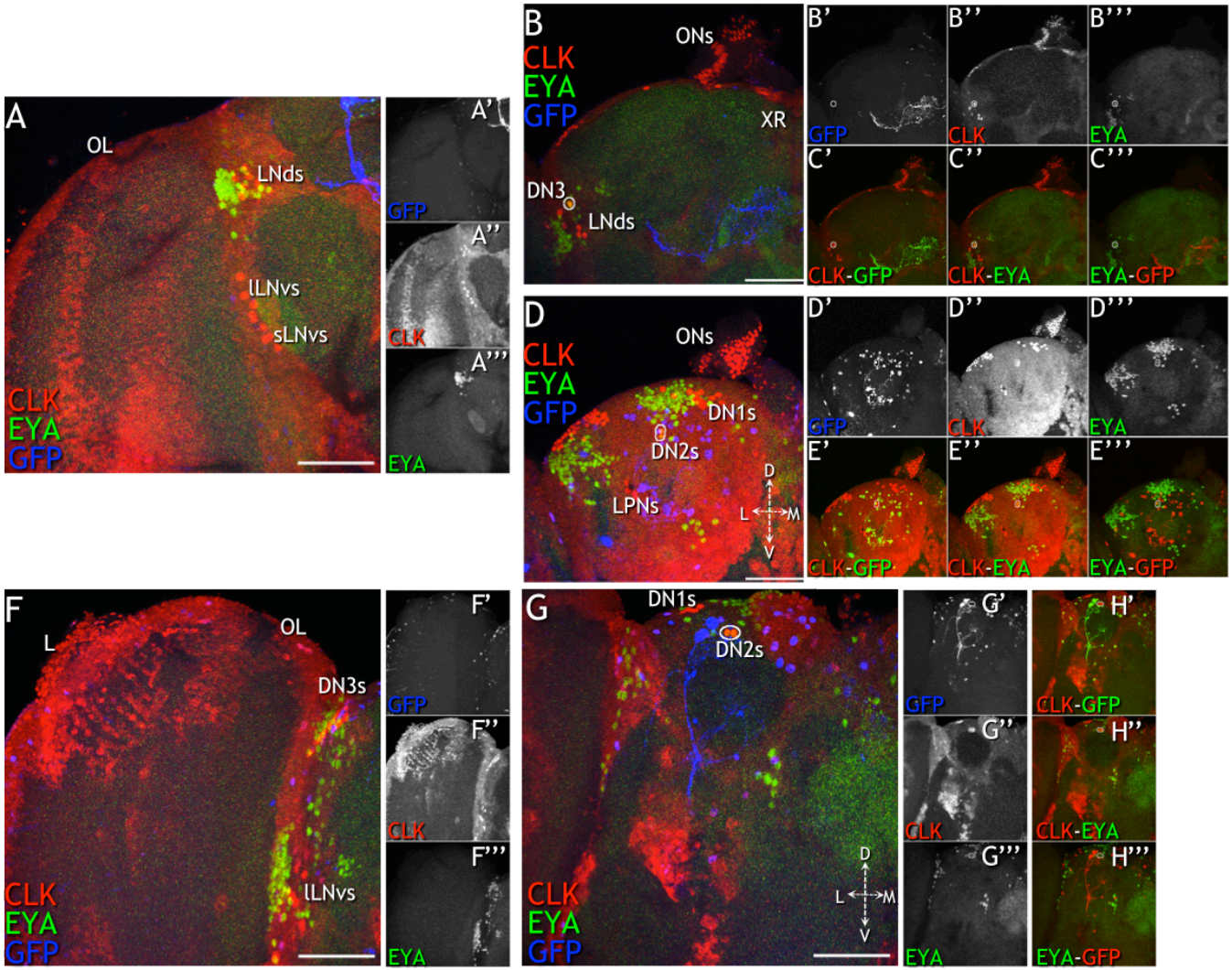

Figure 4.13, Plate 1 *so10-Gal4* adult CNS at ZT3 and ZT9. Minimum *n=3* each, male and female; full legend on page 116.

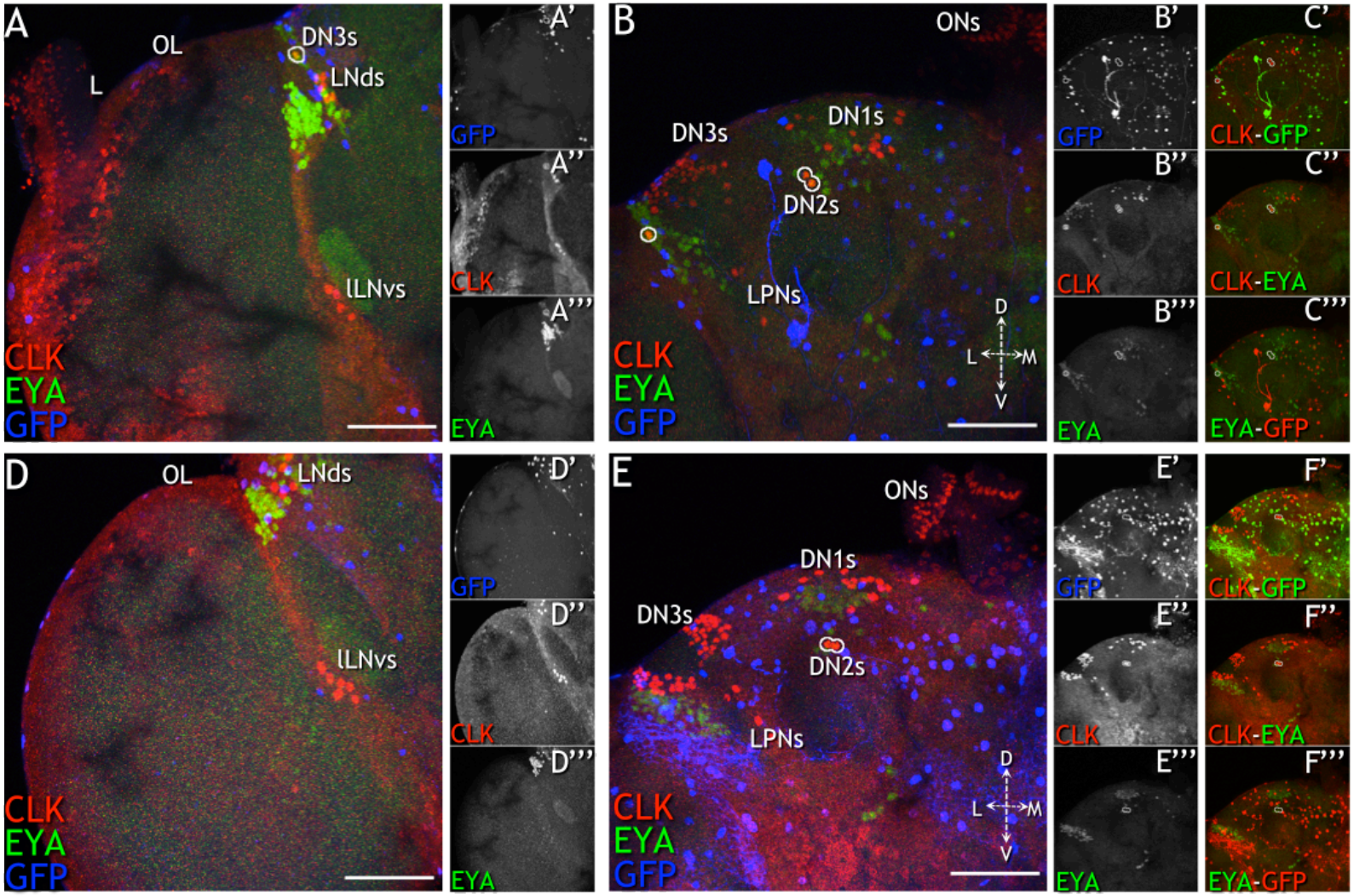

Figure 4.13, Plate 2 *so10-Gal4* adult CNS at ZT15 and ZT21. Minimum *n=3* each, male and female; full legend on page 116.

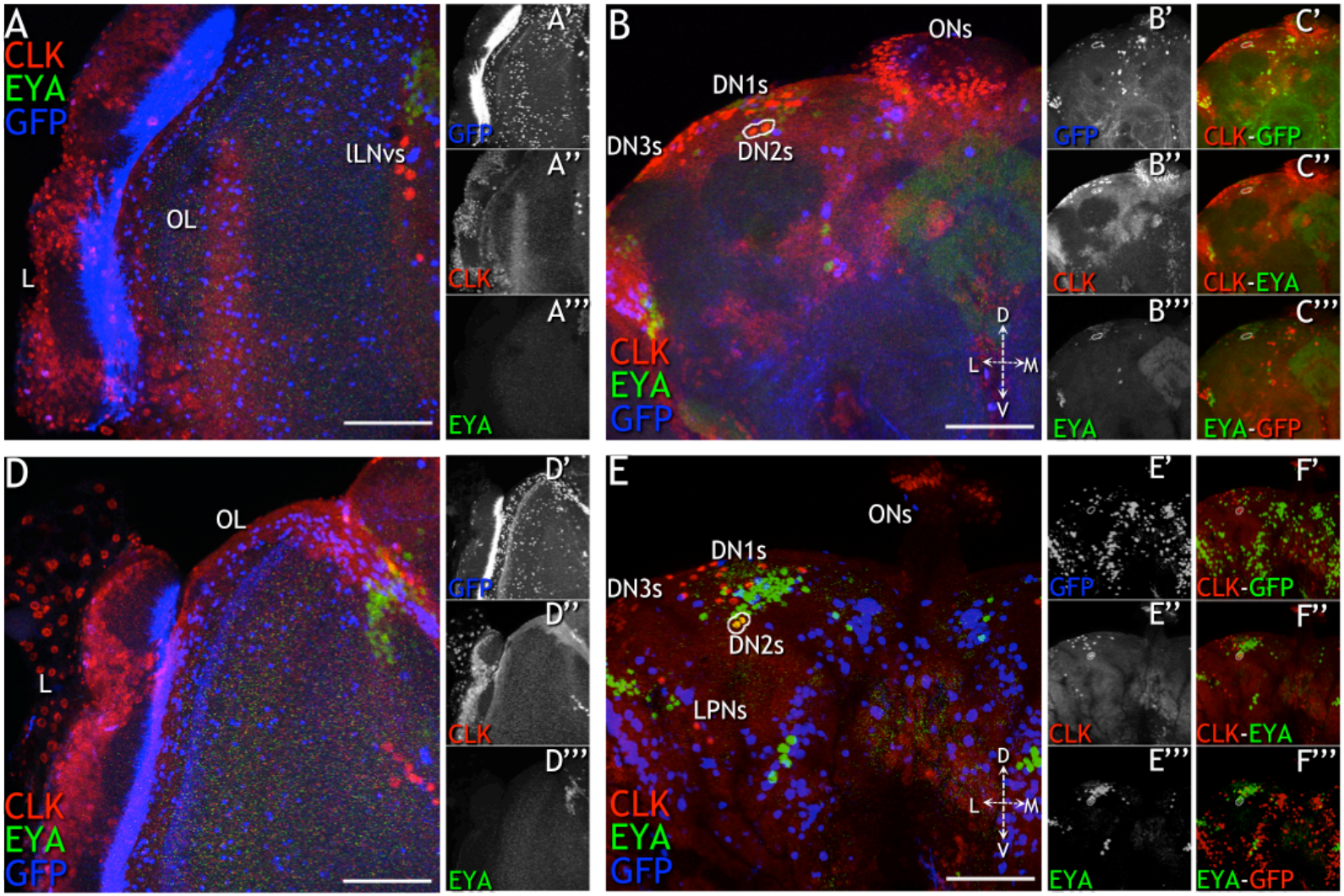

Figure 4.14, Plate 1 *so7-Gal4* adult CNS at ZT3 and ZT9. Minimum *n=3* each, male and female; full legend on page 116.

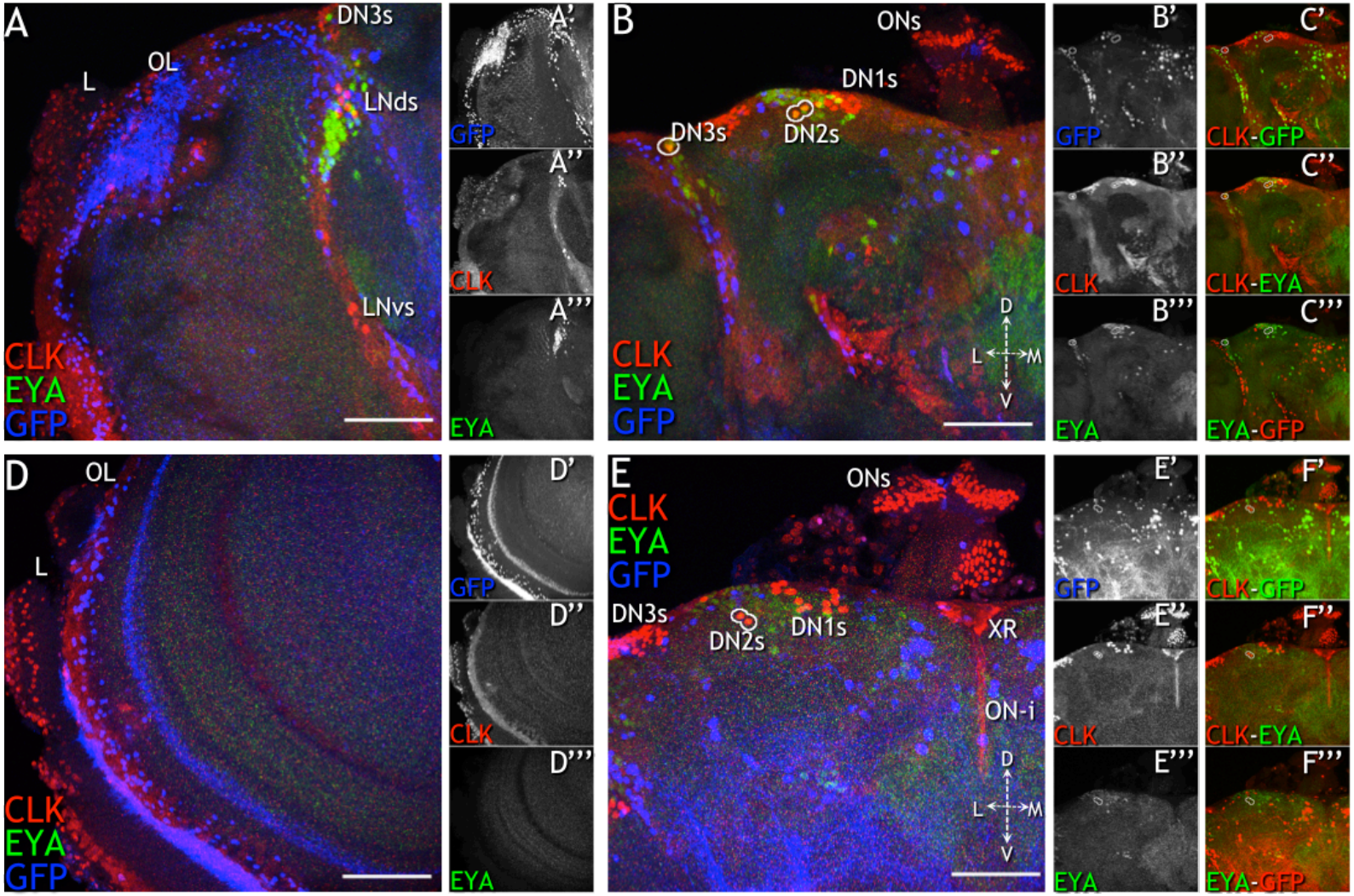

Figure 4.14, Plate 2 *so7-Gal4* adult CNS at ZT15 and ZT21. Minimum *n=3* each, male and female; full legend on page 116.

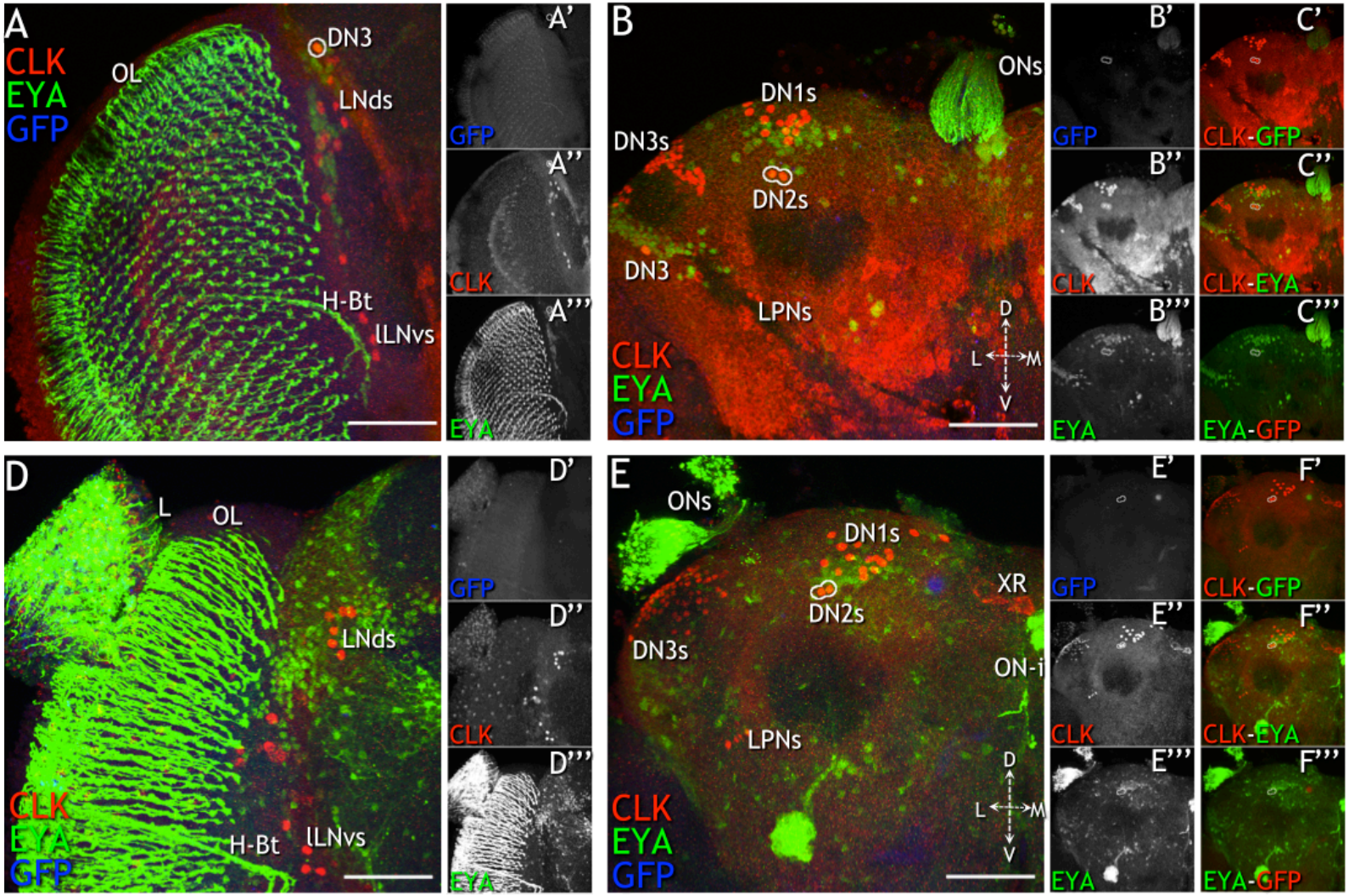

Figure 4.15, Plate 1 *so7+VP-Gal4* adult CNS at ZT3 and ZT9. Minimum *n=3* each, male and female; full legend on page 116.

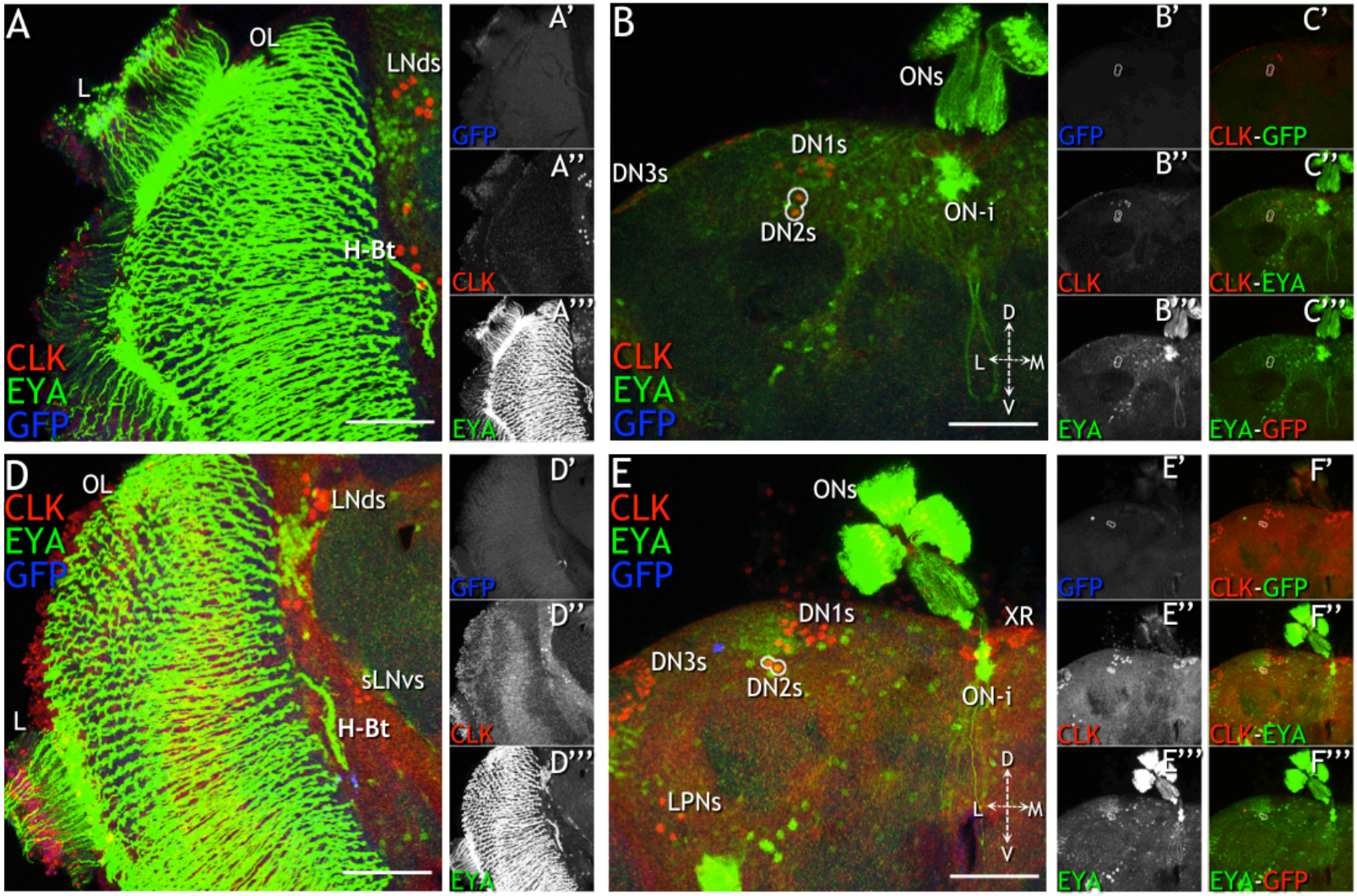

Figure 4.15, Plate 2 *so7+VP-Gal4* adult CNS at ZT15 and ZT21. Minimum *n=3* each, male and female; full legend on page 117.

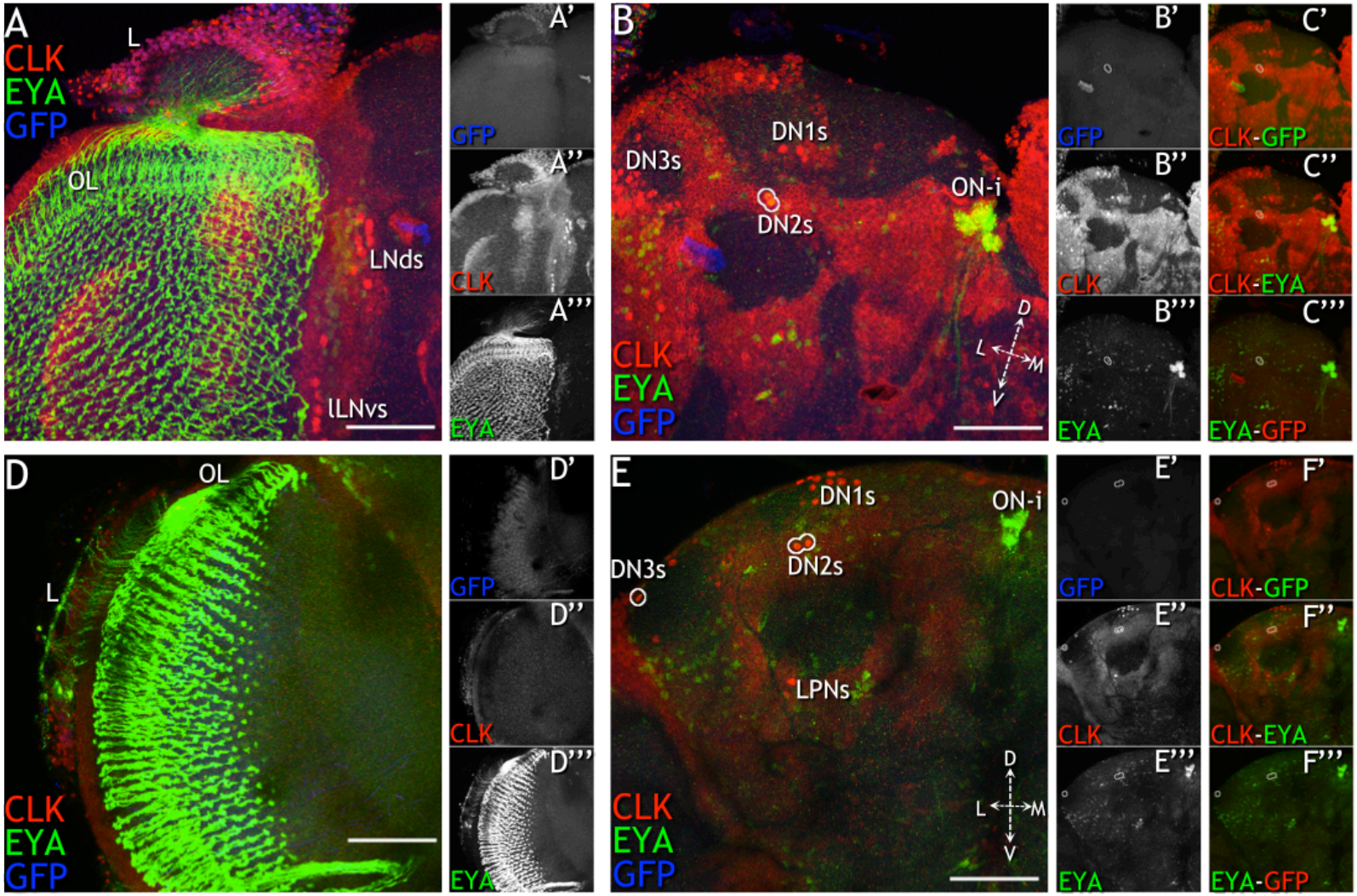

Figure 4.16, Plate 1 *so7+VP[VP-mut]-Gal4* adult CNS at ZT3 and ZT9. Minimum *n=3* each, male and female; full legend on page 117.

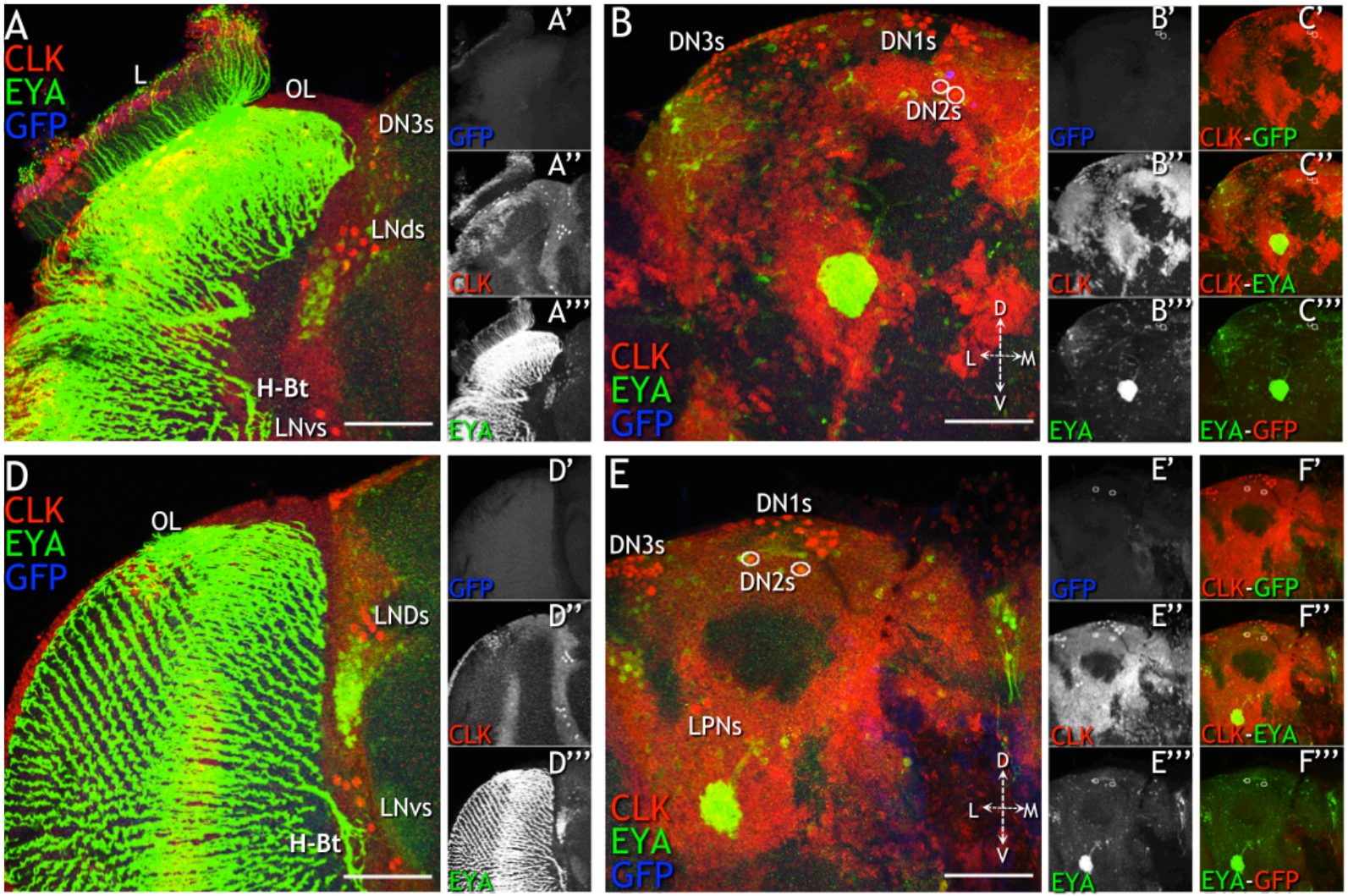

Figure 4.16, Plate 2 *so7+VP[VP-mut]-Gal4* adult CNS at ZT15 and ZT21. Minimum *n=3* each, male and female; full legend on page 117.

Figures 4.12-16 Adult brains expressing GFP and immuno-labelled for CLK and EYA. Plate 1 shows ZT3 and ZT9, Plate 2 shows ZT15 and ZT21. Left hemisphere of brain, midline is to the right and dorsal top, slight deviations of orientation of CNS are shown by representation of axes. Key: (D – V, dorsal ventral; L – M, lateral medial); circled cells are co-labelled for CLK and EYA; OL, optic lobe; L, lamina; ONs, ocellar interneurones; ON-I – ocellar interneuronal tract; H-Bt – Hofbauer-Buchner tract; DN1s, DN2s, DN3s, LNds, LPNs, lLNVs, sLNVs, – oscillator neurone groups; XR, cross-reactivity of donkey anti-guinea pig-Cy5 secondary antibody to SLOB neurones; scale bars are 50μm; minimum *n=3* each, male and female.

Figure 4.12, Panel 1 Wild-type control *w;+;+/UAS-nGFP* A – C’’’, (ZT3); D – F’’’, (ZT9). (A and D) Flattened Z-sections of optic lobe with some attached lamina (A only); individual channels for GFP (A’, D’), CLK (A’’, D’’) and EYA (A’’’, D’’’) also shown. (B, E) Flattened Z-sections of dorsal central brain with ocellar interneurones attached (E only); individual channels for GFP (B’, E’), CLK (B’’, E’’) and EYA (B’’’, E’’’) also shown. (C’-C’’’ and F’-F’’’) two channel merge images of individual channels shown in B’-B’’’ or E’-E’’’, respectively.

Figure 4.12, Panel 2 Wild-type control *w;+;+/UAS-nGFP* A – C’’’, (ZT15); D – F’’’, (ZT21). (A and D) Flattened Z-sections of optic lobe with some attached lamina (D only); individual channels for GFP (A’, D’), CLK (A’’, D’’) and EYA (A’’’, D’’’) also shown. (B, E) Flattened Z-sections of dorsal central brain with ocellar interneurones attached (E only); individual channels for GFP (B’, E’), CLK (B’’, E’’) and EYA (B’’’, E’’’) also shown. (C’-C’’’ and F’-F’’’) two channel merge images of individual channels shown in B’-B’’’ or E’-E’’’, respectively.

Figure 4.13, Panel 1 *so10*-Gal4 A – E’’’, (ZT3); F – H’’’, (ZT9). (A and D) Flattened Z-sections of optic lobe with some attached lamina (F only); individual channels for GFP (A’, F’), CLK (A’’, F’’) and EYA (A’’’, F’’’) also shown. (B, D, E) Flattened Z-sections of dorsal central brain with ocellar interneurones attached (B, D only); anterior (B) and posterior (D) of the same CNS; individual channels for GFP (B’, D’, G’), CLK (B’’, D’’, G’’) and EYA (B’’’, D’’’, G’’’) also shown. (C’-C’’’, E’-E’’’ and H’-H’’’) two channel merge images of individual channels shown in B’-B’’’, D’-D’’’ or G’-G’’’, respectively.

Figure 4.13, Panel 2 *so10*-Gal4 A – C’’’, (ZT15); D – F’’’, (ZT21). (A and D) Flattened Z-sections of optic lobe with some attached lamina (A only); individual channels for GFP (A’, D’), CLK (A’’, D’’) and EYA (A’’’, D’’’) also shown. (B, E) Flattened Z-sections of dorsal central brain with ocellar interneurones attached (E only); individual channels for GFP (B’, E’), CLK (B’’, E’’) and EYA (B’’’, E’’’) also shown. (C’-C’’’ and F’-F’’’) two channel merge images of individual channels shown in B’-B’’’ or E’-E’’’, respectively.

Figure 4.14, Panel 1 *so7*-Gal4 A – C’’’, (ZT3); D – F’’’, (ZT9). (A and D) Flattened Z-sections of optic lobe with some attached lamina (A only); individual channels for GFP (A’, D’), CLK (A’’, D’’) and EYA (A’’’, D’’’) also shown. (B, E) Flattened Z-sections of dorsal central brain with ocellar interneurones attached (E only); individual channels for GFP (B’, E’), CLK (B’’, E’’) and EYA (B’’’, E’’’) also shown. (C’-C’’’ and F’-F’’’) two channel merge images of individual channels shown in B’-B’’’ or E’-E’’’, respectively.

Figure 4.14, Panel 2 *so7*-Gal4 A – C’’’, (ZT15); D – F’’’, (ZT21). (A and D) Flattened Z-sections of optic lobe with some attached lamina; individual channels for GFP (A’, D’), CLK (A’’, D’’) and EYA (A’’’, D’’’) also shown. (B, E) Flattened Z-sections of dorsal central brain with ocellar interneurones attached; individual channels for GFP (B’, E’), CLK (B’’, E’’) and EYA (B’’’, E’’’) also shown. (C’-C’’’ and F’-F’’’) two channel merge images of individual channels shown in B’-B’’’ or E’-E’’’, respectively.

Figure 4.15, Panel 1 *so7+VP*-Gal4 A – C’’’, (ZT3); D – F’’’, (ZT9). (A and D) Flattened Z-sections of optic lobe with some attached lamina (D only); individual channels for GFP (A’, D’), CLK (A’’, D’’) and EYA (A’’’, D’’’) also shown. (B, E) Flattened Z-sections of dorsal central brain with ocellar interneurones attached; individual channels for GFP (B’, E’), CLK (B’’, E’’) and EYA (B’’’, E’’’) also shown. (C’-C’’’ and F’-F’’’) two channel merge images of individual channels shown in B’-B’’’ or E’-E’’’, respectively.

Figure 4.15, Panel 2 *so7+VP*-Gal4 A – C’’’, (ZT15); D – F’’’, (ZT21). (A and D) Flattened Z-sections of optic lobe with some attached lamina; individual channels for GFP (A’, D’), CLK (A’’, D’’) and EYA (A’’’, D’’’) also shown. (B, E) Flattened Z-sections of dorsal central brain with ocellar interneurones attached; individual channels for GFP (B’, E’), CLK (B’’, E’’) and EYA (B’’’, E’’’) also shown. (C’-C’’’ and F’-F’’’) two channel merge images of individual channels shown in B’-B’’’ or E’-E’’’, respectively.

Figure 4.16, Panel 1 *so7+VP*$^{[VP\text{-}mut]}$-Gal4 A – C’’’, (ZT3); D – F’’’, (ZT9). (A and D) Flattened Z-sections of optic lobe with some attached lamina; individual channels for GFP (A’, D’), CLK (A’’, D’’) and EYA (A’’’, D’’’) also shown. (B, E) Flattened Z-sections of dorsal central brain with ocellar interneurones attached; individual channels for GFP (B’, E’), CLK (B’’, E’’) and EYA (B’’’, E’’’) also shown. (C’-C’’’ and F’-F’’’) two channel merge images of individual channels shown in B’-B’’’ or E’-E’’’, respectively.

Figure 4.16, Panel 2 *so7+VP*$^{[VP\text{-}mut]}$-Gal4 A – C’’’, (ZT15); D – F’’’, (ZT21). (A and D) Flattened Z-sections of optic lobe with some attached lamina; individual channels for GFP (A’, D’), CLK (A’’, D’’) and EYA (A’’’, D’’’) also shown. (B, E) Flattened Z-sections of dorsal central brain with ocellar interneurones attached; individual channels for GFP (B’, E’), CLK (B’’, E’’) and EYA (B’’’, E’’’) also shown. (C’-C’’’ and F’-F’’’) two channel merge images of individual channels shown in B’-B’’’ or E’-E’’’, respectively.

4.3 Discussion

4.3.1 VRI binding sites at the eya and so loci

The sequence used for VRI-binding assays is based on that reported for E4BP4/ NF-IL3A (Cowell *et al.,* 1992), as VRI E4BP4/ NF-IL3A is 60% identical, equating to 93% similarity, over 68 amino acids of the DNA-binding, basic domain (George and Terracol, 1997). This site has previously been shown to be bound by VRI and is dependent on the intact basic domain (Glossop *et al.,* 2003). Although Glossop *et al.,* (2003) successfully used the E4BP4/ NF-IL3A binding site as basis for their work, it remains possible that there are small differences between DNA sequence recognition by VRI and E4BP4/ NF-IL3A. For this reason, the -5 and +5 positions of the binding site were not used for data mining. This strategy combined with determination of site recognition by VRI using EMSA revealed that VRI is indeed able to bind some sequences that are non-consensus at bases -5 and/or +5.

Discovery of several sites potentially recognised by VRI is suggestive of direct regulation of these genes by VRI, however, only a few sites were analysed. The sites selected for further analysis were those in closest proximity to

coding regions of the gene and, although enhancers may be found at great distances from the genes they regulate (reviewed by Levine, 2010), for this preliminary work, only these proximal sites were considered for further study.

4.3.2 Intron 6 of so contains a novel enhancer region – is VRI also involved?

A spontaneous mutation, *so*^{1}, has a deletion of 1.3kb within the sixth intron of *so* and results in loss of the compound eyes and ocelli (Cheyette *et al.*, 1994). At the time this work commenced, EY, TOY and SO were reported to regulate expression of *so* for the development of the adult visual system through interactions with the region of intron six deleted in *so*^{1} mutants (Niimi *et al.*, 1999; Punzo *et al.*, 2002; Pauli *et al.*, 2005). Using transgenic reporters and *in vitro* assays, this eye-specific enhancer (*so7*) was shown to be bound at five sites by TOY, three of those sites could also be recognised by EY and a sixth site was bound SO for autoregulation. Moreover, these regions induced reporter expression in the presumptive eye field and rescued the compound eye phenotype and partially rescued the ocelli-less phenotype.

The presence of six activators in close proximity to sites s3 and s4, here hypothesised to be bound by the negative regulator VRI, allows study of the normal regulatory region in transgenic flies. Although very useful for certain paradigms, EMSAs or *in vitro* assays using luciferase reporters in cell cultures are not accurate representations of *in vivo* relationships. In the case of cell cultures, the combination of factors present is different to that found endogenously and may generate false positives. Naturally, transgenic driver-reporter systems (Brand and Perrimon, 1993) have their limitations also – position effect variegation being the primary factor that may affect results, yet it remains one of the gold-standard techniques available for *Drosophila* research. Therefore, I used transgenic reporter analysis for studying variations of the enhancer located in intron six of *so* for assessing the influence of VRI regulation during eye development (and within the CNS) in a near-endogenous context.

It is important to note that I have analysed variations of proposed eye-specific enhancers from the sixth intron of *so* here. Enhancer activity within the CNS of larvae or adults has not been reported and I was interested in clarifying whether the enhancers were active within the CNS. I particularly wanted to examine the oscillator neurones of the central brain in adults as data is emerging that TOY is expressed within these cells and that TOY and SO binding sites are present in the *Clk* locus (Glossop *et al.,* unpublished results). In addition, there is an assumption being made here, that extension of the enhancer will necessarily reflect endogenous interactions with greater accuracy. Furthermore, as I was not able to obtain SO antibody for comparison of protein expression to enhancer activity, assessment of enhancer activity may be somewhat biased towards it's coincidence with EYA.

4.3.2.1 GFP expression in larvae

If VRI is a repressor influencing the *so7* enhancer, a transgenic reporter containing a larger portion of intron 6, from site s3 up to and including *so7* (*so7+VP*), would reduce GFP expression in the anterior eye disc and the PE and mutating the VRI sites of that construct (to make construct *so7+VP*$^{[VP\text{-}mut]}$) would show a pattern more closely resembling *so7*. In fact, in eye discs, the results showed quite the opposite, *so7+VP* increased the intensity but did show gross changes in the regional expression of GFP, although GFP was expressed in additional cells of ocelli precursors. In addition, mutating the VRI binding sites resulted in further up-regulation in intensity of GFP signal, yet regional expression was not affected. This suggests that the VRI sites in intron six do not act as an 'off switch' for this enhancer in the suggested regions. The increase in GFP intensity between *so7+VP* and *so7+VP*$^{[VP\text{-}mut]}$ may have resulted from a loss of VRI binding and de-repression – suggestive of fine tuning of enhancer activity. The persistence of GFP signal in the PE is surprising as EYA and SO (Bonini *et al.,* 1993; Serikaku and O'Tousa, 1994) are not expressed within that region yet *so7* does mediate expression in that region. Other variables, either *cis*-regulatory regions or *trans*-acting factors, must be influencing suppression of SO in the PE.

Enhancer activity in brains of L3 larvae showed some characteristics of that observed in the eye discs. Reporter expression mediated by *so10* was observed in the central brain, VNC and the outer optic anlagen. Expression of reporter by *so7* was observed in all the same regions as with *so10* but in many more cells; only in the outer optic anlagen of brains of both, *so10* and *so7* drivers, was co-expression with EYA observed. Extension of *so7* to *so7+VP* reduced expression of GFP in the VNC and the central brain but increased GFP expression in the outer optic anlagen. As seen in eye discs, mutation of the VRI sites did not change this expression pattern but intensity of GFP expression appeared to have increased. GFP expression in the outer optic anlagen appears restricted to a subset of lamina precursors by the *so10* driver and expanding to additional lamina precursors by the *so7* driver (Yasugi *et al.*, 2008). Cells of the entire outer optic anlagen appear to be expressing GFP mediated by the *so7+VP* and *so7+VP*$^{[VP\text{-}mut]}$ drivers (Yasugi *et al.*, 2008). The reduction of GFP reporter in VNC and central brain suggests that *so7+VP* contains regulatory sites that refine expression mediated by this enhancer to regions connected to the visual system. In both, eye discs and larval brain, observed differences are large between *so7* and *so7+VP* but minimal between *so7+VP* and *so7+VP*$^{[VP\text{-}mut]}$ indicating that the role of VRI at this time within the CNS may be for minor adjustment of the *so* intron six enhancer activity.

4.3.2.2 GFP expression in adult CNS and oscillator cells

Similarly to the larval CNS, *so10* and *so7* mediate a scattered distribution of GFP reporter within the central brain, with an increased number of cells expressing GFP with the *so7* driver. With the *so7* driver, GFP was also observed between the lamina and the optic lobe but could not be localised to cells definitively. Neither *so10* nor *so7* drove GFP in the same cells that showed either, CLK- or EYA- IR signals. Expansion of the enhancer to *so7+VP* or *so7+VP*$^{[VP\text{-}mut]}$ down-regulated expression of GFP in the central brain but increased expression of GFP in the lamina monopolar cells. As suggested for the observations of reporter expression in larval brains, intervening DNA sequence between the VRI sites and the *so7* enhancer is likely being bound by

other regulatory factors that orchestrate the changes observed between *so7* and *so7+VP* enhancer activity. In addition, absence of GFP in oscillator neurones of the brain indicates that the selected regions of the intron are not directing expression of *so* in these cells. If *so* is expressed in the central brain oscillator neurones, other *cis*-regulatory regions will be mediating this expression.

4.3.3 EYA expression within the CNS

4.3.3.1 Endogenous EYA expression in distinct groups of cells

Within the larval CNS, EYA expression in the outer optic anlagen appears to be in the presumptive lamina and neuroepithelium. The lamina precursor cells also express DAC and, together, with expression of *so* suggested by the enhancer driver lines, may be an indication that similar regulation to that observed in eye discs is taking place (Yasugi *et al.*, 2008). Thus, in addition to patterning differentiation of the sensory apparatus of the visual system, *so* appears to also influence the development of the optic lobe (Yasugi *et al.*, 2008). During embryonic development expression of EYA and *so* is observed in neurogenic regions (Kumar and Moses, 2001c) and it is unsurprising that EYA is expressed within the CNS, however, these regions have yet to be described and extensive further study is required to reveal their function.

I have shown five distinct clusters of EYA expressing cells in the adult brain, only two of these were described by Bonini *et al*. (1998) who described them to be within functional rather than anatomical clusters. As for what the function may be has yet to be described. There may be some part played within the oscillator neurones – two cells of EYA+ve 1 group (see Figure 4.12) also show CLK-IR and appear to be DN2 neurones; one cell of the EYA+ve 2 group also shows CLK-IR and appears to be one of the large DN3 neurones. Shafer *et al*. (2006) found that the DN3 group consisted of heterogenous cells – small and large that also differed in reporter gene expression; these cells receive input from the LNs via the PDF receptor (Helfrich-Förster *et al.*, 2007;

Im and Taghert, 2010). DN2 cells meanwhile, are not directly responsive to LD cycles but are instead synchronised to LD by LNs via PDF signalling (Picot *et al.,* 2009). In larvae, the DN2s appear to be the thermocycle response integrators of the oscillator neurone network. As to how EYA fits into the function of these cells – whether it is within oscillator regulation or not requires further study. As we move into a time for finer dissection of oscillator neurone interactions at the level of individual group communication, EYA provides an additional avenue for investigation.

4.3.3.2 Interference of EYA expression by so7+VP – epistatic relationship or insertion position effect?

A wholly unexpected result was that EYA was up-regulated in many cells of the ventral nerve cord and central brain for both transgenic drivers generated in this study. Similar observations were made in adult brains – EYA was up-regulated in tissue from *so7+VP* compared to *so7*. It is possible that the insertion site 51C has an epistatic relationship to EYA and this is the first hypothesis that needs to be tested. Use of two independent sites for insertion of the transgene should, ideally, have been used as a control measure together with generation of an additional transgenic line of the *so7* enhancer at the same insertion sites for direct comparison. In the absence of those controls, immuno-staining of CNS from a fly line with an insertion of a UAS responder (i.e. sequence that is not recognised by endogenous *Drosophila* factors) at site 51C will also reveal whether this phenomenon is a result of the insertion locus. Another possibility is the introduction of non-coding RNAs via the extended enhancer element.

The nearest characterised gene from the insertion target site used for transgenics made in this study, *so7+VP* and *so7+VP*$^{[VP\text{-}mut]}$, *M-Spondin,* is 18.9kb upstream. This gene had been recovered in an enhancer trap screen for genes expressed in PRs that found that promoter-less *Gal4* inserted 179bp upstream of *M-spondin* showed GFP and lacZ expression in the R7 PRs, lamina and medulla (Mollereau *et al.,* 2000). However, the 51C landing platform used as the insertion site for transgenic constructs in this study is 18.9kb from the

position identified in the enhancer trap study by Mollereau *et al*. (2000). Although this distance does not preclude it from also acting as an enhancer trap of *M-Spondin* (Levine, 2010), observations of GFP expression mediated by *so7+VP* and *so7+VP*$^{[VP\text{-}mut]}$ as well as the pattern of EYA up-regulation suggest that it is not merely an enhancer trap.

Firstly, *so7*>GFP in larval VNC correlates somewhat with the position of cells in which EYA is up-regulated in *so7+VP*>GFP – GFP expression is lost in those cells in the latter and EYA is up-regulated. The implication here being that the extended region of the *so7+VP* driver contains sites for factors that co-repress *eya* and *so* and that an additional third copy of the region (the first and second being the endogenous copies on each of the homologous chromosomes) is saturating these repressors – preventing their endogenous role of down-regulating EYA. Next, similarly, the scattered distribution of GFP in adult central brains mediated by *so7* appears to be reflected in brains from the *so7+VP* line but in the expression of EYA rather than GFP. In addition, up-regulation of EYA is observed in cells that do not express *M-spondin*, namely, the ocellar interneurones, the H-B tract and additional compound eye PR axons than R7. There is expression within the lamina, which could result either from the interference with epistatic relationships proposed here or due to some enhancer trap effect of *M-spondin*. It must be conceded that the dramatic increase in EYA is puzzling because, despite the hypothesised alterations in gene regulation in *trans,* increases to such an extent would not be expected. Moreover, EYA is distributed through the cytoplasm, thus far only nuclear localisation of EYA has been described (Bonini *et al.,* 1993); although the aberrant localisation may be attributed to the large amount of EYA protein present. However, this interpretation, though intriguing, must be regarded with caution pending the results from control experiments using flies with a different transgene inserted at site 51C and use of different insertion sites for *so7+VP*.

The gene *CG11145* is present on the minus strand within the sixth intron of *so* and is positioned and oriented such that *so7+VP* is 187bp upstream, the VRI

site s3 being proximal. A small gene of three exons spanning only 690bp from transcriptional start site to end (including introns), it has yet to be annotated with a molecular function or biological process (Tweedie *et al.*, 2009) but one annotated transcript has been described from the cDNA library described in the second release of the *Drosophila* Gene Collection (Stapleton *et al.*, 2002). As there is no data available at present it is possible that regions adjacent to *CG11145* in intron six of *so* regulate this gene which may itself regulate EYA expression.

Chapter 5 eya and so RNA expression over the circadian day

5.1 Introduction

Earlier studies have primarily examined *eya* and *so* gene or protein expression in embryos or larval eye discs (Kumar and Moses 2001a and 2001b; Markstein *et al.,* 2002; Chen *et al.,* 1999; Curtiss and Mlodzik, 2000; Halder *et al.,* 1998; Niimi *et al.,* 1999). Bonini *et al* (1998) show EYA protein is present in cone and pigment cells of ommatidia, in medial cells of ocelli and in clusters in the CNS. Serikaku and O'Tousa (1994) describe SO immunoreactivity in nuclei for the PRs R1-R7, ocelli and in the optic lobe.

A novel technique that can isolate mRNA from specific tissues by transgenic expression of an RNA poly-A binding protein (PABP) utilised a rhodopsin-1 driver line (Yang *et al.,* 2005). PABP was expressed in PRs R1-R6 and isolated mRNA was compared to whole head mRNA from wild-type flies. Although this method does not define the entire transcriptome of R1-R6, it is likely isolating actively expressed transcripts. This approach found that *eya* and *so* transcript levels were >2-fold compared to whole head. Values were provided for *so* but not *eya* (listed in supplementary information) and a dataset has been assembled for the Affymetrix microarray data series of this experiment (Gene Expression Omnibus profile accession number GSE1790, DataSet GDS2479). Inspection of the data indicates that the percentile rank for *so* in whole heads is 55-65% and 80-85% within R1-R6. Percentile rank for *eya* is higher at 70-75% in whole head and 90-98% within R1-R6. These data suggest that, in the adult head, *eya* and *so* transcripts are present PRs R1-R6, and, in the head/ brain of flies that lack compound eye PRs and ocelli (i.e. *eya* mutant). Also indicated is that isolation of R1-R6 PABP-bound transcripts, alters the expression level rank of *eya* and *so* within this trancriptome – raising their profile compared to

whole head. Importantly, the time of day at which samples were collected is not indicated in this study.

The data presented in this chapter, taken together with that by Bonini *et al* (1998), Serikaku and O'Tousa (1994) and Yang *et al* (2005) all indicate that *eya* and *so* transcripts and proteins are expressed within the visual system and the central brain. Protein expression has also been shown within the visual system for both of these genes and, in the case of EYA, is also observed within the central brain at four tested time points (Chapter 4). However, as observed for CLK expression within circadian neurones, protein is constitutively present despite cyclical changes in transcript levels (Glossop *et al.,* 2003; Houl *et al.,* 2006 and 2008). Photoreceptors form the largest complement of oscillator neurones of the adult head (Cheng and Hardin, 1998) and their physiology is influenced by circadian and light changes (Barth *et al.,* 2010). In addition, *eya* and *so* are major upstream determinants of photoreceptors during development (reviewed in Kumar, 2009a and 2009b; Jemc and Rebay, 2007a) and are present in mature photoreceptors (Bonini *et al.,* 1998; Serikaku and O'Tousa, 1994; Yang *et al.,* 2005). Visual system physiology has been shown to alter in a circadian manner (Cheng and Hardin, 1998; Barth *et al.,* 2010). For this interaction between time of day and physiology, there must be communication between the circadian oscillator and the physiological programmes of the eye. Thus far correlations are shown between circadian disruptions on visual functions but molecular links have yet to be established. I hypothesise that circadian factors interact with upstream PR determinants, e.g. *eya* and *so,* to influence changes in physiology. As yet, a time course of *eya* and *so* expression has not been described.

I was interested in examining *eya* and *so* transcript localisation within whole heads and, in addition, whether there were photo-dependent and/ or circadian-regulated changes in transcript expression within and between different regions. Using anti-sense RNA probes directed against *eya* and *so,* I show here preliminary qualitative analyses that reveal that both transcripts are localised to similar regions of the visual system and central brain.

Furthermore, by comparing head sections from flies collected every 4hrs across a 12:12 L:D cycle, it is evident that *eya* and *so* mRNA levels are not constitutively expressed in the brain or compound eye. For *eya,* transcripts are clearly visible during the early light phase (ZT2, 6) but decline to low/ undetectable levels at the end of the light phase and early dark phase (ZT10, 14) before rising in the mid-late dark phase (ZT18, 22). For *so,* transcript levels are high throughout the light phase and early dark phase (ZT2, 6, 10, 14) but decline to low/ undetectable levels in the mid-late dark phase (ZT18, 22). Hence, *eya* and *so* expression are both rhythmic but they show different phasing in the time at which trough levels are reached. Similar results were observed in oscillator-deficient cyc^{01} mutant fly heads. This indicates that the expression of *eya* and *so* is regulated, at least in part, via a circadian-independent mechanism and, hence, predominantly by photoperiod. However, in the cyc^{01} mutant, the intensity of signal of both, *eya* and *so*, was elevated in the visual system, suggesting that the presence of a functional circadian mechanism may be necessary to dampen peak levels of expression in the PRs. Together, the results of this chapter suggest that *eya* and *so* expression in the oscillator (PRs) and non-oscillator (central brain) cells in the adult are predominantly regulated by photoperiod, but in oscillator cells the circadian mechanism may modulate this expression by damping the peak expression of both genes.

5.2 Results

Immunological staining of larval and adult CNS reveals that EYA protein is expressed in several cell clusters. An enhancer element from intron 6 of *so*, and expansions thereof developed in this study, did not mediate reporter gene expression in the same cell clusters as EYA within the CNS. Here, I show *in situ hybridisation* against the *eya* and *so* mRNA transcripts in whole adult head in wild type and oscillator deficient cyc^{01} mutants over a 24-hour period.

Frontal brain sections were applied to slides sequentially to ensure that all samples within a genotype and time of day cohort are from the same set of

animals across the set of RNA probes used. Sense probes did not hybridise at any time point in either genotype. On wild type adult heads, anti-sense probes for *eya* and *so* both hybridised to similar regions of the brain (Figures 5.1-6, images shown here are sections between the ocelli and proboscis along the antero-posterior axis). Signal was seen in (1) components of the visual system: PRs R1-R7, R8 and/ or lamina, lateral medulla and the ocellar region. (2) Within the central brain: dorsal superior protocerebrum, dorso-lateral and ventro-lateral regions. In more posterior sections, staining appeared to encircle the mushroom bodies and extend to the midline. Changes were observed in hybridisation over the course of the day and were synchronous between the visual system and central brain signals but the two different genes showed different phases. Hybridisation of *eya* probes was seen at ZT2, 6, 18 and 22 but reduced to background levels during ZT10 and 14. Hybridisation of *so* probes was high during ZT2, 6, 10 and 14 and reduced to background levels at ZT18 and 22.

It was predicted that any rhythms in *eya* and *so* transcript levels must be driven, either, by the light-dark cycle, or by the circadian clock. To distinguish between these possible mechanisms, *eya* and *so* transcripts were monitored in the oscillator-deficient cyc^{01} mutant background. Generally, the same expression trend observed in wild type head sections persists in cyc^{01} head sections – similar visual system and central brain regions show probe hybridisation; and the down-regulation of *eya* at ZT10 and 14 (compare Figures 5.3, 5.4), and *so* at ZT18 and 22 is maintained (compare Figures 5.5 and 5.6). Preservation of the signals observed in control flies indicates that the oscillator is not necessary for regulating rhythmic expression of these two genes. However, hybridisation signal intensity is higher in the visual system of cyc^{01} head sections indicating that, in the presence of a functioning oscillator, *eya* and *so* transcript levels appear to be dampened.

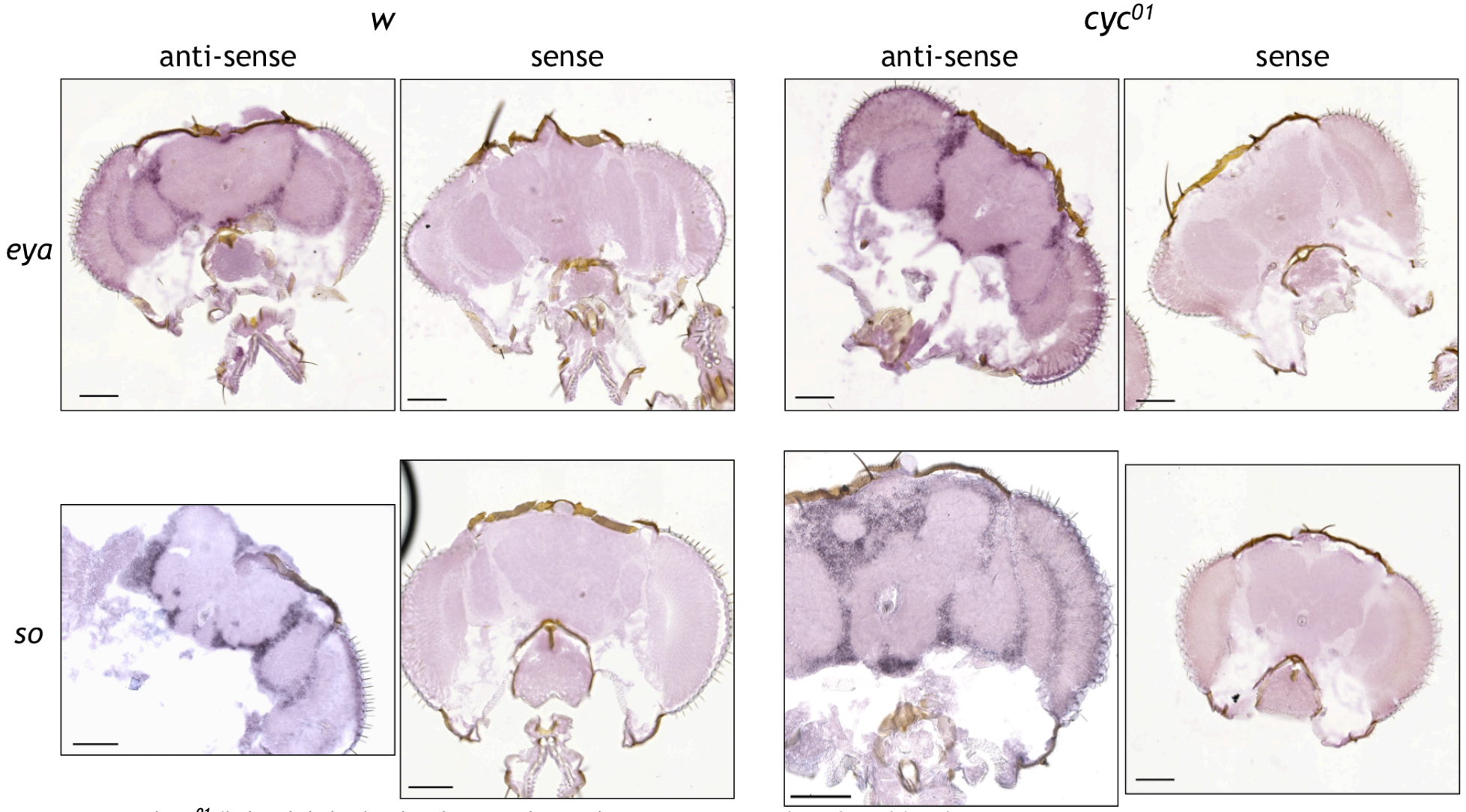

Figure 5.1 *w* and *cyc*^{01} fly heads hybridised with *eya* and *so* probes at ZT2. *n=10* each, male and female.

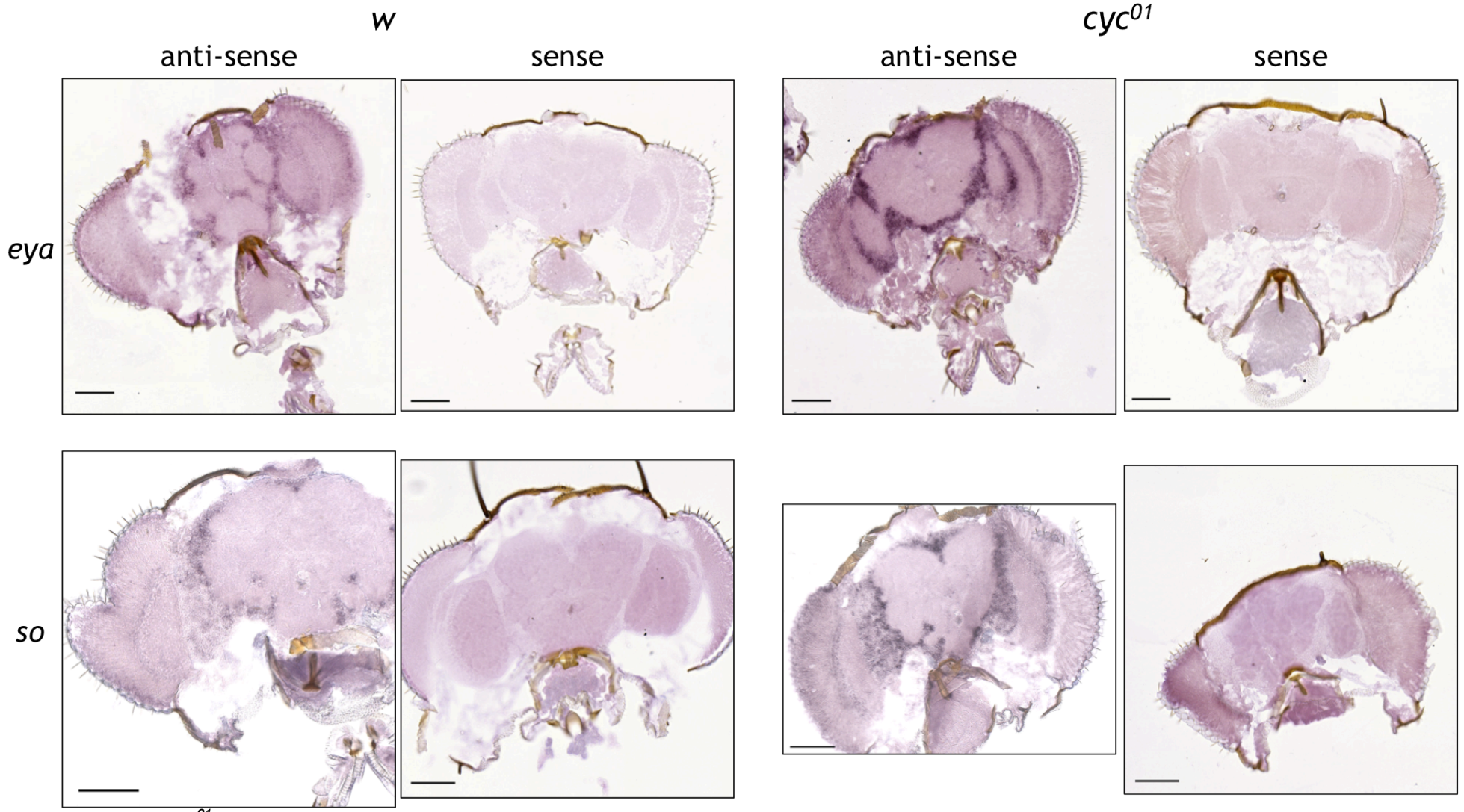

Figure 5.2 *w* and *cyc*^{01} fly heads hybridised with *eya* and *so* probes at ZT6. *n=10* each, male and female.

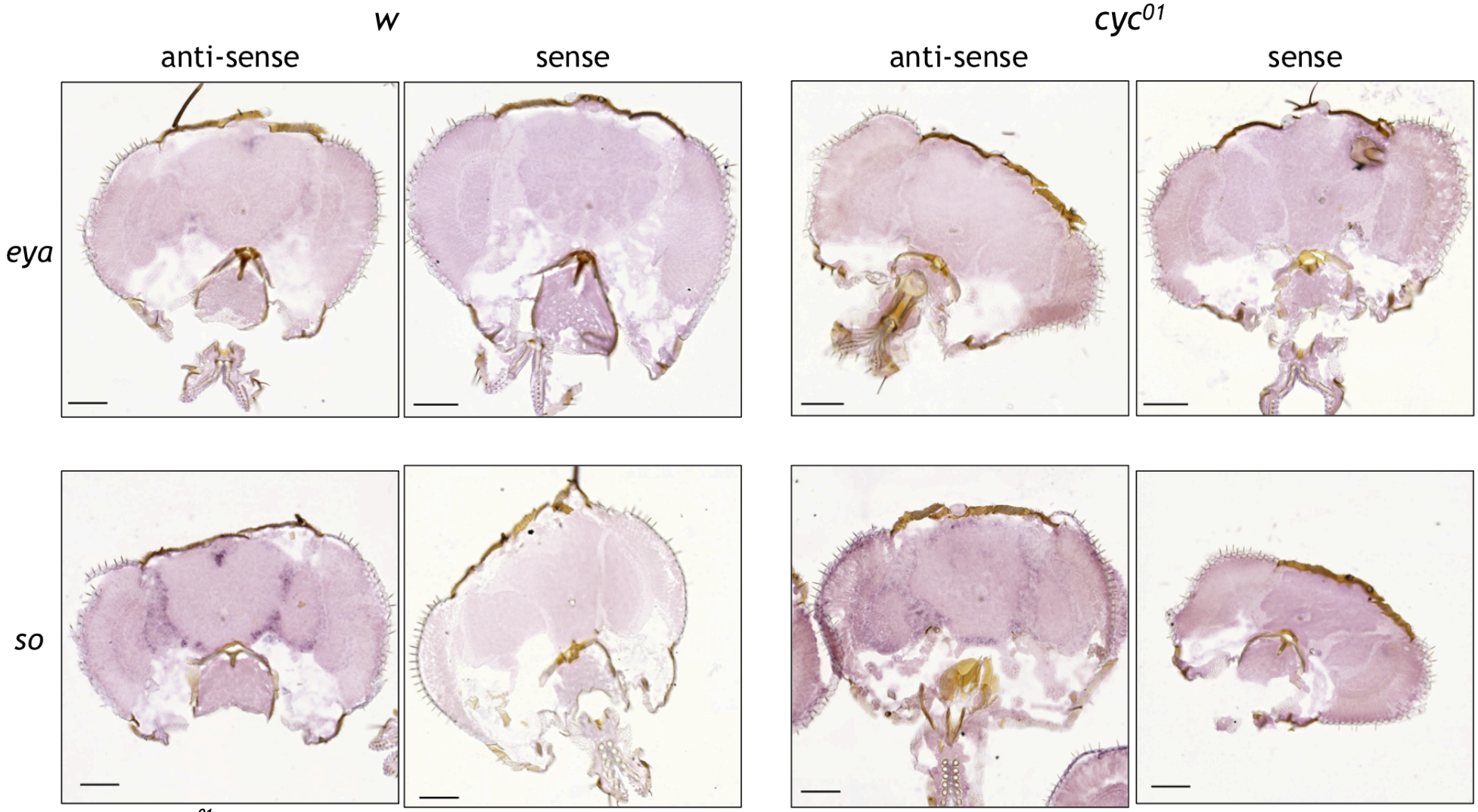

Figure 5.3 *w* and *cyc*^{01} fly heads hybridised with *eya* and *so* probes at ZT10. *n=10* each, male and female.

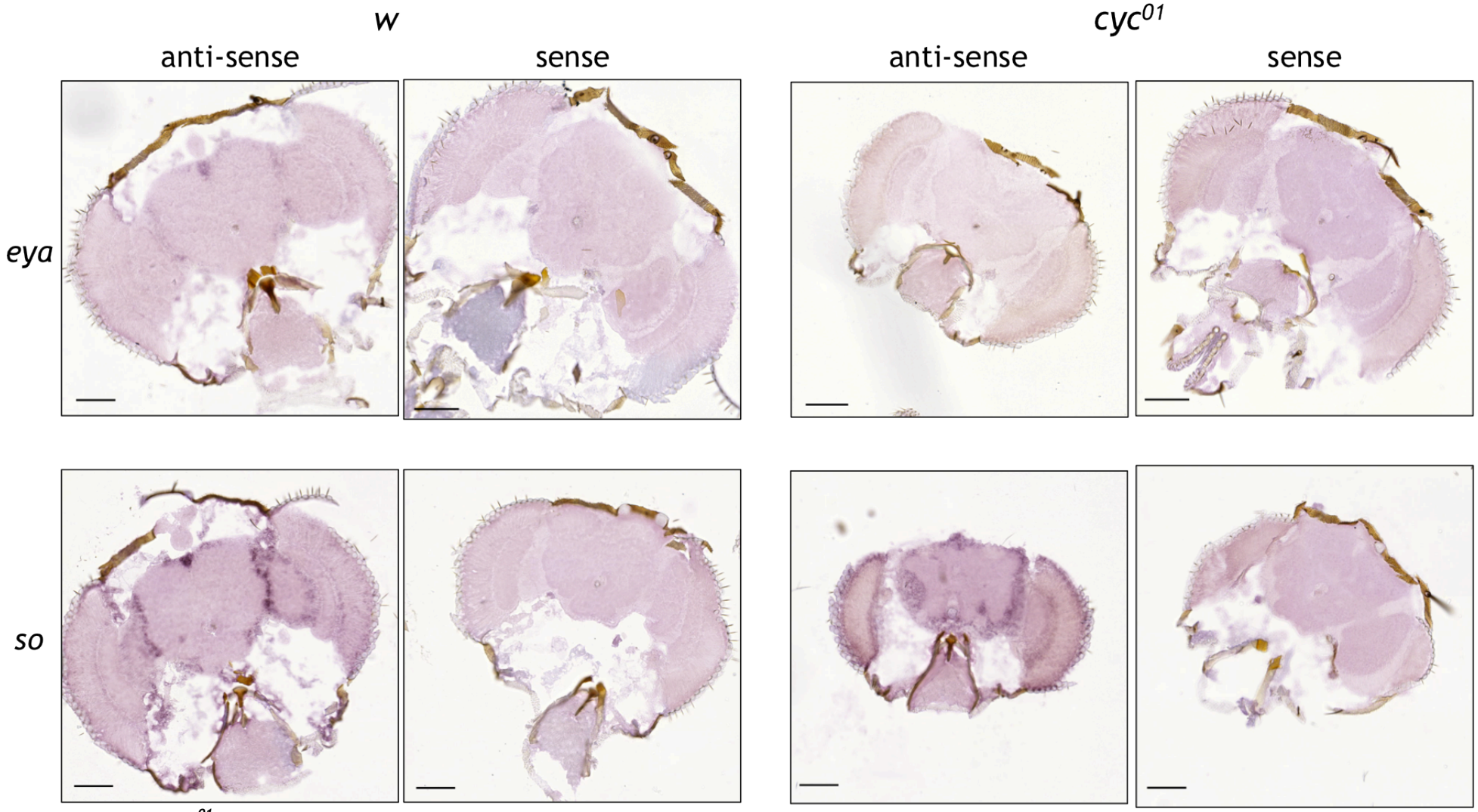

Figure 5.4 *w* and *cyc*^{01} fly heads hybridised with *eya* and *so* probes at ZT14. *n=10* each, male and female.

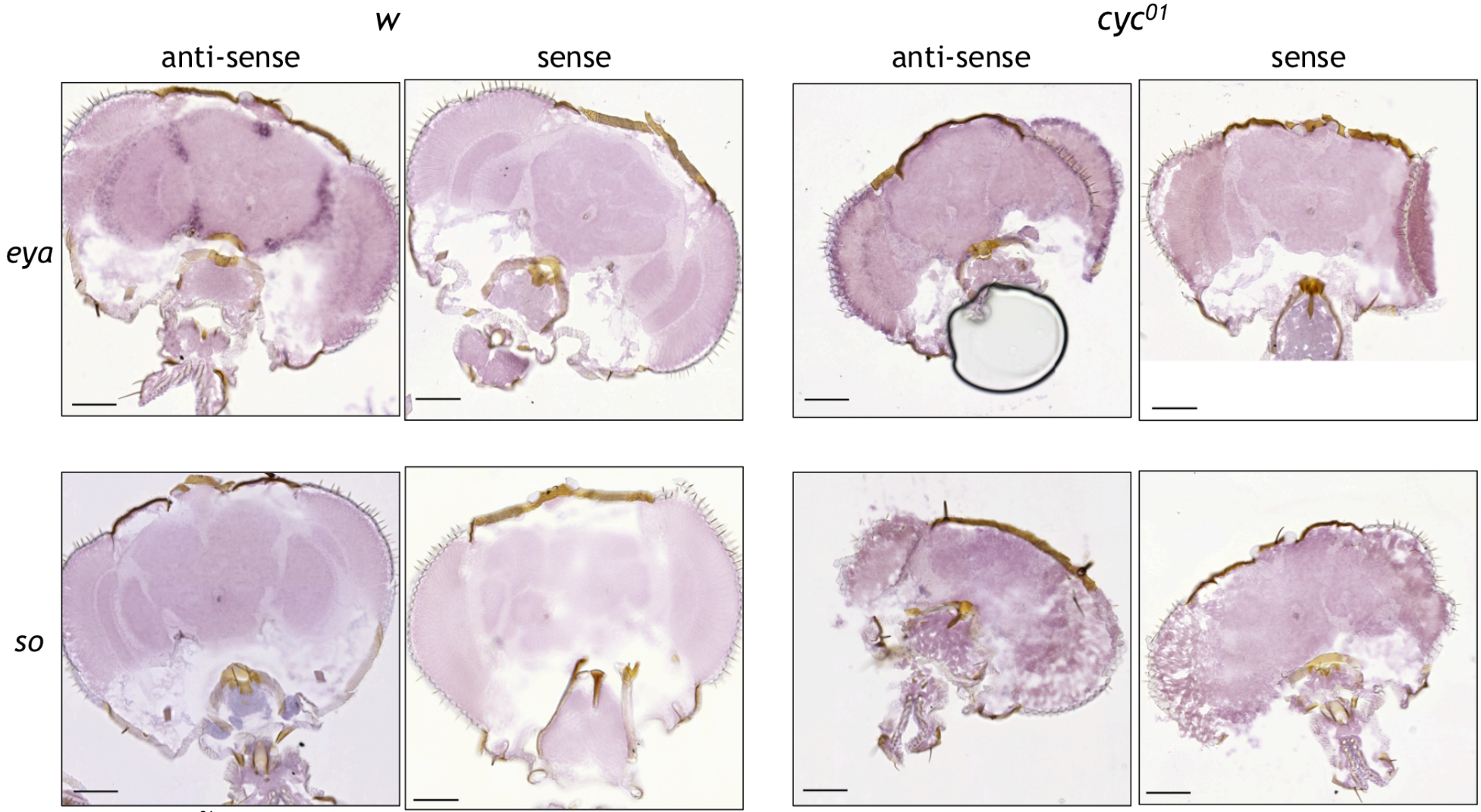

Figure 5.5 *w* and *cyc*^{01} fly heads hybridised with *eya* and *so* probes at ZT18. *n=10* each, male and female.

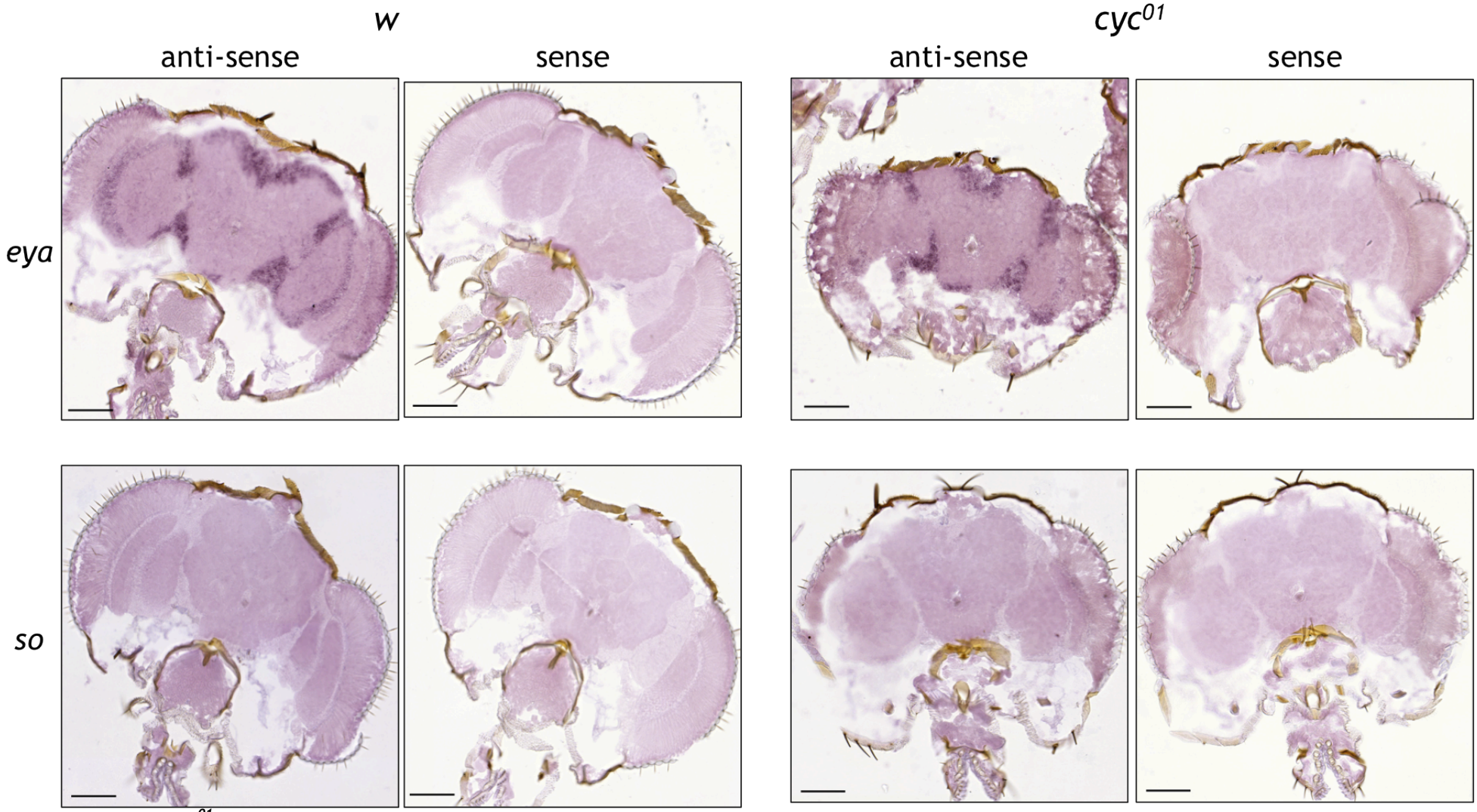

Figure 5.6 *w* and *cyc*^{01} fly heads hybridised with *eya* and *so* probes at ZT22. *n=10* each, male and female.

5.3 Discussion

5.3.1 eya and so are expressed in the visual system and central brain

Hybridisation of full length anti-sense probes of *eya* and *so* seen here support indications that *eya* and *so* are enriched in PRs R1-R6 (Yang *et al.*, 2005). Although preliminary and qualitative rather than quantitative, these data do indicate that there are changes in expression profile over a 24-hour period within the central brain and visual system tissues. In addition, the gross spatial pattern of expression for *eya* and *so* is similar, but the phase of expression differs. As the same expression trend was observed in wild type and circadian rhythm defective strains, it is unlikely that the circadian oscillator mechanism mediates these changes. However, hybridisation signal intensity appears to be higher in the visual system (i.e. PR oscillator cells) of the cyc^{01} mutant. It is possible that although the oscillator does not control spatial expression of these genes, a normal function of the oscillator is to dampen expression levels – i.e. a regulation that is absent in the cyc^{01} mutant. VRI expression is reduced in cyc^{01} flies and it would be possible to determine whether VRI is the modulator here by over-expressing VRI in cyc^{01} mutants.

Collection of heads for sectioning was, by necessity, carried out for a short time in the light. Clearly, this means that flies collected during the dark phase had some light exposure prior to being frozen for further processing. Despite attempts to minimise the duration of these light pulses for dark phase flies, as the kinetics of gene transcription here are unknown, it is possible that the reduction in *so* transcription at ZT18 and 22 is due to an acute clearance of *so* mRNA in response to light. If this is the case, light-mediated clearance mechanisms can only operate in the mid-late night as transcript levels are not affected at ZT14. The reduction in *eya* probe hybridisation at ZT10 and 14 is likely to be an endogenous mechanism of clearance of transcript or down-regulation of transcription; possibly as a result of

photoperiod or an acute response timed to either, lights-on or lights-off. However, without further paradigms, it is possible that the up-regulation of *eya* observed at ZT18 and 22 is due to light pulse activation. Again, if this is the case, up-regulation of *eya* in response to light is only responsive in mid-late night phase.

5.3.2 Functional significance of observed hybridisation signals

To date, functions of EYA and SO in relation to one another for downstream regulation have been most extensively studied. Less well-represented are other functional partners of the two. It is known that SO can partner with GROUCHO and that EYA can form a complex with DAC alone or together with SO. In terms of transcription factor activity, SO contains the DNA binding domain but does not contain nuclear localisation signals and, therefore, requires a protein partner that confers this function. EYA on the other hand, does not have a DNA binding domain but provides the transactivation function and is also a protein tyrosine phosphatase. Transactivation function appears to require phosphatase activity on a target-dependent basis, moreover, phosphatase activity may be required in the cytoplasm as well as the nucleus. Given this information about protein domains and functions, what continues to be uncertain is how early experiments charting ectopic eye development by mis-expression of these proteins, individually, were successful. Certainly, co-expression of EYA and SO in other imaginal discs is synergistic in ectopic eye formation and resulted in a greater percentage of ectopic organs. However, that eye formation proceeded in the absence of one of the partners, suggests that other factors are also able to supplement the complementary functions that EYA and SO require of one another. These unknown aspects may be more or less relevant for the roles of EYA and SO within the developed visual system and CNS.

Based on the expression patterns observed here, it is possible that EYA and SO function as a complex as expression seems to be in similar regions. Further tissue resolution and protein co-incidence confirmation is required as are

studies into the co-incidence of other dimerisation partners of these two proteins. Of particular interest is whether GROUCHO is involved as it partners with SO and is a transcriptional repressor – as SO provides the DNA recognition domain, there is potential for antagonism of the transcriptional output of EYA-SO if expression is coincident. Furthermore, provided the hybridisation signals observed were not artefacts (as mentioned above), spatial and temporal modulations of output are possible. The sketch in Figure 5.7 shows that *eya* and *so* may be co-expressed during the early-mid day; after this *eya* is down-regulated but *so* persists at high levels; this is followed by a fall in *so* expression as *eya* rises. *eya* expression seems to follow a similar phase to that of *Clk* mRNA but does rise whilst VRI is still close to peak levels. Whereas *so* hybridisation signals appear to be high whilst VRI protein levels increase and only fall after VRI reaches peak levels. This is certainly possible if VRI were to be modulating transcription of *so* rather than acting as a primary regulator. Of course, this is speculative and several supportive analyses remain to be carried out to verify the rhythm in expression and quantify it.

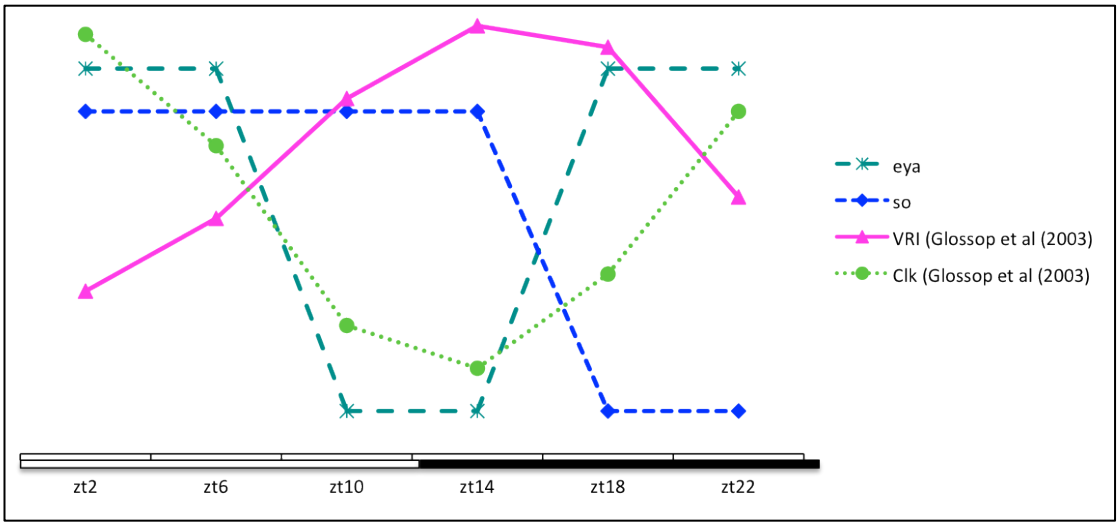

Figure 5.7 Sketch of genes and proteins in whole head. Curves for VRI protein and *Clk* mRNA have been sketched from Glossop *et al* (2003) and superimposed on a sketch of *eya* and *so* transcript levels as qualitatively determined in this study.

Studies in Japanese quail, sheep and mouse indicate that expression of one of the four vertebrate homologues of EYA, Eya3, is regulated by and engages in a photoperiodic response. In sheep, Eya3 peak expression occurred 12hrs after

lights-off within the pars tuberalis – an anterior region of the pituitary gland that receives circadian input and mediates seasonal response. In mice models, Eya3 expression followed somewhat altered kinetics but long photoperiod conditions resulted in an early morning peak in expression. These kinetics mean that on short photoperiod days of 8:16 LD, Eya3 peak was during the dark phase (in sheep, unconfirmed in mice). On long photoperiod days of 16:8 LD, levels were at peak during the light phase in sheep and mice; and in the late day in quail. Regardless of the exact timing of the peak in Eya3 expression, in all three models, *in vitro* reporter assays of the thyrotrophinβ promotor revealed synergistic activation by co-expression of Eya3 and Six1 (one of the six vertebrate *so* family homologues). Thyrotrophin regulates a physiological response to seasons and these data suggest that Eya3-Six1 (and other factors) lie upstream of this regulation. Interactions between Eya3-Six1, thyrotrophin and the oscillator mechanism have not been placed within a model framework as yet. Although, it does place Eya3-Six1 within the overall circadian physiological mechanism.

If *eya* expression in *Drosophila* follows a similar mechanism to that observed for Eya3, the night-time expression at ZT18 and 22 observed here may simply be an acute light activation that is only responsive during the mid-late night and was stimulated by exposure of animals to light during collection. Alternatively, *eya* expression kinetics may be different to that observed in vertebrates and peak expression of *eya* in flies is during the mid-dark phase, different photoperiods may change this expression to be coincident with *so* and regulate a seasonal response.

One of the seasonal phenotypes affected by photoperiod is that of reproductive state. In *Drosophila*, short photoperiods coupled with low temperature lead to reproductive and developmental dormancy, or diapause. At present there is insufficient evidence of the influences of the circadian clock on diapause, either directly and/ or via interactions with photoperiodism and hormonal changes. *eya* is also expressed within *Drosophila* ovaries and, if expression in the ovaries changes over the LD cycle

as observed here in the CNS, may be tracking photoperiod to initiate diapause. Alternatively, photoperiodic tracking within the CNS may interact with the endocrine system to signal to the ovaries to enter diapause.

Chapter 6 General discussion

6.1 Summary of the current study

I have described here initial molecular links between the developmental factors VRI, EYA and SO. Interactions within the eye disc were used as a starting point as the correct expression of all three factors is critical during PR differentiation (George and Terracol, 1997; Szuplewski *et al.*, 2003; reviewed by Kumar, 2009). During early larval growth, a time when cells of the imaginal discs proliferate, VRI is expressed within several imaginal discs including, the pertinent tissue here, the eye disc. As expected, the presence of VRI within the eye disc was not dependent on CLK-CYC, the circadian activator of *vri* (Glossop *et al.*, 2003). I also found that PDP1 protein, of which the ε isoform also binds to VRI sites (Cyran *et al.*, 2003), does not appear to be expressed within the eye disc.

As PR differentiation begins, down-regulation of VRI prior to MF advancement is apparent (Figures 3.2, 3.5). However, initial PR differentiation and ommatidial cluster formation appeared to be unaffected when VRI expression was maintained in the developing neurones (Figures 3.9, 3.10). However, there were differences between cells comprising the developing PR epithelium (Figure 3.10). Endogenous down-regulation of VRI appears to be necessary for the survival of the developed ommatidia since *vri* expression in newly differentiated PRs causes defects during pupal eye maturation and, ultimately, leads to death as pharate adults (Figures 3.12, 3.13). Developing eyes begin to necrose during pupal stages and it is likely that the inflammatory responses to necrosis (Kroemer *et al.*, 1998) result in lethality (Figures 3.12, 3.13).

These results are indicative of a role for VRI that I propose to follow two paths simultaneously; (1) developmental regulation – here targets of VRI

regulation are proposed to be of a more generalised nature, for example, as put forward previously, of cytoskeletal regulation (Szuplewski *et al.,* 2003) or cell proliferation (Gauhar *et al.,* 2009). (2) tissue-specific modulation – here targets of VRI are proposed to be a part of the patterning events of a given tissue. In this case, *eya* and *so* in the eye disc, are responsive to attenuation by VRI and it remains to be seen whether VRI affects other eye-specific factors, either as an attenuator or as a more dominant modulator (Chapter 3).

To further explore a functional relationship between *vri, eya* and *so*, the presence of several putative VRI target sites in *eya* and *so* genomic loci were confirmed *in vitro* (Figure 4.1, Table 4.1). The proximity of two of the indentified sites in the *so* locus to an identified enhancer of *so* located in the sixth intron (Niimi *et al.,* 1999; Punzo *et al.,* 2002; Pauli *et al.,* 2005) might suggest that multiple factors bind intron six to co-ordinate expression of *so*. I have generated novel transgenic animals to determine the contribution of the VRI sites in the intron in regulation of the enhancer (Figure 4.2).

Two variants of the enhancer from the original studies were used for comparison that were 0.4kb (*so10*) and 1.6kb (*so7*) in size and *so7* was modified to contain an additional 2.3kb region of the intron (*so7+VP*). As it is likely that other transcription factor binding sites are present within the additional 2.3kb, the specific contribution of the VRI sites was determined by generation of a second transgenic line in which the VRI sites were specifically mutated (*so7+VP*$^{[VP\text{-}mut]}$). GFP reporter expression mediated by these enhancers was examined in several different tissues. Within all tissues, differences between *so7+VP* and *so7+VP*$^{[VP\text{-}mut]}$ were seen in the signal intensity of the reporter rather than localisation of reporter, higher signal intensity being observed with *so7+VP*$^{[VP\text{-}mut]}$ (Figures 4.5, 4.6, 4.7, 4.10, 4.15, 4.16). An increase in reporter expression, presumably due to ablation of the VRI sites, supports a negative modulatory role for VRI at the *so* locus (as indicated by Chapter 3).

Comparison of *so7* and *so7+VP* within larval and adult CNS shows that extension of the enhancer restricts reporter expression to cells of the visual system – outer optic anlagen of larvae and the lamina of adult brains (Figures 4.9C, 4.10A, 4.14, 4.15). Expression observed within the central brain with *so7* is not seen with *so7+VP*. This is not necessarily an accurate reflection of *so* expression – it is possible that regions of intron six of *so* drive expression of *so* relevant to the visual system and that an alternative enhancer directs central brain expression. This is supported by *so* transcript expression described in Chapter 5 where probes directed against *so* hybridised to regions of the central brain as well as the visual system (Figures 5.1-5.6). The transcript expression in the central brain is not reflected by any of the intron six transgenic reporters (Figures 4.13-4.16). The so^1 mutant has a deletion of the *so7* enhancer and only shows visual system phenotypes (Heitzler *et al.*, 1993; Serikaku and O'Tousa, 1994; Cheyette *et al.*, 1994; Punzo *et al.*, 2002). However, lethal phenotypes are observed for other mutants of *so*. Lethality from certain alleles likely results from developmental lesions in neurogenic regions during embryonic development (Kumar, 2001b). Thus far, only embryonic and eye disc development expression of *so* has been described (Kumar, 2009b) yet it is likely, as seen for EYA, that *so* is expressed within the central brain. Hence, these enhancers are incomplete descriptors of endogenous *so* expression but do highlight interesting aspects of *so* regulation within the visual system, particularly the apparent effect on EYA expression (discussed further below).

Changes in EYA protein levels observed in the CNS of L3 and adults containing the *so7+VP* and $so7+VP^{[VP\text{-}mut]}$ transgenes may indicate that the additional 2.3kb of the intron contains a region that indirectly interferes with *eya* regulation (Phillips, 1998). Initial indications were that insertion of an additional copy of this 3.9kb region of *so* intron six leads to an up-regulation of *eya* expression because regulatory factors that bind to this region appear to be suppressors of *so* expression within the CNS and may also suppress *eya* expression. Insertion of an additional copy of the *so7+VP* region, creating three copies within the genome, may have a saturating effect that relieves

this repression on *eya*, enabling dominance by activators (Chapter 4). However, the dramatic observed increases in *eya* expression implicate the genetic background and positional effect variegation rather than the transgene itself. Non-coding RNAs from the insertion site used for the transgene have not been described as yet but may be a likely influence. In addition, the expression domain of the transgene has not been exhaustively studied and ectopic effects may alter *eya* expression via other routes.

Gene or protein expression within the adult CNS for *eya* or *so* has not been a focus thus far and only been described in brief (Serikaku and O'Tousa, 1994; Bonini *et al.,* 1998; Yang *et al.,* 2005). Neither have they been explored within the field of circadian biology in *Drosophila,* although recent data from Japanese quail, mouse and sheep, that implicate EYA homologues to be part of a pituitary photoperiodic response, may also be relevant to flies (Nakao *et al.,* 2008; Masumoto *et al.,* 2010; Dardente *et al.,* 2010). EYA protein was observed in the DN2s and one of the large DN3 neurones in adult brains but a rhythm in protein expression was not seen (Figure 4.12). This, in itself, does not exclude EYA from circadian regulation as CLK protein does not show rhythmic expression in the oscillator neurones either (Houl *et al.,* 2008). Sectioned adult heads were examined for *eya* and *so* transcripts at 4hr intervals over an LD cycle in wild-type and oscillator-deficient animals. Rhythmic levels of mRNA were observed but the phase was different for *eya* and *so* (Figures 5.1-5.6). Furthermore, *eya* and *so* transcripts were detected in the visual system and the central brain with somewhat altered levels between the wild-type and oscillator-deficient cohorts. Therefore, it appears that although *eya* and *so* show rhythmic expression, this is not mediated by the classical molecular oscillator mechanism. Expression appears to be linked to photoperiod but the oscillator may attenuate this expression as higher levels of hybridised probe were observed in heads of animals lacking an oscillator.

6.2 Conclusions

During eye development, it appears that VRI attenuates expression of *eya* and *so*. However, it is likely that this is a secondary function of VRI expression in the eye disc. Given the necessity of VRI during embryonic development (George and Terracol, 1997) and the expression of VRI in other imaginal tissues (Szuplewski *et al.,* 2003), together with the current study, indicate a function as part of developmental pathways that are common to the imaginal tissues. Expression of EYA within a small subset of oscillator neurones and changes in transcript levels of *eya* and *so* within the PRs suggest that these two eye development factors may interact with the oscillator. However, this is likely to be upstream of the oscillator as changes in transcript levels persist in oscillator-deficient mutant flies. Taken in conjunction with data from Gummadova *et al.,* (2009) and Glossop *et al.,* (unpublished results), a model of interactions between the eye development and oscillator factors is depicted in Figure 6.1.

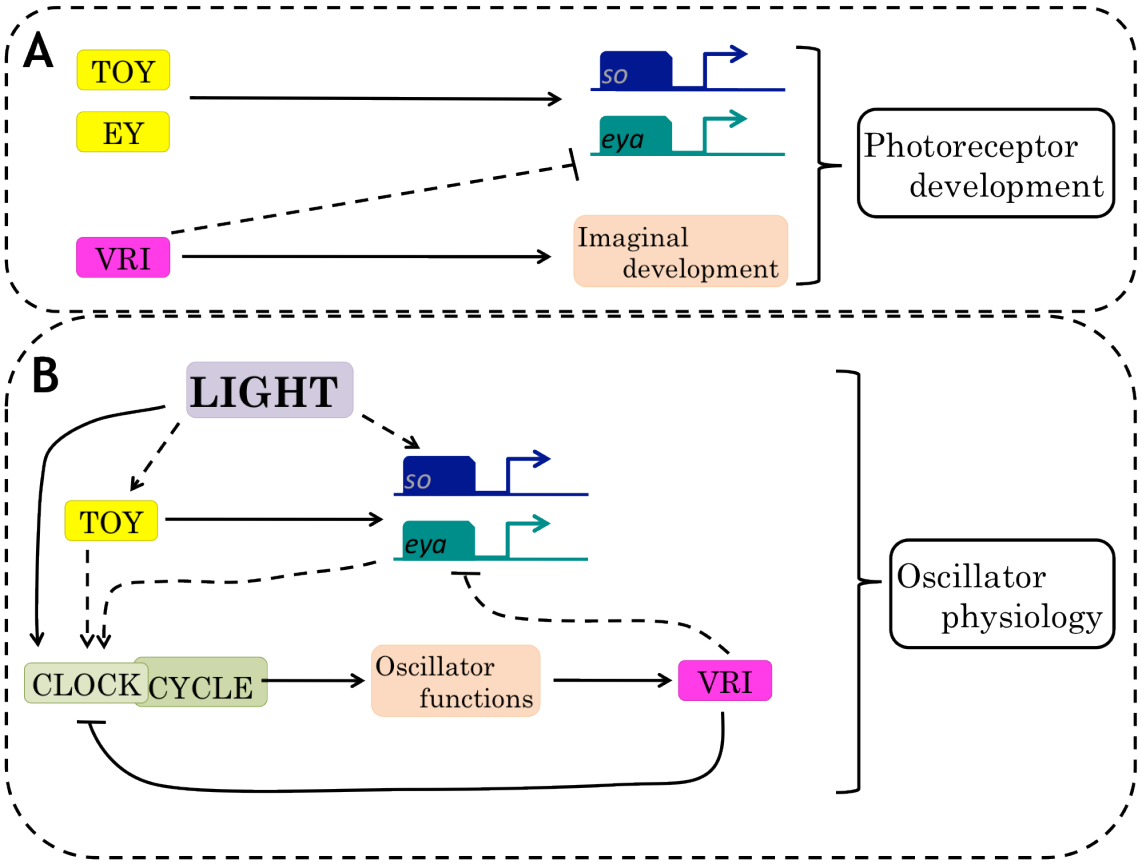

Figure 6.1 Model of interactions between eye development and oscillator factors. (A) Interactions occurring within the developing PRs. (B) Interactions occurring within mature PRs and/ or central oscillator neurones. Solid arrows depict known pathways, dashed arrows depict hypothesised interactions.

6.3 Future directions

A role for VRI in attenuation of *eya* and *so* gene expression is suggested here during eye development (Figure 4.6) and within mature PRs (Figures 5.1-5.6) that are themselves also oscillators (Siwicki *et al.*, 1988; Zerr *et al.*, 1990; Cheng *et al.*, 1998; Meinertzhagen and Pyza, 1999; Barth *et al.*, 2010). Three main proposals for further study are outlined below and their relevance is discussed in the following section.

- To determine the targets of VRI regulation within the eye disc, a chromatin immuno-precipitation (ChIP) assay would be most useful. In order to define the *cis*-acting targets of VRI in the eye disc alone, eye discs collected from over 100 larvae would be required to provide enough DNA

for the procedure. Once the targets of VRI regulation specifically within the eye disc are known, we can begin to answer the questions of whether VRI can be classified as one of the eye DR or as an RDGN factor.

- Gene and protein expression profiles of *eya* and *so* under different photoperiodic conditions should be the next step to expand upon the preliminary results discussed here. In addition it will complement recent findings in vertebrates that *Eya* and *Six* homologues transmit photoperiod information to the pituitary endocrine system (Nakao *et al.*, 2008; Masumoto *et al.*, 2010; Dardente *et al.*, 2010) as well as emerging data on *Clk* regulation by eye development factors (Glossop *et al.*, unpublished results).
- Following expression profiling, it is necessary to pinpoint the actual targets of EYA and SO. To fully grasp their influence in developmental and photoperiodic pathways, functional description of EYA and SO is now necessary.

6.4 Perspectives and outlook

The circadian oscillator mechanism is described as an interlocked feedback loop model that is self-sustaining. The effect of these feedback loops is monitored in two ways, (1) as cyclical changes in gene and protein expression of the factors comprising the mechanism requiring approximately 24hrs. And, (2) physiology of the organism that is adaptive to the challenges and requirements that the organism encounters in relation to the light-dark cycle. External inputs to the oscillator mechanism are indicated by isolation of novel enhancers in the *Clk* gene that do not contain binding sites for the only known activator of *Clk* at present (Cyran *et al.*, 2003; Gummadova *et al.*, 2009). Furthermore, early indications are that the eye development regulator TOY acts via direct and indirect mechanisms on these novel enhancers (Glossop *et al.*, unpublished results).

It must be noted that the popularity of *Drosophila* as a research model is due to a high degree of homology with vertebrate genes. *vri, eya, so, toy* and *Clk*

are all conserved within vertebrates. The congenital disorders that result from disruption of *eya, so* and *Pax-6* together with other diseases, notably cancer, that can result from disruptions of *eya, so* and the oscillator, necessitate their study.

Study of the developing eye disc and circadian rhythms are each somewhat of a double-edged sword. On one side, data on molecular regulatory interactions between transcriptional networks orchestrating the mechanisms is plentiful and we can describe exquisite details of these systems. Conversely, these data have revealed several levels of feedback regulation between networks and individual factors such that mapping these interactions makes for an intricate genetic network. Mathematical modelling approaches for depicting these interactions has already begun in order to plot eye development events (Graham *et al.,* 2010) and oscillator maintenance (Fromentin *et al.,* 2010). As we progress, a dual approach incorporating both, molecular biology techniques and mathematical simulations, will be required as each will be required to complement and inform the other.

References

Baonza and Freeman. Control of Drosophila eye specification by Wingless signalling. Development (2002) vol. 129 (23) pp. 5313-22

Barth et al. Circadian plasticity in photoreceptor cells controls visual coding efficiency in Drosophila melanogaster. PLoS ONE (2010) vol. 5 (2) pp. e9217

Bessa et al. Combinatorial control of Drosophila eye development by eyeless, homothorax, and teashirt. Genes Dev (2002) vol. 16 (18) pp. 2415-27

Bischof et al. An optimized transgenesis system for Drosophila using germ-line-specific phiC31 integrases. Proc Natl Acad Sci USA (2007) vol. 104 (9) pp. 3312-7

Blake et al. Perplexing Pax: from puzzle to paradigm. Dev Dyn (2008) vol. 237 (10) pp. 2791-803

Blau and Young. Cycling vrille expression is required for a functional Drosophila clock. Cell (1999) vol. 99 (6) pp. 661-71

Bodenstein, D., The Postembryonic Development of Drosophila, in Biology of Drosophila, M. Demerec, Editor. 1994, Cold Spring Harbor Laboratory Press: Plainview, N.Y.

Bonini et al. Multiple roles of the eyes absent gene in Drosophila. Developmental Biology (1998) vol. 196 (1) pp. 42-57

Bonini et al. The Drosophila eyes absent gene directs ectopic eye formation in a pathway conserved between flies and vertebrates. Development (1997) vol. 124 (23) pp. 4819-26

Bonini et al. The eyes absent gene: genetic control of cell survival and differentiation in the developing Drosophila eye. Cell (1993) vol. 72 (3) pp. 379-95

Brand and Perrimon. Targeted gene expression as a means of altering cell fates and generating dominant phenotypes. Development (1993) vol. 118 (2) pp. 401-15

Campos-Ortega, J.A. and Hartenstein, V., The embryonic development of Drosophila melanogaster. 1985, Berlin: Springer-Verlag.

Cavodeassi et al. The Iroquois homeobox genes function as dorsal selectors in the Drosophila head. Development (2000) vol. 127 (9) pp. 1921-9

Chanut and Heberlein. Role of decapentaplegic in initiation and progression of the morphogenetic furrow in the developing Drosophila retina. Development (1997) vol. 124 (2) pp. 559-67

Chen et al. Signaling by the TGF-beta homolog decapentaplegic functions reiteratively within the network of genes controlling retinal cell fate determination in Drosophila. Development (1999) vol. 126 (5) pp. 935-43

Chen et al. Dachshund and eyes absent proteins form a complex and function synergistically to induce ectopic eye development in Drosophila. Cell (1997) vol. 91 (7) pp. 893-903

Cheng and Hardin. Drosophila photoreceptors contain an autonomous circadian oscillator that can function without period mRNA cycling. J Neurosci (1998) vol. 18 (2) pp. 741-50

Cheyette et al. The Drosophila sine oculis locus encodes a homeodomain-containing protein required for the development of the entire visual system. Neuron (1994) vol. 12 (5) pp. 977-96

Cohen, S.M., Imaginal Disc Development. The Development of Drosophila melanogaster, ed. M. Bate and A. Martinez Arias. Vol. II. 1993, Plainview, N.Y.: Cold Spring Harbor Laboratory Press.

Cowell et al. Transcriptional repression by a novel member of the bZIP family of transcription factors. Mol Cell Biol (1992) vol. 12 (7) pp. 3070-7

Curtiss and Mlodzik. Morphogenetic furrow initiation and progression during eye development in Drosophila: the roles of decapentaplegic, hedgehog and eyes absent. Development (2000) vol. 127 (6) pp. 1325-36

Cyran et al. vrille, Pdp1, and dClock form a second feedback loop in the Drosophila circadian clock. Cell (2003) vol. 112 (3) pp. 329-41

Dahl et al. Pax genes and organogenesis. Bioessays (1997) vol. 19 (9) pp. 755-65

Daniel et al. The control of cell fate in the embryonic visual system by atonal, tailless and EGFR signaling. Development (1999) vol. 126 (13) pp. 2945-54

Dardente et al. A Molecular Switch for Photoperiod Responsiveness in Mammals. Curr Biol (2010) pp.

Durgan and Young. The cardiomyocyte circadian clock: emerging roles in health and disease. Circulation Research (2010) vol. 106 (4) pp. 647-58

Ellis et al. Expression of Drosophila glass protein and evidence for negative regulation of its activity in non-neuronal cells by another DNA-binding protein. Development (1993) vol. 119 (3) pp. 855-65

Ferris, G.F., External Morphology of the Adult, in Biology of Drosophila, M. Demerec, Editor. 1994, Cold Spring Harbor Laboratory Press: Plainview, N.Y.

Freeman. Reiterative use of the EGF receptor triggers differentiation of all cell types in the Drosophila eye. Cell (1996) vol. 87 (4) pp. 651-60

Fromentin et al. Hybrid modeling of biological networks: mixing temporal and qualitative biological properties. BMC Syst Biol (2010) vol. 4 pp. 79

Gallego and Virshup. Post-translational modifications regulate the ticking of the circadian clock. Nat Rev Mol Cell Biol (2007) vol. 8 (2) pp. 139-48

Gauhar et al. Genomic mapping of binding regions for the Ecdysone receptor protein complex. Genome Research (2009) vol. 19 (6) pp. 1006-13

Geiser et al. Integration of PCR fragments at any specific site within cloning vectors without the use of restriction enzymes and DNA ligase. BioTechniques (2001) vol. 31 (1) pp. 88-90, 92

George and Terracol. The vrille gene of Drosophila is a maternal enhancer of decapentaplegic and encodes a new member of the bZIP family of transcription factors. Genetics (1997) vol. 146 (4) pp. 1345-63

Glossop et al. VRILLE feeds back to control circadian transcription of Clock in the Drosophila circadian oscillator. Neuron (2003) vol. 37 (2) pp. 249-61

Graham et al. Modeling bistable cell-fate choices in the Drosophila eye: qualitative and quantitative perspectives. Development (2010) vol. 137 (14) pp. 2265-78

Gummadova et al. Analysis of the Drosophila Clock promoter reveals heterogeneity in expression between subgroups of central oscillator cells and identifies a novel enhancer region. J Biol Rhythms (2009) vol. 24 (5) pp. 353-67

Halder et al. Eyeless initiates the expression of both sine oculis and eyes absent during Drosophila compound eye development. Development (1998) vol. 125 (12) pp. 2181-91

Halder et al. Induction of ectopic eyes by targeted expression of the eyeless gene in Drosophila. Science (1995) vol. 267 (5205) pp. 1788-92

Hardin. The circadian timekeeping system of Drosophila. Curr Biol (2005) vol. 15 (17) pp. R714-22

Hauck et al. Functional analysis of an eye specific enhancer of the eyeless gene in Drosophila. Proc Natl Acad Sci USA (1999) vol. 96 (2) pp. 564-9

Heitzler et al. Genetic and cytogenetic analysis of the 43A-E region containing the segment polarity gene costa and the cellular polarity genes prickle and spiny-legs in Drosophila melanogaster. Genetics (1993) vol. 135 (1) pp. 105-15

Helfrich-Förster et al. Development and morphology of the clock-gene-expressing lateral neurons of Drosophila melanogaster. J Comp Neurol (2007) vol. 500 (1) pp. 47-70

Helfrich-Förster. The neuroarchitecture of the circadian clock in the brain of Drosophila melanogaster. Microsc Res Tech (2003) vol. 62 (2) pp. 94-102

Helfrich-Förster et al. The extraretinal eyelet of Drosophila: development, ultrastructure, and putative circadian function. J Neurosci (2002) vol. 22 (21) pp. 9255-66

Helfrich-Förster et al. The circadian clock of fruit flies is blind after elimination of all known photoreceptors. Neuron (2001) vol. 30 (1) pp. 249-61

Houl et al. CLOCK expression identifies developing circadian oscillator neurons in the brains of Drosophila embryos. BMC Neurosci (2008) vol. 9 pp. 119

Houl et al. Drosophila CLOCK is constitutively expressed in circadian oscillator and non-oscillator cells. J Biol Rhythms (2006) vol. 21 (2) pp. 93-103

Im and Taghert. PDF receptor expression reveals direct interactions between circadian oscillators in Drosophila. J Comp Neurol (2010) vol. 518 (11) pp. 1925-45

Ivanchenko et al. Circadian photoreception in Drosophila: functions of cryptochrome in peripheral and central clocks. J Biol Rhythms (2001) vol. 16 (3) pp. 205-15

Jemc and Rebay. Identification of transcriptional targets of the dual-function transcription factor/phosphatase eyes absent. Dev Biol (2007b) vol. 310 (2) pp. 416-29

Jemc and Rebay. The eyes absent family of phosphotyrosine phosphatases: properties and roles in developmental regulation of transcription. Annu Rev Biochem (2007a) vol. 76 pp. 513-38

Kammermeier et al. Differential expression and function of the Drosophila Pax6 genes eyeless and twin of eyeless in embryonic central nervous system development. Mech Dev (2001) vol. 103 (1-2) pp. 71-8

Kenyon et al. Partner specificity is essential for proper function of the SIX-type homeodomain proteins Sine oculis and Optix during fly eye development. Developmental Biology (2005) vol. 286 (1) pp. 158-68

Kroemer et al. The mitochondrial death/life regulator in apoptosis and necrosis. Annu Rev Physiol (1998) vol. 60 pp. 619-42

Kumar. The molecular circuitry governing retinal determination. Biochim Biophys Acta (2009b) vol. 1789 (4) pp. 306-14

Kumar. The sine oculis homeobox (SIX) family of transcription factors as regulators of development and disease. Cell. Mol. Life Sci. (2009a) vol. 66 (4) pp. 565-83

Kumar and Moses. Expression of evolutionarily conserved eye specification genes during Drosophila embryogenesis. Dev Genes Evol (2001c) vol. 211 (8-9) pp. 406-14

Kumar and Moses. The EGF receptor and notch signaling pathways control the initiation of the morphogenetic furrow during Drosophila eye development. Development (2001b) vol. 128 (14) pp. 2689-97

Kumar and Moses. EGF receptor and Notch signaling act upstream of Eyeless/Pax6 to control eye specification. Cell (2001a) vol. 104 (5) pp. 687-97

Landskron et al. A role for the PERIOD:PERIOD homodimer in the Drosophila circadian clock. Plos Biol (2009) vol. 7 (4) pp. e3

Lee et al. PER and TIM inhibit the DNA binding activity of a Drosophila CLOCK-CYC/dBMAL1 heterodimer without disrupting formation of the heterodimer: a basis for circadian transcription. Molecular and Cellular Biology (1999) vol. 19 (8) pp. 5316-25

Lévi et al. Implications of circadian clocks for the rhythmic delivery of cancer therapeutics. Philos Transact A Math Phys Eng Sci (2008) vol. 366 (1880) pp. 3575-98

Lim et al. Clockwork orange encodes a transcriptional repressor important for circadian-clock amplitude in Drosophila. Curr Biol (2007) vol. 17 (12) pp. 1082-9

Malpel et al. Larval optic nerve and adult extra-retinal photoreceptors sequentially associate with clock neurons during Drosophila brain development. Development (2002) vol. 129 (6) pp. 1443-53

Mardon et al. dachshund encodes a nuclear protein required for normal eye and leg development in Drosophila. Development (1994) vol. 120 (12) pp. 3473-86

Markstein et al. Genome-wide analysis of clustered Dorsal binding sites identifies putative target genes in the Drosophila embryo. Proc Natl Acad Sci USA (2002) vol. 99 (2) pp. 763-8

Masumoto et al. Acute Induction of Eya3 by Late-Night Light Stimulation Triggers TSHß Expression in Photoperiodism. Curr Biol (2010) pp.

Matsumoto et al. A functional genomics strategy reveals clockwork orange as a transcriptional regulator in the Drosophila circadian clock. Genes & Development (2007) vol. 21 (13) pp. 1687-700

McDonald and Rosbash. Microarray analysis and organization of circadian gene expression in Drosophila. Cell (2001) vol. 107 (5) pp. 567-78

McGarry and Lindquist. The preferential translation of Drosophila hsp70 mRNA requires sequences in the untranslated leader. Cell (1985) vol. 42 (3) pp. 903-11

Meinertzhagen and Pyza. Neurotransmitter regulation of circadian structural changes in the fly's visual system. Microscopy research and technique (1999) vol. 45 (2) pp. 96-105

Milner et al. The role of the peripodial membrane in the morphogenesis of the eye-antennal disc ofDrosophila melanogaster. Dev Genes Evol (1983) vol. 192 (3) pp. 164-170

Mollereau et al. A green fluorescent protein enhancer trap screen in Drosophila photoreceptor cells. Mech Dev (2000) vol. 93 (1-2) pp. 151-60

Moses and Rubin. Glass encodes a site-specific DNA-binding protein that is regulated in response to positional signals in the developing Drosophila eye. Genes & Development (1991) vol. 5 (4) pp. 583-93

Nagoshi et al. Dissecting differential gene expression within the circadian neuronal circuit of Drosophila. Nat Neurosci (2010) vol. 13 (1) pp. 60-8

Nakao et al. Thyrotrophin in the pars tuberalis triggers photoperiodic response. Nature (2008) vol. 452 (7185) pp. 317-22

Niimi et al. Direct regulatory interaction of the eyeless protein with an eye-specific enhancer in the sine oculis gene during eye induction in Drosophila. Development (1999) vol. 126 (10) pp. 2253-60

Ostrin et al. Genome-wide identification of direct targets of the Drosophila retinal determination protein Eyeless. Genome Res (2006) vol. 16 (4) pp. 466-76

Pappu, K. and Mardon, G., Retinal Specification and Determination in Drosophila, in Results and problems in cell differentiation; Vol. 37: Drosophila eye development, K. Moses, Editor. 2002, Springer-Verlag: Berlin.

Pappu et al. Dual regulation and redundant function of two eye-specific enhancers of the Drosophila retinal determination gene dachshund. Development (2005) vol. 132 (12) pp. 2895-905

Pappu et al. Mechanism of hedgehog signaling during Drosophila eye development. Development (2003) vol. 130 (13) pp. 3053-62

Pauli et al. Identification of functional sine oculis motifs in the autoregulatory element of its own gene, in the eyeless enhancer and in the signalling gene hedgehog. Development (2005) vol. 132 (12) pp. 2771-82

Pelham and Bienz. A synthetic heat-shock promoter element confers heat-inducibility on the herpes simplex virus thymidine kinase gene. EMBO J (1982) vol. 1 (11) pp. 1473-7

Phillips. The language of gene interaction. Genetics (1998) vol. 149 (3) pp. 1167-71

Picot et al. A role for blind DN2 clock neurons in temperature entrainment of the Drosophila larval brain. Journal of Neuroscience (2009) vol. 29 (26) pp. 8312-20

Pignoni et al. The eye-specification proteins So and Eya form a complex and regulate multiple steps in Drosophila eye development. Cell (1997) vol. 91 (7) pp. 881-91

Plautz et al. Independent photoreceptive circadian clocks throughout Drosophila. Science (1997) vol. 278 (5343) pp. 1632-5

Poulson, D.F., Histogenesis, Organogenesis, and Differentiation in the Embryo of Drosophila Melanogaster Meigen, in Biology of Drosophila, M. Demerec, Editor. 1994, Cold Spring Harbor Laboratory Press: Plainview, N.Y.

Punzo et al. Differential interactions of eyeless and twin of eyeless with the sine oculis enhancer. Development (2002) vol. 129 (3) pp. 625-34

Reddy et al. Circadian clocks: neural and peripheral pacemakers that impact upon the cell division cycle. Mutat Res (2005) vol. 574 (1-2) pp. 76-91

Reddy et al. The Drosophila PAR domain protein 1 (Pdp1) gene encodes multiple differentially expressed mRNAs and proteins through the use of multiple enhancers and promoters. Dev Biol (2000) vol. 224 (2) pp. 401-14

Richier et al. The clockwork orange Drosophila protein functions as both an activator and a repressor of clock gene expression. J Biol Rhythms (2008) vol. 23 (2) pp. 103-16

Schaeren-Wiemers and Gerfin-Moser. A single protocol to detect transcripts of various types and expression levels in neural tissue and cultured cells: in situ hybridization using digoxigenin-labelled cRNA probes. Histochemistry (1993) vol. 100 (6) pp. 431-40

Seimiya and Gehring. The Drosophila homeobox gene optix is capable of inducing ectopic eyes by an eyeless-independent mechanism. Development (2000) vol. 127 (9) pp. 1879-86

Serikaku and O'Tousa. sine oculis is a homeobox gene required for Drosophila visual system development. Genetics (1994) vol. 138 (4) pp. 1137-50

Shafer et al. Reevaluation of Drosophila melanogaster's neuronal circadian pacemakers reveals new neuronal classes. J Comp Neurol (2006) vol. 498 (2) pp. 180-93

Siwicki et al. Antibodies to the period gene product of Drosophila reveal diverse tissue distribution and rhythmic changes in the visual system. Neuron (1988) vol. 1 (2) pp. 141-50

Stapleton et al. The Drosophila gene collection: identification of putative full-length cDNAs for 70% of D. melanogaster genes. Genome Res (2002) vol. 12 (8) pp. 1294-300

Stoleru et al. Coupled oscillators control morning and evening locomotor behaviour of Drosophila. Nature (2004) vol. 431 (7010) pp. 862-8

Suzuki and Saigo. Transcriptional regulation of atonal required for Drosophila larval eye development by concerted action of eyes absent, sine oculis and hedgehog signaling independent of fused kinase and cubitus interruptus. Development (2000) vol. 127 (7) pp. 1531-40

Szuplewski et al. vrille is required to ensure tracheal integrity in Drosophila embryo. Dev Growth Differ (2010) vol. 52 (5) pp. 409-18

Szuplewski et al. The Drosophila bZIP transcription factor Vrille is involved in hair and cell growth. Development (2003) vol. 130 (16) pp. 3651-62

Tanaka-Matakatsu and Du. Direct control of the proneural gene atonal by retinal determination factors during Drosophila eye development. Developmental Biology (2008) vol. 313 (2) pp. 787-801

S. Tweedie, M. Ashburner, K. Falls, P. Leyland, P. McQuilton, S. Marygold, G. Millburn, D. Osumi-Sutherland, A. Schroeder, R. Seal, H. Zhang, and The FlyBase Consortium. FlyBase: enhancing Drosophila Gene Ontology annotations. Nucleic Acids Research (2009) 37: D555-D559; doi:10.1093/nar/gkn788.

Umemiya et al. M-spondin, a novel ECM protein highly homologous to vertebrate F-spondin, is localized at the muscle attachment sites in the Drosophila embryo. Developmental Biology (1997) vol. 186 (2) pp. 165-76

Voas and Rebay. Signal integration during development: insights from the Drosophila eye. Dev Dyn (2004) vol. 229 (1) pp. 162-75

Vosshall et al. A spatial map of olfactory receptor expression in the Drosophila antenna. Cell (1999) vol. 96 (5) pp. 725-36

Wernet et al. Homothorax switches function of Drosophila photoreceptors from color to polarized light sensors. Cell (2003) vol. 115 (3) pp. 267-79

Wolff, T.R., Donald F., Pattern Formation in the Drosophila Retina, in The Development of Drosophila melanogaster, M.M.A. Bate, Alfonso, Editor. 1993, Cold Spring Harbor Laboratory Press: Plainview, N.Y

Xiang et al. Light-avoidance-mediating photoreceptors tile the Drosophila larval body wall. Nature (2010) pp.

Yang et al. Isolation of mRNA from specific tissues of Drosophila by mRNA tagging. Nucleic Acids Res (2005) vol. 33 (17) pp. e148

Yasugi et al. Drosophila optic lobe neuroblasts triggered by a wave of proneural gene expression that is negatively regulated by JAK/STAT. Development (2008) vol. 135 (8) pp. 1471-80

Zerr et al. Circadian fluctuations of period protein immunoreactivity in the CNS and the visual system of Drosophila. J Neurosci (1990) vol. 10 (8) pp. 2749-62

Zhang et al. Direct control of neurogenesis by selector factors in the fly eye: regulation of atonal by Ey and So. Development (2006) vol. 133 (24) pp. 4881-9

Zheng et al. An isoform-specific mutant reveals a role of PDP1 epsilon in the circadian oscillator. J Neurosci (2009) vol. 29 (35) pp. 10920-7